A Novel *in vitro* Framework for Understanding Aroma Interactions with the Oronasal Mucosa

Clive Ford

A Thesis in the Field of Food Sciences
for the Degree of PhD

University of Nottingham

Abstract

An overview is presented of the olfactory mucosa, volumetric air flow through the geometry of the nasal and oral cavity and a review of the constituent parts of oro-nasal surfactants, saliva and nasal mucus. Discussed is the physical chemistry of dictating the behaviour of aroma in aqueous solutions. Previous investigations into the techniques deployed to describe aroma interactions with proteins, lipids, and biological system such as the oro-nasal mucosa.

A review on the theory and use of APCI-MSMS, an analytical instrument used for real time detection of volatilised aroma through the MS NOSE interfaces.

An overview is provided on the development of a novel volatile delivery system for the real time injection of volatilised aroma samples to air-solution interfaces housed within custom reaction vessels.

A chapter discussing the sensitivity gains achievable in APCI analysis by adopting a dual mass filtering approach using MRM techniques, validation of isobaric resolution is also presented for *in vitro* and *in vivo* systems, including a novel method for persistence of inhaled volatiles, a previously unseen use of APCI.

Gas phase aroma deposition techniques are compared with dynamic headspace techniques for model lipid emulsion systems to highlight the developed techniques applicability in the investigation into interfacial aroma interactions with a medium of interest. *In vivo* aroma deposition data is compared with *in vivo* solution persistence of aroma and parallels are drawn between the two systems through robust statistical analysis.

Investigations consider the impact of mucin on aroma absorbance and release under shear stress and after modulation by salt. Absorption kinetics are a new topic for discussion not fully explored in the literature as is the identification of mucin induced Marangoni effects, that is the homogenisation of aroma absorption caused by surface tension gradients. Finally, mass transfer and surface permeability are used to explain some of the observed aroma-mucin interactions *in vitro*.

Dedication

For Jack and Alice, my little horrors, my own little contribution to the Cthulhu mythos.

For Helen, the owner of an impossibly radiant smile. Her love, her support and belief has improved the lot of my life. You are the perfect partner for dancing, whiskey cocktail swigging and extreme heavy metal gigging.

For Chris, band mate and best mate, there is no one better to achieve "A bridge over trebled water" with… whilst drinking… with pizza.

And finally, for my Ma and Pa who managed to keep me out of trouble just long enough to get this far.

Acknowledgments

Prof. Ian Fisk

Prof. Steve Howdle

Dr. Rob Linforth

Dr. Gary Adams

Dr. Ni Yang

Dr. Marion Doyennette

Dr. Sara Martins

Dr. Anne-Marie Williamson

Dr. Scott Singleton

Dr. Charfedinne Ayed

Dr. Lisa Rull

Sharon Lim

Dr. Vlad Dinu

EPSRC

Unilever PLC

Contents

Table of Figures

List of Tables

Abbreviations in order of appearance

ORNs = Olfactory receptor neurons

OR = Odour receptors

K_{am} = air/mucosa partition coefficients

OBP = Odour binding proteins

BOBP = Bovine odour binding protein =

P_i^o (T) = vapour pressure for the pure component i (Pa)

P_T = gas phase total pressure (Pa)

∇_g = molar volumes of the gas phase

∇_l = molar volumes of the liquid phase

γ_i = activity coefficient

QSPR = Quantitate structure property relationship

X_i = mole fraction of i

K_i = proportionality constant of i

BLG = β-lactoglobulin

CID = Collision induced dissociation

SIR = Single ion recording

MRM = Multiple reaction monitoring

APCI-MSMS = Atmospheric pressure chemical ionisation tandem mass spectrometry

K_H = Henry's law constant

RF = Radio frequency

UPLC-MSMS = Ultra-Pure Liquid Chromatography-tandem mass spectrometry

RHI = Relative headspace intensity

k_{ae} = air-emulsion partition coefficient

K_{aw} = air partition coefficient K_{aw}

PCA = Principal component analysis PCA

EPA = Environment protection agency

V_f =volatilisation factor (V_f)

PRPs = proline-rich proteins

rpm = Revolutions per minute

ANOVA = analysis of variance

HSD = Honest significant difference

BSM = Bovine submaxillary mucin

PGM = porcine gastric mucin

RIM = rat intestinal mucin

ABS% = Percentage absorbed (total)

$ABS\%_s$ = Percentage absorbed during infusion

K_s = Rate of interface saturation

K = Rate of release

K_{slow} = Rate of release during slow decay

K_{fasr} = Rate of release during fast decay

Chapter 1 - General Introduction

1.1.1 Introduction

This project aims to develop an *in vitro* system that able to explain, characterise and ultimately, predict the *in vivo* interfacial interactions of aroma compounds with the oro-nasal mucosa. Several fundamental questions need to be asked to unravel this complex system. How does the physical chemistry of the aroma compound and the interface constituents affect the nature of the interactions? How strong are these interactions? What is the nature of these interactions? What is the temporal aspect of these interactions? How does the physical chemistry of the aroma compound affect the compounds ability to reach the oronasal mucosa?

To begin, a review of the physiology of the oro-nasal mucosa, the structure of the nasal cavity, physical chemistry describing partitioning behaviour of volatile compounds between phases and modelling approaches for characterising the behaviour of aroma compounds in both *in vitro* and *in vivo* systems.

1.1.2 Olfactory system

Aroma compounds are volatile organic compounds with a molecular weight of <400 $gmol^{-1}$ that are sufficiently volatile enough at atmospheric pressure to reach the olfactory mucosa (Tegoni *et al* 2000). In mammals, aroma compounds or odorants are detected by olfactory receptors at the olfactory mucosa.

The mammalian olfactory system is comprised of the olfactory mucosa - a sensory organ, and the olfactory bulb - a specific olfactory brain region. Covering a large surface area, the olfactory mucosa is located mainly in the superior-posterior areas of the nasal

cavity and covers both the turbinate bones and the nasal septum (Moran *et al* 1982). The olfactory mucosa is not continuous, instead, areas of respiratory mucosa are interspersed throughout the olfactory mucosa. Every 6-8 weeks, the olfactory neurons are completely replaced. This process of continuous neurogenesis is thought to be the cause of the discontinuous spread of the olfactory mucosa throughout the nasal cavity (Leopold *et al* 2000).

The olfactory mucosa is comprised of an epithelium and a lamina propria separated by a basement membrane. A specialised mucus secretion gland, the Bowman's gland, is present in the lamina propria (Moran *et al* 1982). Distributed amongst the epithelium are the specialised basal and sustentacular (supporting) cells. Sustentacular cells contain biotransformation enzymes such as cytochrome P450 that detoxify potentially dangerous chemicals that have gained access to the nasal cavity (Vogallis *et al* 2005, Nomura *et al* 2004). Bowman's gland and the specialised cells of the olfactory epithelium also secrete xenobiote metabolising enzymes to the mucus where enzyme mediated biotransformation via Phase I (hydroxylation and other reactions increasing hydrophilicity) of aroma compounds also occurs (Nagashima & Touhara 2010).

Olfactory receptor cells terminate into processes that are further subdivided into microvilli, named olfactory cilia which are displayed on the lumen side of the nasal cavity. Olfactory epithelium neuron axons run through the epithelium and coalesce into larger fascicles called the fila olfactoria in the lamina propria. The fila olfactoria traverse the cribiform plate and join the olfactory bulb. Where they defasciculate and synapse with the mitral cells of the olfactory bulb in a specialised, glomeruli structure (Mackay-Slim and Royet 2006).

Proteomic analysis of rat olfactory cilia identified 377 proteins. Eighty percent of the olfactory sensory neurons and olfactory cilia's

protein function has been characterised (figure 1). Several protein types are over-represented in the cilia proteome. Although olfactory cilia are not motile cilia, cytoskeleton proteins necessary for cell structure and mobility feature heavily. The continuous process of neurogenesis of in olfactory mucosa result in the olfactory cilia proteome featuring an enriched profile of proteins involved in neurogenesis. Xenobiotic clearance proteins are also prominent in the olfactory cilia reflecting the precarious situation of sensory apparatus. By necessity, the sensory apparatus is exposed to the outside environment; the sensory apparatus requires a means of protection from harmful foreign material. Finally, an overexpression of proteins key to intracellular traffic is observed in the olfactory cilia proteome. These findings are consistent with previous findings that the cilia protein profile contains the full complement of proteins that contribute to the current model of chemoelectrical transduction (Frings 2001).

Over a quarter of the protein profile was for plasma membranes (9.9% membrane associate and 15.6% membrane which reflect the large number of membrane transport proteins and proteins required for chemoelectrical transduction (Mayer *et al* 2009).

Lipid content of the olfactory mucosa cilia has a distinct composition. The lipid content of rat olfactory mucosa is dominated by phospholipids, 81% (by weight). Prominent phospholipid type includes Phosphatidylcholine (46% of total phospholipids) and phosphatidylethanolamine (26%). Phosphatidylinositol (8%), sphingomyelin (6%), and phosphatidylserine (7%) are the next most abundant phospholipids, with cardiolipin (4%) and phosphatidic acid (1%) present in lesser amounts. Phospholipids displayed a high degree of poly-unsaturation, with arachidonic acid (20:4) and docosahexaenoic acid as the most abundant species.

However, the sphingomyelin fatty acids were predominantly unsaturated in nature with 24:0 and 20:1 variety dominating (Russell *et al* 1989). The levels of lipid poly-unsaturation observed are similar to that of the photoreceptor cells and other sensory epithelium (Rabinowitz *et al* 1986, Anderson *et al* 1976). Poly-unsaturated lipids promote membrane fluidity, cell differentiation by modulating between lipid raft modulation and signal transduction (Reedy, 2010).

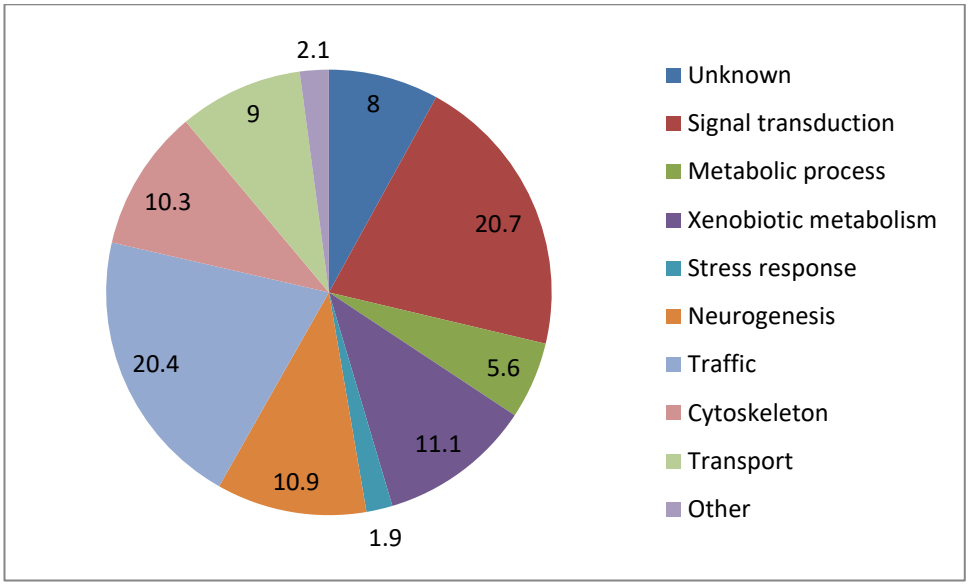

Figure 1 Functional groups of the 377 proteins in the olfactory cilia proteasome of the rat by percentage

The structure of the olfactory mucosa and the interactions of odour compounds results in a chromatographic separation of odour compounds, which sorb at different rates to the mucosa. A chromatograph column with the standard lining replaced with that of a bullfrog olfactory sac produced different retention times for 15 tested volatiles, a finding that supported the hypothesis that the olfactory mucosa is able to distinguish between different volatiles using a chromatographic effect (Mozell *et al* 1973). A chromatographic-like separation was also observed with the

exposure of butanol and octane to a bullfrog olfactory mucosa. A sorption gradient across the mucosa was observed for butanol, with the gradient reversing direction depending on whether stimulus was applied at the external or internal naris. An even pattern of sorption was observed for octane regardless of stimulus origin. The sorption gradient observed for butanol was not affected with alterations in flow rate, partial pressure and volume of the stimulus, suggesting that the separation was based on the physicochemical parameters of the volatile (Hornung and Mozell 1977).

In conjunction with computer simulations, experimental studies have found that deposition patterns onto the olfactory mucosa are not only odorant specific but also dependent on odorant mucosa solubility and also the nasal flow field. Odorant mucosa solubility conforms to the trend that odorants with lower water solubility are more soluble in the mucosa than would be predicted by water solubility alone. Other physicochemical parameters influence odorant solubility in the mucosa and include the local air/odorant flow distribution patterns, odorant mucosal solubility and odorant diffusive transport (Kurtz *et al* 2004, Zhao *et al* 2006, Yang *et al* 2007).

The presence of OR's (odour receptors) in the mucosa affects the sorption of odorants to the olfactory mucosa. Hornung *et al* (1986) compared the air/mucosa partition coefficients (K_{am}) of a normal adult bullfrog's olfactory mucosa with that of an adult bullfrog olfactory mucosa without OR's. For the more water-soluble compounds tested (butanol and isobutyric acid) both mucosae absorbed the same amounts of aroma, suggesting to the authors that uptake was a function of water on the mucosa. For the more water insoluble compounds tested (octane and amyl acetate), the

mucosa containing receptors displayed significantly more sorption than the receptor-less mucosa.

1.1.3 Mucus and odour binding proteins

Human saliva coats the oral mucosa and is secreted by the salivary glands. 93% of saliva is secreted by the salivary glands with the remaining 7% secreted by the minor glands. The role of saliva is complex and varied and includes lubrication, antimicrobial action (lysozyme, lactoperoxides, immunoglobulins, etc.), maintaining mucosa integrity, cleansing, digestion and maintaining oral pH (Dodds *et al* 2015).

Daily saliva secretions range from 500ml up to 700 ml, average mouth volume is ~1.1ml. Secretion of saliva increases to 1.5 mL/min during mechanical and electrical stimuli from a resting rate of ~0.25 mL/min (Lena-Puy 2006)

A wide range of proteins are present in saliva and nasal mucus, table 1 compares the basic protein profiles of saliva and nasal mucus. A study carried out to identify proteins unique to saliva revealed that most salivary proteins are present in comparable levels in other mucosal secretions with the only salivary specific secretions being histatins and acidic PRPs – proline-rich proteins (Shenkels *et al* 1995)

Composition of human nasal mucus and saliva are summarised in table 2 (Jackson *et al* 1999) Nasal mucus contains a higher concentration of mucins than saliva with mucins contributing up to 80% of the dry weight of mucus. Mucins are secreted by both goblet cells and the seromucinous glands of the lamina propria at the apical epithelium.

Table 1: Distribution of salivary and nasal mucus proteins

PROTEIN	SALIVA	NASAL MUCUS
MUCINS	++++	++++
ACIDIC PRPS	++++	-
ALPHA AMYLASE	+++	+
BASIC PRP	++	+
BASIC PRG	++	
SECTRETROY IGA	+	++++
CYSTATINS	+	+
STATHERIN	+	+
IGG	+	+
EP-GP	+	+
VEGH	+	-
HISTATINS	+	-
LYSOZYME	+	++++
KILLIKRIEN	+	+
LACTOFERRIN	+	++++
LACTOPEROXIDASE	+	+
HAPTOCORRIN	+	+
B-MICROSMINOPROTEIN	+	++
IGM	+	+
ALBUMIN	+	+

- not detected; + < 1 % of the total protein amount, or detected but not estimated; ++ between 1 % and 5% of the total protein amount; +++ between

5% and 15% of the total protein amount; ++++ > 15% of the total protein amount; empty spaces indicate "not determined".

Mucin fibres are entwined, bundled, and densely glycosylated proteins with 25-30 carbohydrate chains per 100 amino acids. A consequence of glycosylation is an increase in the viscoelastic properties of mucus. The increase of negatively charged sugars such as sialic acid introduce greater instances of repulsion stretching out the protein chains increasing protein-protein interactions resulting in increased viscosity of the medium (Wiley 1999) Increases in viscosity result in a general decrease of diffusion through the mucus medium (Lai *et al* 2009).

Table 2: Composition of human nasal mucus and saliva

	Saliva (%)	Nasal mucus (%)
Water	99	95
Mucin	<1	2.5-3.5
Salts	<1	1
Enzymes etc.	<1	<1

Present in the mucus of the nasal cavity are OBPs (odour binding proteins) which belong to a class of proteins known as lipocalins, a family of protein that reversibly bind small, hydrophobic molecules. Lipocalins as a class reversibly bind small hydrophobic molecules including steroids and retinoids. OBPs specifically, are lipocalins that reversibly bind odorants in the nasal cavity. Subclasses of OBP exist, for instance there is a subset of lipocalins that bind odour pheromones exclusively.

BOBP (bovine odour binding protein) show a broad range of specificity for small hydrophobic odour compounds. Ligands the with the highest affinity for OBP possess binding constants of between 0.1-1 μM. Ligands with the highest binding constants are heterocyclic derivatives (alkyl substituted pyrazines and thiazoles),

terpenes and derivatives (menthol, thymol) and medium sized aliphatic alcohols and aldehydes. Ligands with poor affinities include round shaped terpinoids (camphor) and polar compounds (Tegoni *et al* 2000).

Several theories of the role OBPs have been hypothesised in the literature such as peripheral odour coding, solubilizing odorants, a buffering effect, as a scavenger protein that prevents saturation of the OR's and for the transfer of odorants to and from the ORs (Pevsner et al. 1986, Bignetti et al. 1987, Pevsner and Snyder 1990, Pevsner et al. 1990, Pelosi 1994, Steinbrecht 1998, Lobel et al. 2002 Taylor et al. 2008)

Comparative studies of artificial and human saliva that showed no significant differences for the partitioning behaviour of volatiles (van Ruth and Roozen, 2000; Friel and Taylor, 2001). A significant trait of the artificial saliva for each study lacked OBP, with the only proteins present being mucin and amylase.

1.1.4 Air flow and deposition of compounds

Orthonasal Olfaction (figure 2) begins with the inspiration of air which enters the nasal cavity via the naris of the nostrils, molecules are transported to the olfactory region by air flow. The olfactory region is not immediately accessible to airborne compounds, odorants travel through airways featuring widespread sorbative surfaces. When bulk flow of odorant loaded air traverses the upper posterior area of the nasal cavity, olfactory perception occurs. The air flow enters the ventral tip of the naris and travels to and through the olfactory slit. Air flow passes through the slit in an almost straight path without the formation of separated recirculating zones (Keyhani *et al* 1996). The passageways of the nasal cavity narrow at the nasal valve and widen as they reach the mid-section of the nasal turbinates' (or conchae), wing shaped structures that occur on

both the lateral walls and the roof of the lumen (Lang 1989, Proctor 1977 and Proctor and Andersen, 1982). The septum divides the nasal cavity into two separate passageways that terminate near the nasopharynx. Towards the rear of the nasal valve lies the inner surface of the nasal cavity, a surface of ciliated epithelial cells. Like all conductive passageways of the respiratory tract the region of the turbinates' is lined with pseudostratified, ciliated and columnar cells (Eccles and Mygind 1985, Van Cauwenberge *et al* 2004).

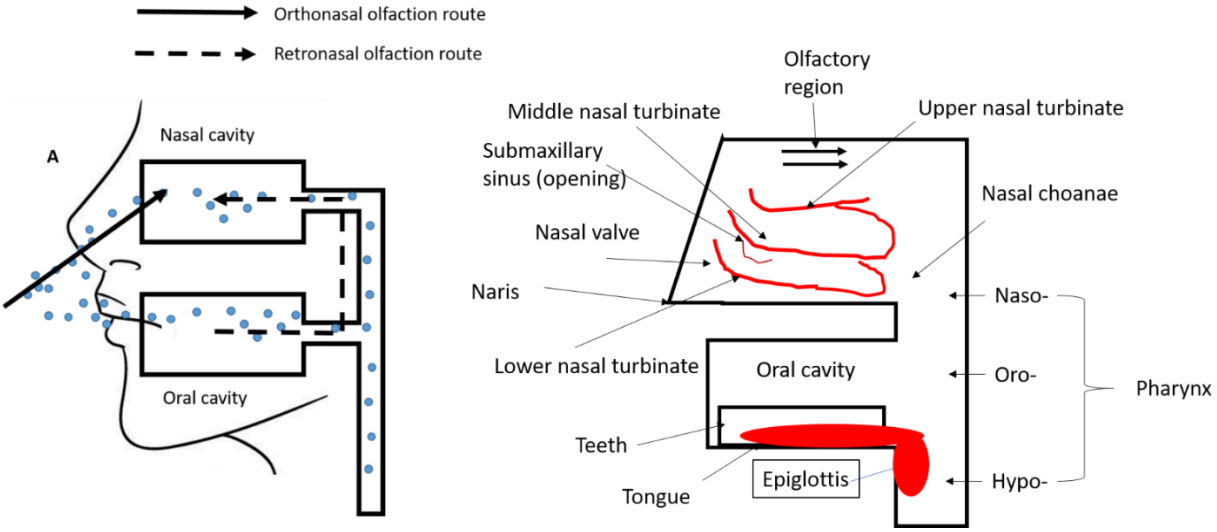

Figure 2 Odorant routes to the olfactory mucosa

Nasal breathing acts as a defence against invading xenobiote particles and conditions inspired air to mimic the condition of air in the alveolar maintaining the warm conditions where gas exchange occurs. Table 3 summarises the air conditions found in the nasal vestibule, nasal valve area, anterior turbinate area, and nasopharynx (Elad *et al* 2008)

Literature values for human air flow rates of restful breathing through the nasal cavity are ~250 mL/s, the right nostril (~143 mL/s) has a higher rate of flow than the left nostril (~105 mL/s). Nasal cavity volumes also differ between gender. The mean volume

of the nasal cavity is 5.95 ± 0.10 cm^3 and 7.01 ± 0.18 cm^3, for the concha nasalis media (meatus) 0.56 ± 0.22 cm^3 and 0.67 ± 0.31 cm^3, for concha nasalis inferior (conchae) 1.45 ± 0.68 cm^3 and 1.59 ± 0.98 cm^3 for female and male respectively (Emirzeoglo *et al* 2012)

Table 3: Distribution of temperature and humidity in the nasal passageway during quiet breathing at room temperature (25 °C, 8.06 mg H2O/l)

Location	Inspiration temperature (°C)	Expiration absolute humidity (mg H2O/L)	Temperature (°C)	Absolute humidity (mg H2O/L)
Nasal vestibule	25.3	9.5	34.2	33.8
Nasal valve area	29.8	19.8	35.1	36.8
Anterior turbinate area	32.3	24	35.1	37.6
Naspharynx	33.9	32.1	36.2	39.6

The highest airflow rate occurs in the lower meatus whilst the second largest airflow peak is experienced by the middle meatus. Approximately 8% of the external naris airflow from the right nostril reaches the olfactory mucosa and approximately 2% from the left nostril, although inter-individual variation of between 5-10% of total naris airflow (left and right nostril) is quoted in the literature (Hahn 1993).

An alternative route for odour molecules to reach the olfactory epithelium is via the mouth (retronasal olfaction). A significant difference between orthonasal olfaction (via the nose) and retronasal olfaction is that perception of orthonasal delivered odour originates from outside the nasal cavity, i.e. from the surroundings whilst retronasal olfaction is perceived as arriving from the mouth

and is often mistaken for taste rather than the perception of an odour (Rozin 1982).

Sensory panel assessment of hydro-alcoholic solutions containing a single aroma active compound attempted to ascertain differences in odour intensities of 8 different compounds for retronasal and orthonasal perception. Panellists oronasal olfaction was more sensitive to compounds with low water solubility whereas retronasal olfaction was more sensitive to high solubility compounds with low volatility (Ferreria *et al* 2006). Sensory panels validated instrumental studies, findings that volatility of an aroma, measured by log K_{aw} or log K_H (Henry's constant), play a significant role in persistence and also that persistence is relative to orthonasal or retronasal delivery.

Lamina airflow is a good approximation for restful breathing where a strong sniff is best described by turbulent airflow. Sniffing behaviour produces a turbulent nasal airflow of > 300 ml/s and has been linked with increased mucosal odorant deposition and an associated increase in odour detection. However, using computational fluid dynamics and human nasal cavity models Zhao *et al* (2006) found no difference in odorant flux (g cm^2/s) for laminar vs turbulent air flow at 300 and 1000 mL/s and no difference for odorants with different mucosal solubility. Sniffing action produced higher resistance to mass transport from the mucosal phase to the air phase resulting in an increased odorant flux to the nasal/olfactory mucosa but a decreased cumulative total uptake of odorants. The sniff duration is, therefore, important but sniff strength is not, suggesting a limit of aroma interfacial movement.

1.2.1 Physical chemistry pertinent to aroma partitioning, aroma diffusion and aroma binding

The proposed aroma delivery system for this project will make use of a system that continuously flushes the headspace above an aqueous aroma compound solution. It is therefore necessary to review the physics governing the behaviour of volatile compounds in such a system.

Distribution of aroma compounds between systems of different phases is described by the aroma compounds affinity for each phase and thus the tendency for the compound to partition. Partitioning coefficients provide a measure of a compounds partitioning behaviour for systems at equilibrium.

1.2.2 Air-water partition coefficient, K_{aw}

The air-water partition coefficient is one of the simplest equilibrium parameters of partitioning between two-phase systems. K_{aw} (equation 1) is a ratio of the concentration of aroma compounds in the air (C_i) above an ideal solution of aroma compound and water (C_l) at equilibrium (Taylor 1998)

$$K_{aw} = \frac{C_g}{C_l} \tag{1}$$

Caveats as to the voracity of experimental K_{aw} measurements accompany many literature values (Taylor 2002). Several methods are available using a range of analytical techniques (Turner 1996, Hu-Sheng 2010).

Several methods for calculating K_{aw} are available. Calculation of K_{aw} can be achieved using thermodynamic parameters (equation 2)

$$K_{aw} = \left(\frac{\gamma_i P_i^o(T)}{P_T}\right) \frac{\nabla_L}{\nabla_g} \quad (2)$$

P_i^o (T) = vapour pressure for the pure component i (Pa),

P_T = gas phase total pressure (Pa)

∇_g = molar volumes of the gas phase

∇_l = molar volumes of the liquid phase

γ_i = activity coefficient

The activity coefficient and therefore the term $\gamma_i P_i^o$ (T) where, (T) can be assumed to be constant if the solution exists in a state of infinite dilution. Determining partition coefficients from the thermodynamic data requires values for pure compounds vapour pressure, another parameter that is not well described in the literature, however these parameters can be successfully estimated (Taylor 2002).

QSPR (quantitate structure property relationship) approaches have previously determined the vapour pressure and solubility of 411 structurally diverse compounds. A five-descriptor equation derived from the chemical structure of each compound produced R^2 values of 0.949 and 0.879 for vapour pressure and solubility, respectively. The QSPR correlation equations for vapour pressure and solubility were then used to predict K_{aw} for each compound (Karitzky *et al* 1998)

1.2.3 Odour partitioning between oil and water phases, Log P

Measurements expressing the preferred partitioning behaviour of aroma between phases other than air and water must also be considered such as k_{ow}, octanol-water partition coefficient, K_{ow} also expressed in logarithmic form as the parameter log P. Log P

provides a measure of compounds solubility through oil and is therefore, an important parameter of compounds hydrophobicity and for relating the interactions of an aroma compound with a lipid phase. Using the Log P scale, hydrophobic compounds have a positive value and hydrophilic compounds have negative values. The value of Log P to the current study can be seen in the work of Sangster (1997) who was able to show that the partitioning behaviour of compounds in a water-biological membrane system closely followed the behaviour observed in octanol-water system.

1.2.4 Henry's law and Raoult's law

Aroma compounds are molecules that are sufficiently volatile so as to allow for transport to the olfactory apparatus. A tendency for an aroma compound to break free from the confines of a solution, food system, biological organism, etc. is given by compounds volatility, a descriptor that provides a measure of the rate at which a compound evaporates. A common measure of volatility used in the literature and central physicochemical parameter databases such as EPIsuite, is the saturated vapour pressure – the equilibrium pressure exerted by a substance in a closed system at a specified temperature (Perring 1999). As previously mentioned, vapour pressure can be used to calculate other thermodynamic parameters such as partition coefficients that can be used to determine the distribution of aroma compounds in multiphase systems. This is because vapour pressure is directly related to the molar fraction of aroma compounds contained within the air phase of a system (Voilley 1991)

Compounds behaviour in solution can be expressed in terms of adherence to Henry's law. Henry's law (equation 3) states that, the partial pressure of a component in the vapour above a solution is directly proportional to the concentration of that component in solution.

$$P_i = X_i K_i \quad (3)$$

X_i = mole fraction of i

K_i = proportionality constant of i

Raoult's law (equation 4) states that the vapour pressure of an ideal solution is proportional to the mole fraction of solvent.

$$P_i = X_i P_i^* \quad (3)$$

X_i = mole fraction of i

P^*_i = partial pressure I, pure solvent

For a pure solvent or a solution that is nearly pure, the vapour pressure of the solvent is proportional to the mole fraction with a gradient of P*I, the vapour pressure for the pure component. If the solvent is the minor component of the solution the constant of proportionality is K^i not P^*_i. Under dilute conditions, solvent molecules are in a similar environment to that of the pure liquid (i.e. water in aqueous systems), the aroma compound conversely is surrounded by solvent molecules. Consequently, the solvent molecules obey Raoult's law and the aroma compounds obey Henry's law because they exist in a state far removed from the pure state, unless the solvent molecules and the aroma molecules are very similar, in which case they conform to Raoult's law (Atkins and de Paulo 2010). Henry's law is a limiting law; it is only applicable in a range of conditions. The law is only applicable if volatile compounds are present at infinite dilution. In practice, this means that only relatively low concentrations of volatiles can be used in the proposed volatile delivery system (from mg/kg^{-1} to µg/ kg^{-1}) to ensure that the volatile solutions obey henry's law (Taylor 1998).

It is important to note that dimensionless expression of Henry's law constants is also a measure of K_{aw}.

Relevant to the proposed volatile delivery system are the mechanistic models produced and validated experimentally to characterise the release of aroma compounds from aqueous systems at equilibrium and under dynamic conditions (Marin *et al* 1999). Under dynamic conditions, factors determining the rate of release of volatiles is dependent on the value of Kaw, if Kaw < 10^{-3} then Kaw determines release, if Kaw > 10^{-3} then mass transport in the gas phase determines release.

1.3.1 Mass transfer

Thermodynamic and kinetic factors dictate the release of aroma compounds from food systems. Partitioning behaviour of aroma compounds in liquid systems is comparatively easier to study than more complex systems such as viscous and solid foods where parameters such as diffusion have a greater effect. Rate of mass transfer can be thought of as the driving force to move materials and the arising resistance to the materials flow. For aroma compounds, this chemical potential difference is characterised by differences in partial pressure or vapour pressure (Voilley 2006)

Although a full review of mass transfer is beyond the scope of a generalised introduction, the fundamentals are however presented. Two important parameters for characterisation of material flux are the diffusion coefficient, D and the mass transfer coefficient, Km.

1.3.2 Diffusion coefficient, D

In an immobile system mass transfer is categorised as diffusional, the movement of groups of molecules is negligible compared to the movement of individual molecules. If the direction of the molecules movement is independent from the properties of the system; then the system is isotropic.

Fick's first law (equation 5) describes an immobile, isotropic, permanent system.

$$\frac{dm}{dt} = -A\,D\,\frac{dC}{dx} \tag{5}$$

M = quantity of diffusing molecules (kg) passing normally across the element, dA (m^2) in time dt (s).

D = diffusion coefficient m^2/s

dC/dx = concentration gradient

C =concentration (kg/m^3)

x = distance (m)

Fick's second law (equation 6) describes non-permanent systems by expressing point by point variations in concentration as a function of time.

$$\frac{\partial C}{\partial t} = D\left(\frac{\partial^2 C}{\partial x^2} + \frac{\partial^2 C}{\partial y^2} + \frac{\partial^2 C}{\partial z^2}\right) \tag{6}$$

(Atkins and de Paulo 2010)

1.3.3 Mass transfer coefficient, k

The simplest view of mass transfer between mucosa and surfactant, (i.e. the buccal mucosa and saliva) can be thought of as a biphasic system. If mass flux is to occur in a biphasic system with a moving liquid, there must be a uniform boundary layer of distance Δx that exists at the interface in which all flow is laminar. Mass transfer beyond the boundary layer is infinitely rapid, turbulent and maintains a mean concentration of C1 (figure 3).

Mass flux, after derivation can be expressed by equation (7)

$$\frac{dm}{dt} = A\,k(C_2 - C_1) \quad (7)$$

Under equilibrium conditions the concentration at the interface, C2 reaches similar levels to those reached at C1, i.e. (equation 8).

$$\frac{dm}{dt} = A\,k(C_1^* - C_1) \quad (8)$$

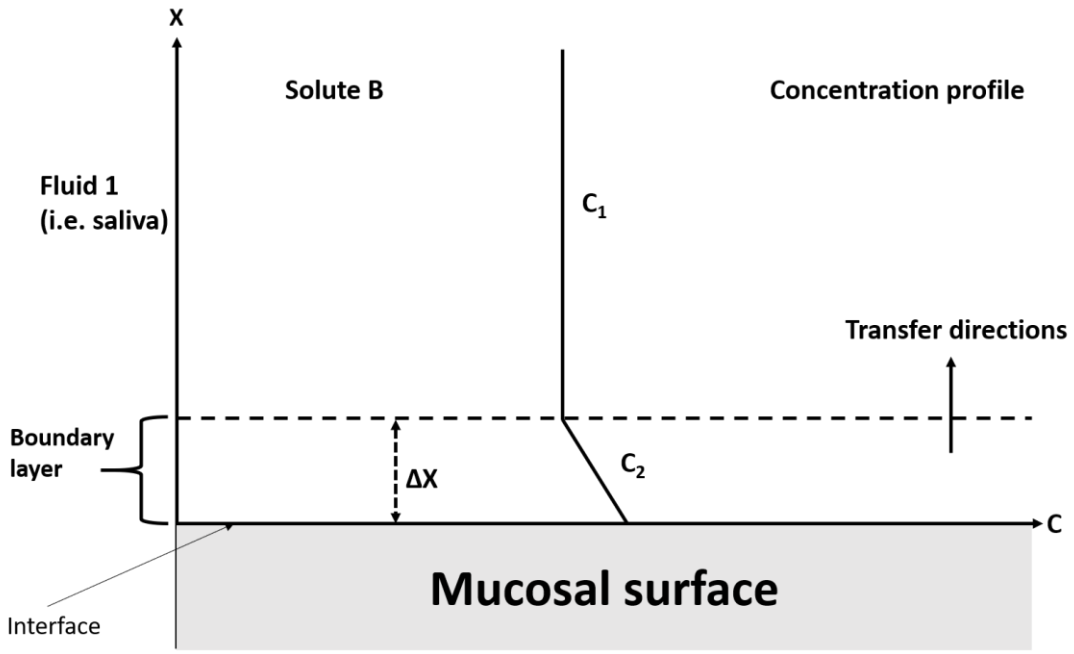

Figure 3 Mass transfer in a biphasic mucosa-saliva system

Odour transport to the olfactory mucosa in (based on canine studies) can be subdivided into four stages (figure 4). The first; advective-diffusive transport of an odorant-air mixture from the internal environment of the nasal passageways; the second; sorption of odorant on to the mucus layer; the third diffusion of odorant through the mucus layer to the epithelial surface and finally; the consumption of odorants at the epithelial surface (Lawson *et al* 2012)

Nasal flow of inspired air delivers odorants from the external environment to the olfactory recess. In the vapour phase, odorants

are passive scalers, molecules that have no effect on the motion of the inspired air, in the nasal air flow. Odorants behaviour is expressed by the equation (equation 9):

$$u_i \frac{\partial C_a}{\partial x_i} = D_{0a} \frac{\partial C_a}{\partial x_i \partial x_i} \quad (9)$$

Here, u_i is the velocity of the air stream, D_{0a} is the binary diffusion coefficient of odorant in air, and C_a is the non-dimensional air-phase odorant concentration. In canines, transport of air is dominated by advection (Lawson *et al* 2012). In humans, transport is not only dependent on convective transport (local airflow rate), but also on the concentration of the remaining odorant in the local air stream (Zhao *et al* 2004). However, odorant transport in the nasal cavity can be expressed by equation (equation 9) if it is assumed that the effect of odorant concentration on the velocity field is negligible for the typical low odorant concentration inhaled through the nose.

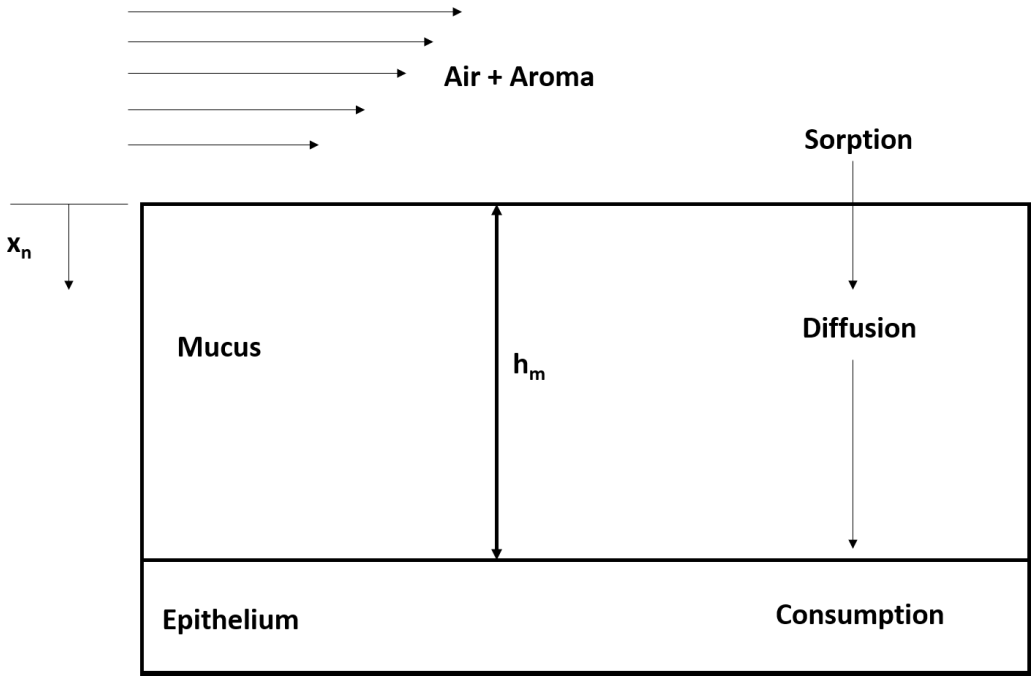

Figure 4 Odorants move from the external environment to the olfactory recess, sorb into the mucus, diffuse through the mucus to the olfactory epithelial layer where they are consumed.

Sorption of odorants begins at the air-mucus interface. Transport across the air-mucus interface is governed by Henry's law (equation 10) and the conservation of mass (equation 11).

$$C_a\left[\, x_{n=0} = K_p C_m\right] x_{n=0} \tag{10}$$

$$D_{0a} = \frac{\partial C_a}{\partial x_n}\left[x_{n=0} = D_{0m}\,\frac{\partial C_m}{\partial x_n}\right] x_{n=0} \tag{11}$$

Where, C_m is concentration of the odorant in the mucus layer, D_{0m} is the binary diffusion coefficient of odorant in the mucus layer, and K_p is the equilibrium partition coefficient, a measure of odorant solubility. x_n is the direction normal to the air–mucus interface. Henry's law allows for a discontinuous movement of odorant concentration across the air-mucus interface. Most odorants have an air-mucus, K_{am} of less than 1, which amplifies the concentration of odorants across the air-mucus interface. Because transport through the nasal passageways is a function of airflow only, the difference in K_{am} is responsible for the difference in deposition patterns of different aromas (Lawson *et al* 2012).

Flow behaviour of mucus at the olfactory mucosa is approximately stagnant. Parallel movement of odorant molecules in the mucus is generally not taken into consideration due to the thinness of the mucus (10 μm), therefore, diffusion through the mucus can be expressed by the one-dimensional diffusion (equation 12) (Menco 1980).

$$\frac{\partial u}{\partial t} = D\,\frac{\partial^2 u}{\partial x^2} \tag{12}$$

Odorants generally take <0.1s to diffuse through the mucus layer. Odorants bind to embedded G protein-coupled receptors at the ciliated mucosa surface. Dwell time at the receptor site is 0.001s, much less than the time taken to diffuse through the mucus layer (Bhandawat *et al* 2005). Odorants are metabolised by enzymes (Pelossi 1996), OBPs (steinbrecht 1998) or vascular clearance (Hahn 1994). If the diffusion time of odorants exceeds the binding and clearance time of odours at the epithelial surface, then there is no saturation of odorants at the epithelial surface and the concentration of odorants at the epithelial surfaces is effectively zero. However, adherence and aggregation of odorants to the lipids and other proteins of the plasma membrane have not been considered.

1.4.1 Aroma compounds interactions with macro molecules

Distribution of aroma compound through complex systems such as a food matrix which can contain several phases is governed by the aroma compounds physical characteristic (molecular weight, shape and moieties) and the thermodynamic properties of the compound (activity coefficient, phase solubility, volatility and partition coefficients). Retention and release of aroma compounds is dependent upon the interactions of the aroma compounds with the constituents of the system, i.e. water, carbohydrates, protein and lipids.

Several key discoveries derived from the field of food flavour release have important ramifications for the study of aroma compound mucosal partitioning, such as the interactions of aroma compounds with the lipids and proteins, the major constituents of the cell plasma membranes.

Fluid mosaic model of plasma membrane describe (figure 5) the components that form a cell membrane. Mammalian cell membranes contain, lipids, proteins, glycoproteins, sterol and glycolipids (Cooper 2002). The structure of each constituent will be briefly covered followed by a summary of the known interactions between aroma compounds and the major plasma membrane macromolecules – proteins and lipids.

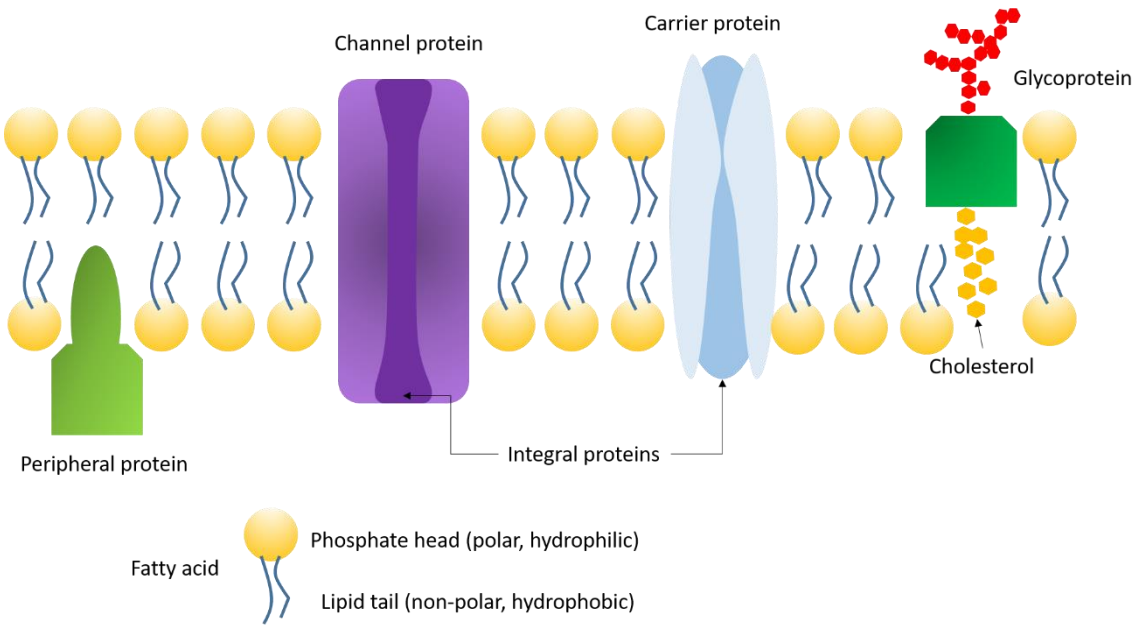

Figure 5 Fluid mosaic model of the cell membrane

(Lombard 2014)

Proteins compromise ~50% (by weight) of the cell membrane. Proteins are formed of 20 amino acids linked by peptide bonds to form long chains structures that are able to fold into varied, unique, and complex structures. The 20 amino acids possess different functional groups and therefore have different water solubility. The suite of amino acids a protein possesses dictate a proteins structure based on how they interact with water (with the assistance of

chaperone proteins). The 3D shape of a protein directly determines the function of a protein. Proteins are the biochemical machinery of a cell and perform a diverse range of roles such as DNA replication, signal transduction and lipid processing (Berg *et al* 2010).

The field of flavour release has produced studies examining aroma compounds interactions with proteins. Food matrix proteins contain little flavour in themselves, however they bind aroma compounds. The strength and the nature of the aroma compound protein complex, set the release of aroma compounds and therefore, impact on overall perception (Guichard 2002)

The structure of a protein influences the residues accessible to the external environment. Globular proteins fold in such a way as to reduce the number of hydrophobic residues presented on the surface in an aqueous environment. Hydrophobic effects are the driving force of interactions between aroma and protein under these conditions. The molecular structure of a protein will determine the nature of interactions with aroma compounds (McClements 2002)

Globular proteins are used for thickening, emulsification etc. in the food industry and consequently, β-lactoglobulin (BLG) is one of the best characterised proteins from the food industry. BLG is part of the super family of proteins, lipocalins of which OBP is a member (Flower 2000). BLG is structurally similar to retinol binding protein. The binding site for retinol was discovered by Monaco *et al* (1987) by x-ray diffraction methods. Retinols binding site was located in a hydrophobic pocket on the outer surface of the protein. Furthermore, Wu *et al* (1999) located the binding site for palmitate in a similar hydrophobic pocket, and Naryan and Berliner (1997) located binding sites for the simultaneous binding of retinol and fatty acids.

A systematic instrumental analysis of the interactions between BLG and 35 flavour compounds of different chemical classes. Protein-ligand binding constants were assessed by affinity chromatography. Flavour compounds affinity for BLG was measured by the calculation of the binding constant, K_B (equation 13).

$$K_B = \frac{t_R^- t}{c_p t_0} \quad (13)$$

Where t_g is the retention time of the compound on the column containing the protein, t is the retention time, c_p is the protein concentration (mol dm^3) and to is the void time.

For esters, pyrazines and phenolic compounds, K_B, increased with hydrophobic chain lengths resulted in increased affinity for BLG. Generally, excluding, terpenic compounds evaluated, K_B increased with increasing values of Log P (Reiners *et al* 1999).

The plasma membrane, of a cell is comprised of ~50% lipids (by weight). The interfacial interactions of an aroma compound and oro-nasal mucosa will include interactions with the lipids of the plasma membrane.

The simplest definition of lipids is based on solubility, i.e. lipids are insoluble in water but soluble in organic solvents. With the genesis of lipidomics (whole characterisation of a subject's lipid profile, i.e. cellular, organellular) the lipid MAPS consortium developed a more encompassing definition of lipids. "Hydrophobic or amphipathic small molecules that may originate entirely or in part by carbanion-based condensation of thioester (fatty acyls, glycerolipids, glycerophospholipids, sphingolipids, saccharolipids, and polyketides) and/or by carbocation-based condensations of isoprene units prenol lipids and sterol lipids" (Brugger 2014).

The literature provides examples of the effects lipids have on the release of aroma compounds from lipid-containing solutions and model food systems. Previous studies highlight the importance of compounds hydrophobicity (log P) in flavour release. In a liquid bullion model food, the retention of aroma compounds strongly correlated with the intrinsic physicochemical property, Log P. It was summarised that non-volatile food lipids are efficient at binding aroma compounds (Rièra *et al* 2006). Emulsion systems provide additional examples of the preponderance of Log P as a governing factor in the release of aroma compounds. Frank *et al* (2011) observed that the release of volatiles conformed to the theory that volatile with a high Log P (>1) will be retained to a greater extent than volatiles with a low Log P (<1) for the release of volatiles from the intravenous feeding emulsion IVELIP. Carey *et al* (2000) reported similar findings for cloud emulsions where the statistically significant factors affecting flavour release were Log P, Dipole Vector, log Solubility and oil fraction.

1.5.1 Modelling flavour Release (*in vivo* and *in vitro*)

There exist, two possible approaches for modelling flavour release, a mechanistic approach, and an experimental, empirical approach. Modelling approaches developed for the elucidation of flavour release mechanism can potentially be further refined to characterise the interfacial interactions of aroma compounds at the oro-nasal mucosa.

A mechanistic model uses the theories and principles of chemistry and physics to describe flavour compounds behaviour in a given system. A mathematical description is built up of the system, and equations are used to determine the behaviour of the compound based upon interactions between flavour compound and system. A mechanistic model is a theoretical approach and requires

experimental validation; however, a considerable advantage of using a model of this form is the ability to provide form to a system that analytical techniques are not yet sensitive enough to penetrate.

An empirical approach requires experimental data on a observation such as the headspace concentration above an aqueous system. Physiochemical parameters identified in theoretical models and parameters provide descriptors for the differences in the compound in conjunction with data it is then used to create a model to describe the variation in results for each compound in the system (Linforth 2010).

1.5.2 Mechanistic models – flavour release *in vitro* and *in vivo*

Buttery (1973), mathematically described the partitioning behaviour of volatiles in an emulsion system by combining the Kaw with K_{ow} to produce the air/emulsion coefficient, K_{ae} (equation 14).

$$K_{ae} = \frac{1}{\left(\frac{F_o}{K_{ao}} + \frac{F_w}{K_{aw}}\right)} \qquad (14)$$

Subsequent refinements were made to the model to account for factors such as pH of the system and pKa (de Roos and Sarelse 1996)

A different approach was taken by Harrison and Hills (1997a), who produced an early model to describe the release of volatiles from an emulsion. The model assumed that the rate-limiting step was due to the resistance of mass transfer across the emulsion/gas interface (penetration theory). Partitioning of flavour molecules across the gas/emulsion interface is much slower than the comparatively rapid movement of flavour molecules across the aqueous/oil interface (equilibrium properties at the gas/emulsion interface). The mass transfer coefficients dependence on viscosity, oil fraction and droplet

size were also incorporated into the model. In summary, the major physical factors affecting flavour release in this model included the mass transfer coefficient, flavour concentration and gas/emulsion partition coefficients. Subsequent Harrison and Hills models (1997b) expanded previous work to describe flavour release from systems containing aroma-binding macromolecules. The model incorporated first order chemical kinetics to describe the reversible interactions of aroma with polymer. The rate-limiting step was the transport of aroma compounds across the air/liquid interface, not the chemical binding step. These early models, whilst influential, did not accurately describe *in vivo* conditions. The surfaces and volumes were assumed to be constant; the models used a closed system so that equilibrium was eventually reached and there was no incorporation of dynamic physiological factors such as dilution by salivary flow. Harrison and Hills (1997) further refined their original models by introducing an air flow to simulate a subject's cyclic breathing patterns and thus created an open system to introduce parity between the theoretical model and *in vivo* conditions.

Seeking to refine the equations developed by Harrison and Hills to describe better the conditions of aroma behaviour during the consumption of food, parameters to describe individual physiology were introduced. The selected parameters sought to describe the effects of salivary flow, periodic breathing, saliva volume changes and the effects of chewing and swallowing on the total surface area of the food (Wright and Hills 2003, Normand *et al* 2004, Wright *et al* 2003). Improvements to the existing models was to consider the release of aroma compounds *in vivo* , that results from a bolus deposits in the pharyngeal mucosa after the bolus is consumed. Normand (2003) proposed a model that included release from equilibrium batch extraction (pertinent for a few breaths after

swallowing) and release from mucosa that remained coated with liquid after the initial swallow. These models describe the case for *in vivo* conditions and the consumption of food.

1.5.3 Empirical models of *in vivo* aroma persistence

Empirical models are data driven. Theoretical mechanistic models can be used to identify physicochemical parameters for investigation. A data series (i.e. headspace concentration of volatiles) is gathered with sufficient variation in the parameters so as to describe the differences in the observed data.

Limitations inherent to empirical modelling include the adjustment of the data gathered using mathematical functions that have no connection with the observed behaviour of the system.

Studies by Linforth and Taylor (2000) and Buffo *et al* (2005) made use of MS and MS Nose APCI-MS to measure the persistence of volatiles *in vivo* after consumption of flavoured solutions. The ratio of the concentration of volatiles present in the first exhaled breath and the second exhaled breath was used as an indicator of *in vivo* persistence. Using physicochemical parameters and a Chemometrics modelling program (Design Expert 6) Linforth and Taylor (2000) produced a polynomial function ($R^2 = 0.83$) to predict the release.

With an R^2 value of 0.83, Linforth and Taylor (2000) used physicochemical parameters and the data from 65 volatiles to produce a polynomial function to predict the persistence of volatile *in vivo* . The statistically significant factors to the function are volatiles values for Log P and the estimate of the vapour pressure of the molecule, Log pL.

Individual physiological variance of subjects, the concentration of volatile and replications within the subjects were found to be not

statistically significant in Buffalo *et al* (2005) models. Saturated vapour pressure was the most statistically significant factor for predicting a compounds *in vivo* persistence with a regression coefficient of $R^2 = 0.73$.

A study aiming to correlate the duration of 8 compounds after smell and various physiochemical parameters was undertaken by Ferreria *et al* (2006). The most significant correlation was between the log of the purging constant Kp – an alternative measurement for volatility. The study suggests that an inverse relationship exists between the volatility of an odorant and the duration of its aftersmell. The model produced was hindered by not considering any other parameters such as interfacial interactions between mucosa and odorant or interactions between salivary constituents and odorant.

Long-term persistence of volatiles in breath was modelled by Hodgson *et al* (2004). Nose space concentration of 5 volatiles with a range of Kaw values were monitored by APCI-MS after consumption of an aqueous volatile solution. Decay of the volatiles signal proceeded in two stages, an initial rapid decline in concentration that lasted up to a minute and a second period of greatly reduced signal decay. Both stages of decay are related to desorption of volatiles from the nasal mucosa. Breath by breath decay of volatiles was modelled using a power law, $Y = Mx^{-p}$, ($R^2 = 0.96$). However, the first breath could not be modelled by this function. The first breath contained the volatiles that had not partitioned to mucosal lining, rather, they had portioned into the lining of the mouth. Subsequent breaths contained volatiles that had desorbed from the mucosal lining. The release of volatiles from the mucosal lining was modelled from the second breath onwards

and produced a measure of long-term persistence using the function (equation 15):

$$C = C_1\, t^{*-P} \qquad (15)$$

C_1 is the volatile concentration in breath after the first minute whilst P is the decay rate of the volatile in the breath of the subject, t* is dimensionless. What was found was that the long-term persistence of compounds does not depend on the physiochemical properties of the volatile.

Further work conducted by Hodgson *et al* (2005) attempted to refine the understanding of the relative contribution of the gas and liquid phases to aroma transport and how the composition of the liquid phases can modulate *in vivo* aroma persistence. Breath volatile concentration was monitored from the second breath onwards after consumption of emulsions of varying lipid content. Variation in the hydrophobicity of the studied compounds (2,5–dimethyl pyrazine and menthone) was assigned as the physicochemical parameter responsible for the variation in persistence behaviour between the two compounds. Persistence of 2,5-dimethylpyrazine, a hydrophilic volatile, showed little variation with changes in emulsion fat concentration. This is conformation of the presence of emulsion residue in the throat, if volatile release was only occurring from depositions on the mucosal layer then, the release profile of menthone would not be adjusted by the modification of fat content. It was also noted that initial spikes in aroma concentration during APCI-MS breath analysis was due to the transfer of a portion of the buccal gas phase concentration being delivered to nasal mucosa by the tidal breath flow.

Rabe and colleagues (2004) undertook a study to assess the influence of physiological factors on the release of dynamic in mouth flavour release for aqueous solutions. A previously validated mouth model apparatus (Rabe *et al* 2002) was used to simulate and investigate the effects of saliva (artificial), shear rate, airflow, in-mouth headspace volume and human epithelial cells (modelling mucosa) on the initial dynamic flavour release on liquids. *In vitro* approaches were used so as to bypass the inherent limits of human chemoreception i.e. lack reproducibility and inter individual variation as detailed by Laing and Jinx (2001).

Kinetic data for the first 30 seconds of dynamic flavour release under simulated mouth conditions were assessed. The results identified three statistically significant factors for *in vitro* flavour release: shearing/ mastication – results in increased surface area and increased distribution of undissolved flavour molecules, headspace volume and volumetric airflow rate

For liquid food, using the developed *in vivo* mouth model, artificial saliva and the oral mucosa mimetic were of insufficient statistical significance.

1.6.1 Investigating *in vivo* interfacial phenomena *in vitro*

Generally, in APCI-MSMS vivo analysis (figure 6) consists of two events. Initially, a period of interface saturation as volatile compounds partition into the various phases of the oro-nasal mucosa results in an increase in detected signal. A maximum point is reached that corresponds either to the end of an eating/drinking (swallowing) event or the saturation of interfaces, the volatile compounds are the lost through the breath. Secondly, after a maximum is reached, a period of decay begins. The decay period corresponds to the loss of volatiles partitioning into the gas phase to be removed by the breathing cycle. The saturation event provides

a measure of interfacial deposition, interfacial capacity and the kinetics of saturation. The decay event provides a measure of compounds persistence at the oro-nasal mucosa and also (in real systems) any residual volatile release caused by remaining artefacts such as the mucosal lubrication.

Molecules physicochemical parameters, particularly, octanol-water partition coefficient (Log P), air-water partition coefficient, vapour pressure and solubility will govern the how each compound will interact with the surrounding environment.

Consider a solution composed of water and a volatile compound. The solution sits in a subject's mouth before swallowing, volatile compounds begin to leave the area that spans only a few microns at the interface of the solution and enter the oral cavity, this event will be governed by the tendency for the volatile to volatilise and enter the air phase. The rate and amount of volatilisation will be governed by the compounds affinity for air and water, measures given by the physicochemical parameters K_{aw}, and vapour pressure. A compounds volatility will also be affected by its water solubility (for this example) a measure provided by the solubility of a compound.

Molecules transported to the nasal cavity mucosa by air flow arrive at a fresh interface, mucus a mostly water surfactant. Partitioning into the mucus will be governed by K_{aw}, movement through the mucus governed by solubility. Once at the mucosal surface, volatiles will then be met by the lipid bilayer of the cells that compose the mucosa. Interactions will be then governed by hydrophobic interactions, a factor characterised by the physicochemical parameter, Log P. Kaw, vapour pressure, solubility and Log P will be significant factors in describing a volatiles behaviour.

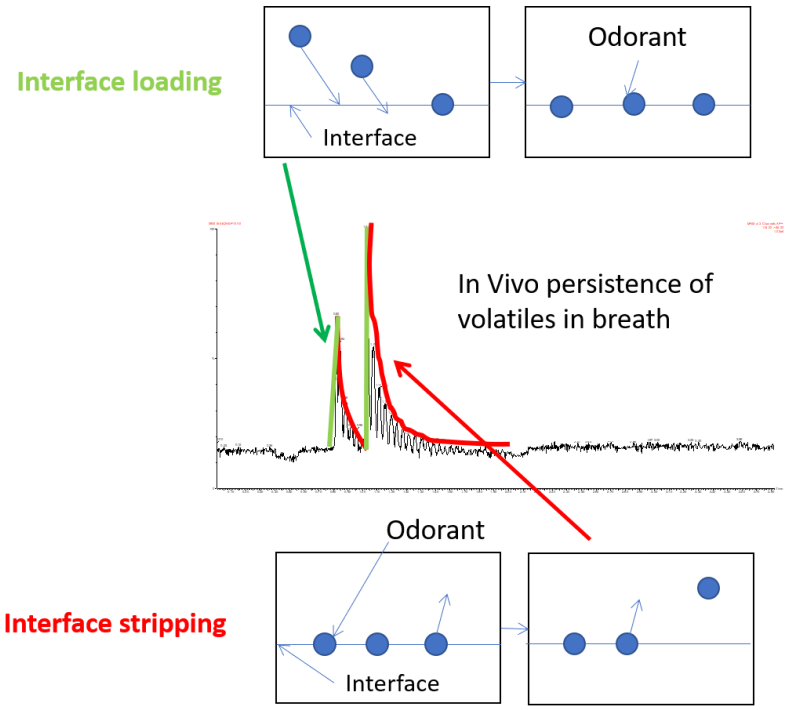

Figure 6 Breath by breath release of aroma and the proposed events occurring at the interface

Volatiles will also meet other constituents, such as OBP, proteins and glycoproteins. The current study aims to characterise the events of *in vivo* persistence and saturation with an *in vitro* system with varying surface composition such as high fat systems and saliva containing systems. For systems composed of water and oil/water, movement from the interface will be greatly affected by K_{aw} and Log P. Decay rates will be dictated by the freedom of movement to establish a concentration gradient. For instance, in high fat systems volatiles with high Log P values will decay to a quicker extent and volatiles with high Kaw values will have higher decay rates in aqueous systems and low-fat systems. Proposed *in vitro* systems will attempt to identify the physical phenomena occurring at the interface of air-solution systems (figure 7).

In vitro systems used to explain, characterise and ultimately predict the interactions of volatile compounds at the oro-nasal mucosa interface

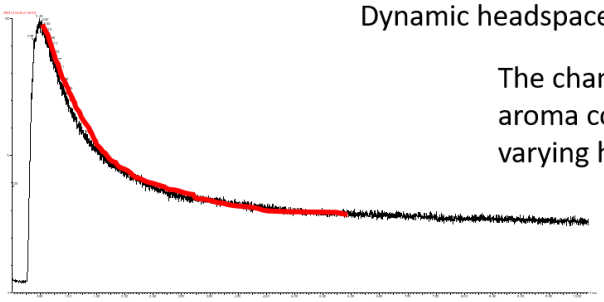

Dynamic headspace analysis – **In vitro system 1**

The change in persistence of aroma compounds in systems of varying hydrophobicity

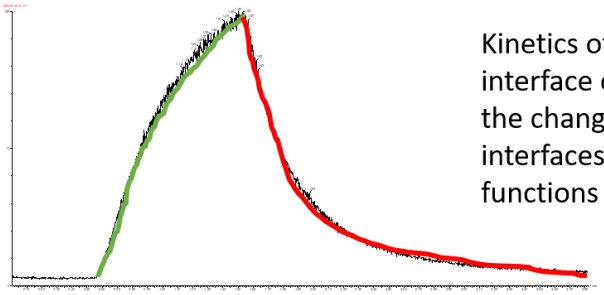

Persistence of volatiles at an interface – **In vitro system 2**

Kinetics of interfacial saturation of interface of differing hydrophobicity and the change in persistence of volatiles at interfaces of varying hydrophobicity as functions of time and concentration

Figure 7 Application of *in vitro* systems to explain *in vivo* mucosa loading and stripping and persistence.

2.1.1 APCI-MSMS – Atmospheric pressure chemical ionisation tandem mass spectrometry

The MS Nose APCI-MSMS interface is a powerful tool for characterising the real-time fluctuations of gas phase compounds in a compartment such as a glass vessel or nasal cavity. Studies by Linforth and Taylor (2000) and Buffo *et al* (2005) made use of MS and MS Nose APCI-MS to measure the persistence of volatiles *in vivo* after consumption of flavoured solutions. More recently, Gan *et al* (2015) developed an APCI-MSMS, in conjunction with GC-MS headspace analysis technique for predicting the maturity of Cheddar cheese based on the cheese aroma profile.

The MS-Nose APCI-MSMS set up comprises of the MS Nose interface, an APCI ionisation chamber followed by a triple quadrupole tandem mass spectrometer. Volatiles contained within the headspace above a flavoured solution are sampled through the MS Nose interface and transported to the ionisation source where molecular adducts are formed by charge transfer reactions. Newly protonated volatiles are declustered by imparting energy to ion clusters. Ions progress to the first mass analyser where ions are separated based upon the m/z. Depending on the operating mode parameters, ions either pass through to the detector or are undergo collision induced fragmentation (CID) followed by a second mass analysis step before moving through to detection (figure 8).

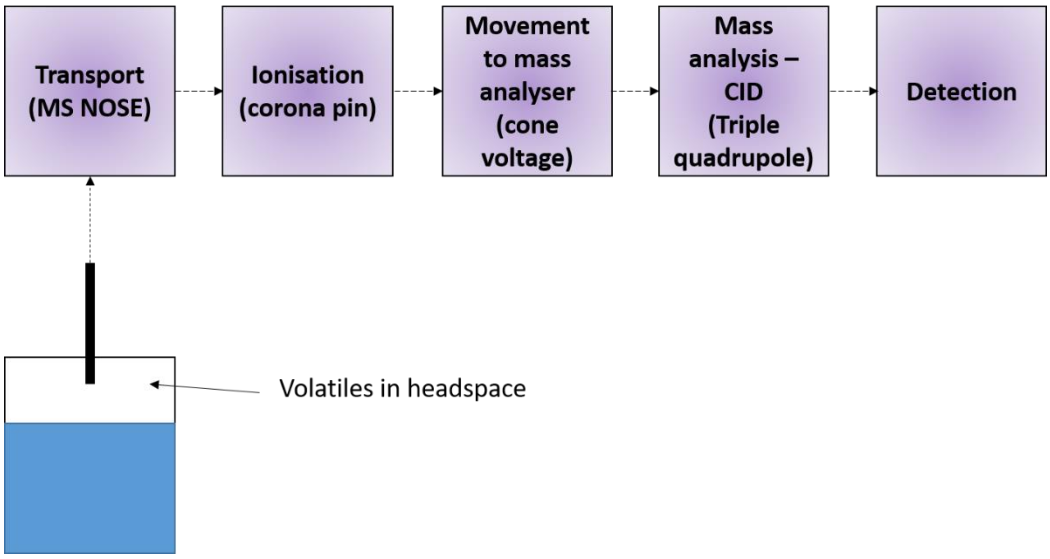

Figure 8 Volatile pathway through MS Nose interface and APCI-MSMS

2.1.2 MS Nose interface

MS Nose is an interface for mass spectrometers and is the component responsible for delivery of volatised compounds from a sampling space to the ionisation source. The interface is composed of a heated transfer line, which encases a fused silica column. The heated transfer is joined to the APCI at the sampling port, the silica tubing continues on into a heated APCI capillary to the venturi region. The location of the silica in the venturi region is finely adjustable and is the method of sampling rate control (figure 9).

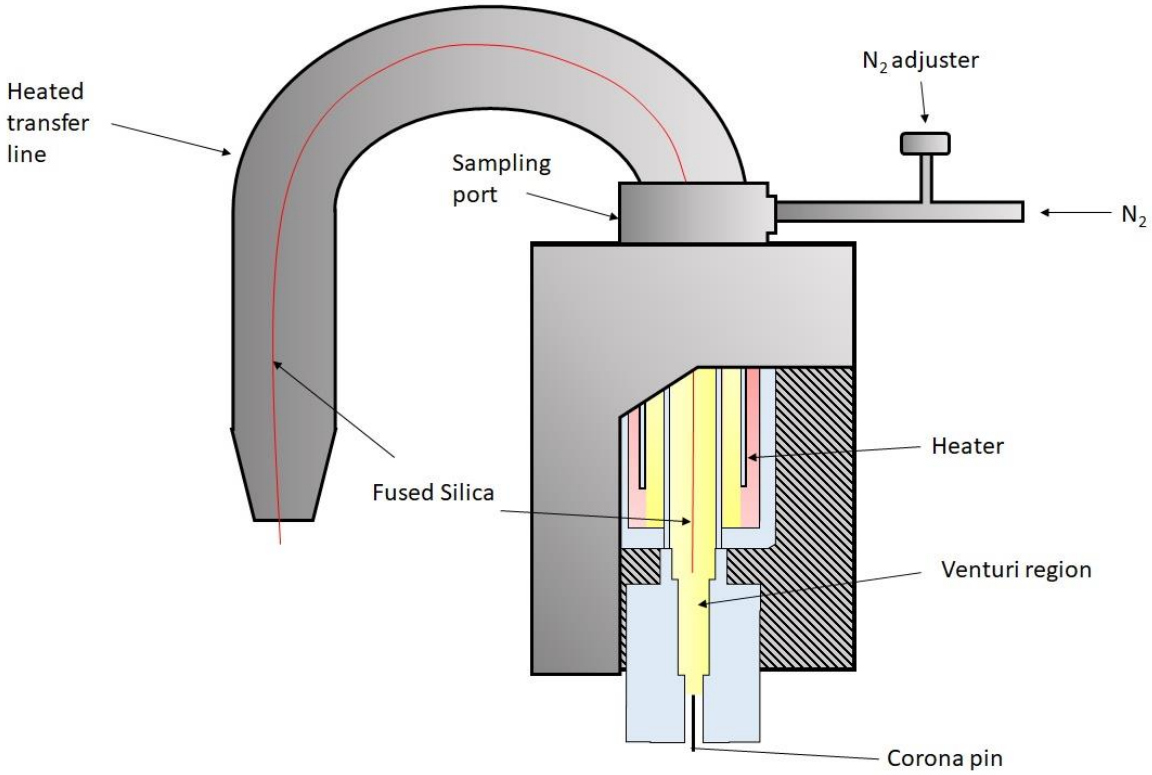

Figure 9 MS Nose schematic.

The general purpose of the MS nose interface is to deliver a gas phase sample at atmospheric pressure to an ionisation source in preparation of mass separation by mass spectrometry. The heated transfer line encasing the silica line facilitates provides thermal energy to facilitate the movement of volatiles through the silica tubing. The rate of a samples movement to the ionisation source is achieved by the generation of a vacuum by the venturi effect. The venturi effect describes the behaviour of a liquid or gas flow through a conduit, such as a pipe, where a region of the conduit is constricted (Jitschen 2014) (figure 10).

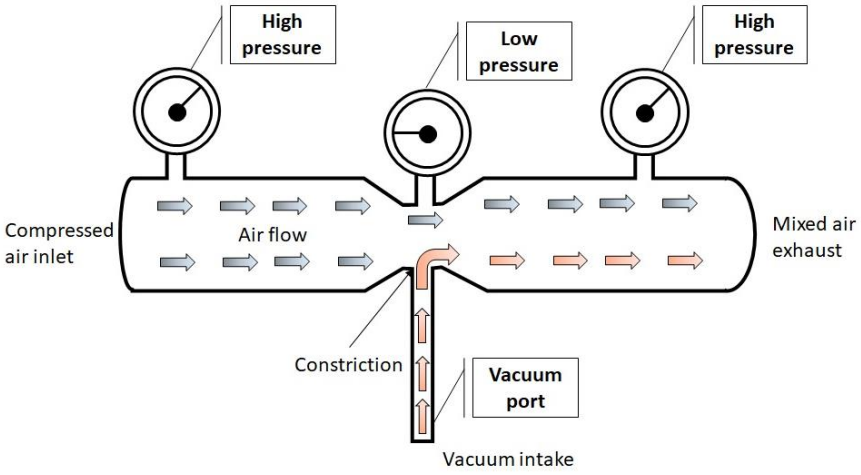

Figure 10 The venturi effect. Constriction a localised constriction of a pipe results in an increase in flow velocity and a decrease in pressure relative to that of unrestricted regions

At the point of constriction, flow velocity increases which results in a drop-in pressure. Mass flow through a duct with no leakages remains constant, flow rate at the duct inlet is the same at the outlet. When a constricted section is present, flow velocity increases with a consequential drop in pressure (Jitschen 2004).

2.2.1 APCI – a soft ionisation technique

APCI is a soft ionisation technique where minimal fragmentation of analyte compounds occurs (Aznar *et al*, 2004). When operating in positive ion mode compounds are ionised by charge transfer reaction, where a proton from a hydronium ion is transferred to the analyte producing an adduct ion with a net positive charge, $M[H]^+$. A high potential voltage (5 – 10 kV) is applied to a corona pin situated at the terminus of the heated region, which produce spontaneous electrical discharges of 1 – 5 μA. When nitrogen is the nebulising and desolvation gas the environment in the ionisation source at 1 atm is that of atmospheric water and nitrogen. Molecular

collisions and charge transfer processes form a plasma region (high energy gas where some electrons dissociate from atoms) is formed around the corona pin (figure 11). The primary ion formed is a type of cluster ions of the general form of $H_3O^+(H_2O)n$ (Brydwell 2001).

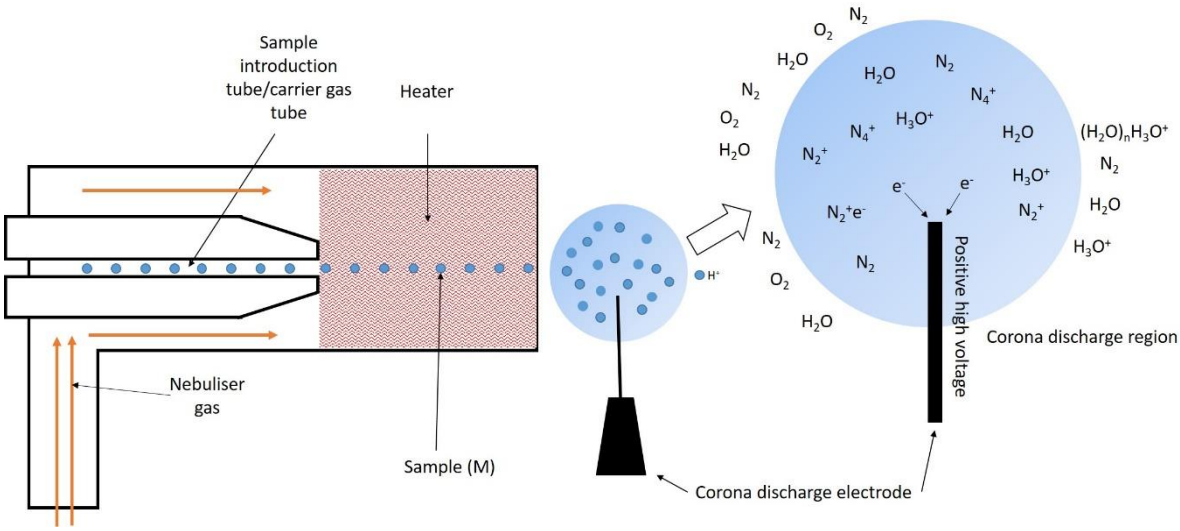

Figure 11 APCI soft ionisation

A complex series of reaction cascades are involved in the formation of the $H_3O^+(H_2O)_n$ cluster ions. The plasma region generated by around the corona pin facilities the loss of electrons from nitrogen (figure 12):

$$N_2 + e \rightarrow N_2 + 2e \qquad (16)$$

Nitrogen cations react with nitrogen forming N_4^+ ions:

$$N_2 + 2N_2 \rightarrow N_4^+ + N_2 \qquad (17)$$

N_4^+ react with atmospheric water:

$$N_4^+ + H_2O \rightarrow 2N_2 + H_2O^+ \quad (18)$$

Followed by successive reactions with water to form hydronium ions and hydroxide ions:

$$H_2O^+ + H_2O \rightarrow H_3O^+ + OH^- \quad (19)$$

Further reactions occur between hydronium ions, atmospheric water and nitrogen:

$$H_3O^+ + H_2O + N_2 \rightarrow H_3O^+(H_2O)_2 + N_2 \quad (20)$$

Reactions continue to form $H_3O^+(H_2O)_n$ clusters:

$$H_3O^+(H_2O)_{n-1} + H_2O + N_2 \rightarrow H_3O^+(H_2O)_{n-1} + N_2 \quad (21)$$

Electron loss from oxygen and nitric oxide also results in formation of $H_3O^+(H_2O)_n$ cluster ions and are succinctly presented in (Carroll *et al* 1975).

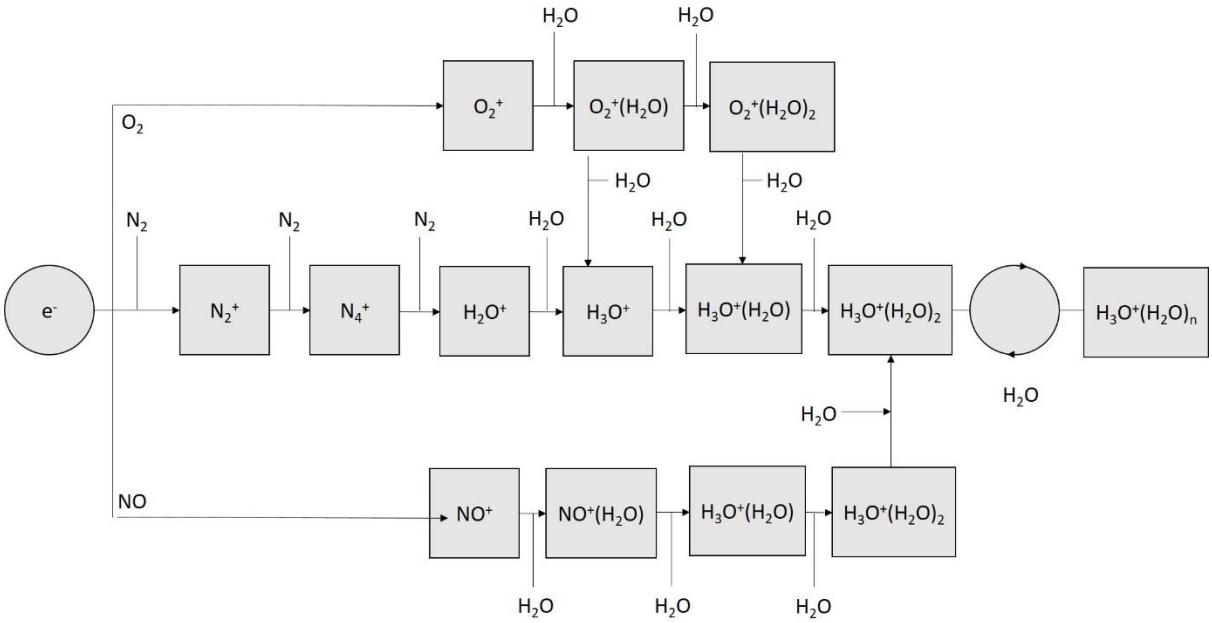

Figure 12 APCI reaction cascade

Collisions of analyte molecules undergo repeated collisions with H_3O^+ and $H_3O^+(H_2O)_{n=}$ ions form the protonated pseudomolecular adduct ions of the general form $M[H]^+$ (Herrera *et al* 2008) (figure 13). Adduct ions are then accelerated towards the mass analyser by action of declustering potential.

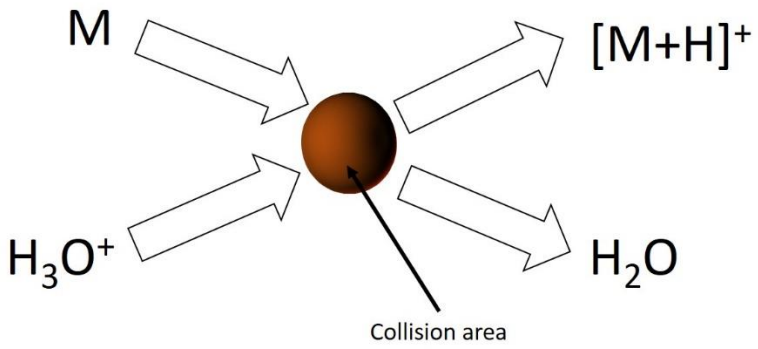

Figure 13 Collision-induced dissociation

When coupled to LC, eluents can also undergo charge transfer reactions in the plasma region, however, these reactions are not a consideration for this study which exclusively uses the MS Nose interface for compound delivery.

2.2.2 Acceleration to mass analyser – declustering potential

Increasing declustering potential by altering cone voltage settings alters energy imparted to the ions facilitating decluttering. Generally increasing the cone voltage increase the energy imparted to ions with an associated increase in ion declustering. Increased declustering potentials can positively impact signal to noise ratios and/or signal intensity by reducing chemical noise from ion clustering (Niessen, 2006). However, exceeding optimal voltages can lead to in source fragmentation resulting in decreased sensitivity of ions interest (Ashraf *et al* 2009).

2.2.3 Tandem mass spectrometry – Mass analyser and CID

Quadrupole mass analyser consists of four cylindrical rods set parallel to one another and is the component of a mass spectrometer responsible for mass analysis/filtering. Quadrupoles are connected to radio frequency and direct-current power supplies. Through application of DC and AC currents, two opposing poles hold identical charge, which is the opposite charge to the other two opposing poles. Ions enter the area between the quadrupole at low velocity (<5eV) in order to interact with oscillating electromagnetic field generated by the charged rods. Two rods set at opposing locations experience a short period of negative charge when the RF voltage exceeds the positive DC voltage favouring passage of relatively high m/z ions. The same is true for the other two opposing ions when the poles experience a short period of positive voltage favouring the passage of low m/z ions. Application of AC and DC currents to all poles generates a band filter where only specific m/z through to the

detector. Altering absolute values of DC and AC current but keeping ratios constant allows for the acquisition of the mass spectra. Because a low velocity entry of ions into mass analyser an ion acceleration step is not required (Somogyi, 2008) (Mellon, 2003) (Reuben *et al* 1996).

Altering the operating mode of APCI-MSMS alters the behaviour of ions through the triple quadrupole. Operating in MS Scan mode stabilises the trajectory of all ions within a specified m/z range through the quadrupoles producing a full mass spectrum of all ions within that range. Single ion recording (SIR) mode feature a single mass filtering step. A m/z is specified, RF, AC and DC settings favour a stable trajectory of that m/z through the quadrupole. The mass filtering quadrupole can be either a single quadrupole or all quadrupoles contribute to mass filtering. Product scan mode fragments a specified precursor ion and generates mass spectrum for all product ions. Precursor ions refers to the initial ion of interest, usually the adduct ion generated in the initial ionisation step. Precursor ions are mass filtered at the first quadrupole. Fragmentation is carried out in the collision cell second quadrupole or hexapole situated at quadrupole 2. The collision cell is pressurised with an inert collision gas such as argon fragmenting the precursor ion, ions passing through to the third quadrupole and then detector are referred to as product ions. Multiple reaction monitoring (MRM) makes use of the precursor-product ion transitions obtained from product scans for a highly selective detection protocol. The first quadrupole is responsible for mass filtering for the precursor ion, the collision cell fragments precursor ions to product ions (figure 14). Finally, the third quadrupole filters for the desired product ion (Keinhus and Geerdink, 2000) (Chang *et al* 2014). For instance, the detection of ethyl butyrate would be

performed by monitoring transitions from ion m/z 117 to 71. Q1 would perform the initial mass filtering for ion m/z 117. Ions that achieve these criteria are fragmented at Q2 and finally Q3 mass filters for ion m/z 71 (Coscollà *et al* 2011. Note, Q2, dependant on the device may be collision cell, quadrupole or hexapole arrangement.

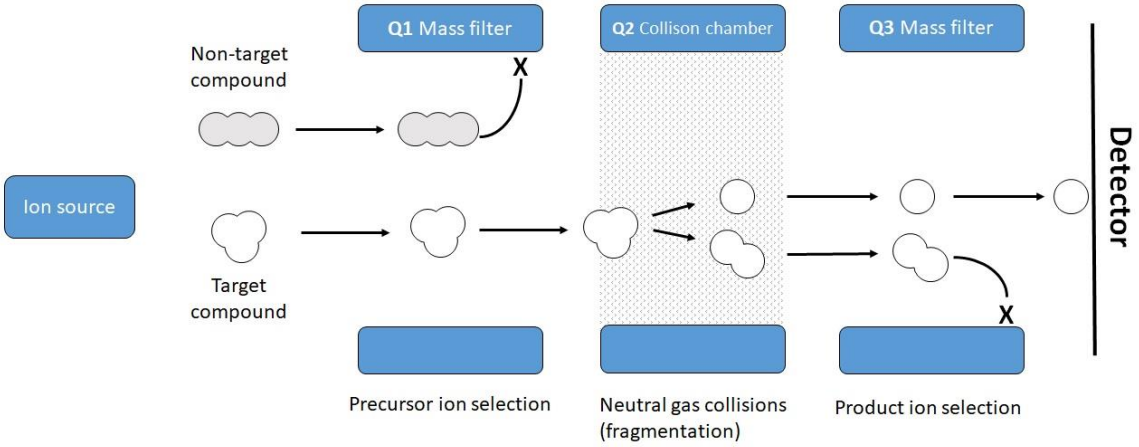

Figure 14 Schematic for a triple quadrupole mass spectrometer. Precursor ions are mass filtered in the first quadrupole (Q1) and fragmented to product ions in the second quadrupole (Q2). Mass filtering of product ions is performed in the third quadrupole (Q3), before proceeding to a detector.

Chapter 3 – Method development of the *in vitro* framework for volatile sorption and desorption at the gas-liquid phase interface

3.1.1 Introduction

In considering the nature of volatile organic compounds interactions with biological surfaces, not only are the physicochemical properties of volatiles and surface constituents of importance but also the surroundings in which they exist. Airflow in the nasal cavity is modified not just by inhalation and exhalation events but also nasal cavity geometry. An assortment of additional parameters require consideration such as inter-individual variability, oro-nasal volume, mucus consistency, incumbent fauna populations and inhalation-exhalation cycles (Ambatipudi *et al* 2009, Mishellany-Dutour *et al* 2012, Frank *et al* 2019).

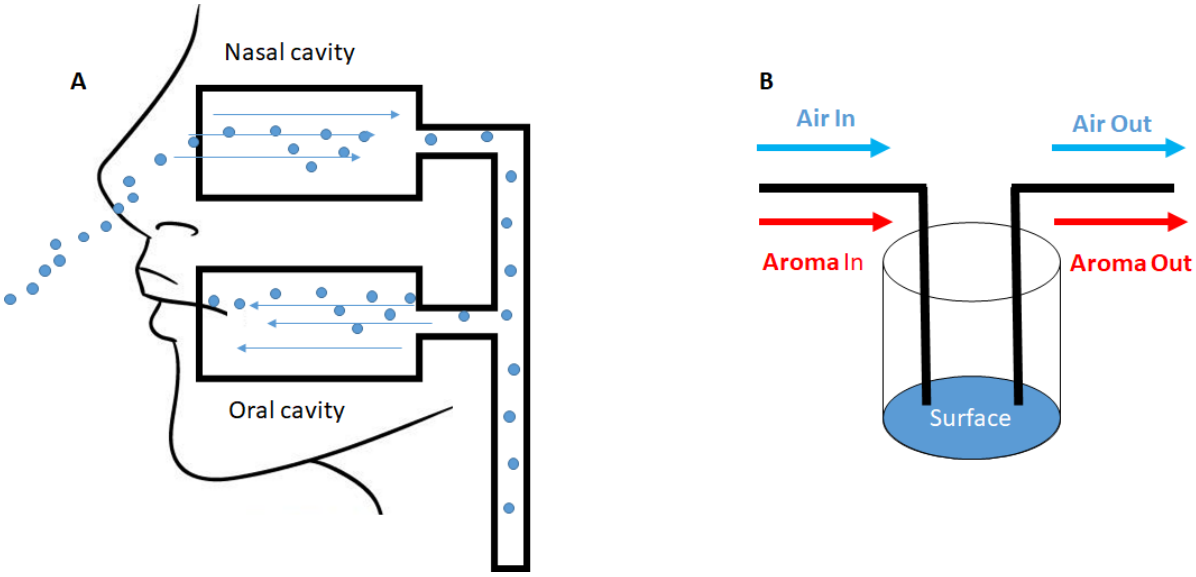

Figure 15 [A] Inhalation of aroma into the nasal cavity and [B] an *in-vitro* system for delivery of aroma to the headspace above a surface.

Developing a mechanistic understanding of volatiles interactions with a biological surface, therefore, requires an analytical framework that can mimic the dynamic nature of an aroma inhalation event in a uniform cavity (figure 15).

The remit for the *in vitro* framework is threefold, firstly, to produce a reaction vessel where the absorption and release of aroma compounds by a defined medium can be assessed in real time. Secondly, to develop a method for the repeatable introduction of defined quantities of aroma to the reaction vessel. Finally, to identify and characterise an appropriate measure describing the absorption and release of aroma by a defined medium.

3.2.1 Prototype *in vitro* system for assessing aroma interactions with the constituents of the oro-nasal mucosa

The analytical framework devised to answer the questions postulated by this study expands upon the previous dynamic headspace APCI-MSMS studies outlined in the work of Marin *et al* (1999) and Tsachaki *et al* (2005) which described the persistence of aroma in the headspace above a solution. Typically, in dynamic headspace studies, a flavoured solution with an equilibrium distribution of aroma between liquid and gas phase (headspace) before a dilution stream is introduced to the system, purging the equilibrium headspace from the vessel. The ability of an aroma to sustain a presence in the headspace is then monitored over the time course of an experiment, typically less than ten minutes in order to reduce bulk solution concentration contributions. Aroma solutions must be sufficiently dilute to minimise aroma-aroma interactions, generally, solution concentrations of less than 50 ppm are sufficient. Dynamic headspace studies can be thought of as an interface stripping procedure.

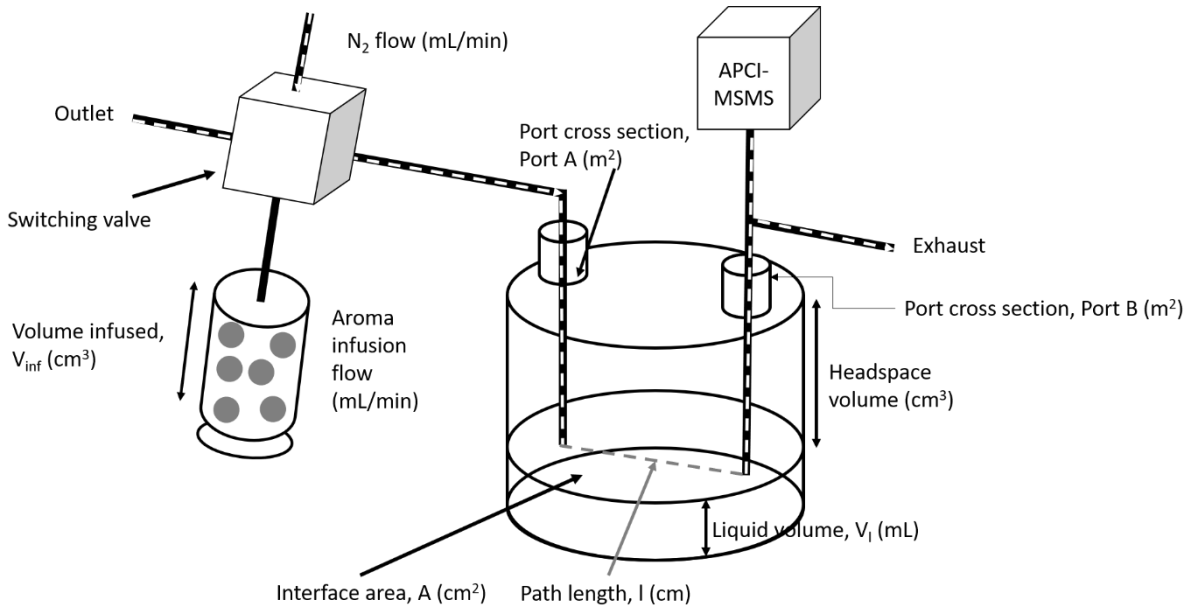

Figure 16 Modified dynamic headspace system with addition of an automated syringe dispenser enable real-time injection of aroma into diluting stream for transportation to the air-liquid interface contained within other reaction vessel.

The presented novel volatile delivery system adds several additional refinements to the dynamic headspace method, namely a humidity source and a method for introducing volatiles to the airflow (figure 16). The proposed system features a reaction vessel or cavity containing an interface of interest, an inlet port, accommodating a dilution stream and an outlet port through which the cavity headspace is flushed.

The addition of humidity to the system is designed to replicate the moist conditions of the nasal and oral cavities. Humidity is introduced in one of two ways. Either, the entire system is housed within an oven set to a desired temperature or the dilution stream is first passed through a heated vessel containing water. When humidity is not a requisite of an investigation then the humidity system is removed.

The reaction vessel is designed to mimic the oral or nasal cavity. The surface area of the air-liquid interface, A (m^2) is an analogue of the saliva/mucus coated mucosal surfaces whilst the headspace volume, V_a (m^3) represents the air compartment of the oro-nasal cavities. Liquid volume V_l (m^3) is the depth of the solution, inhaled aroma laden air is mimicked by the volume of infused aroma, V_{inf} (m^3) and the cross-sectional areas of ports A and B, A_{pA} and A_{pB} (m^2) are the inlet and outlet ports represent entry and exit points such as nostrils or mouth. An additional measurement, which is important for the calculation of mass transfer constants, is given by the length of the 2D path taken by aroma from the sampling infusion port to the sampling port is referred to as l (m).

Breathing cycles of inspired and exhaled air through are mimicked by the application of continually applied dilution stream. Several measures of air-aroma flow velocity are considered in descriptions of the dynamic aroma infusion system (figure 17).

Flow velocity of either the dilution stream or the infused aroma at port A is given by V_A (m/s). Flow velocity is also considered at port B and is termed V_B (m/s). Finally, V_{inf} (m/s) refers to the velocity of aroma infusion when the velocities of the dilution stream and aroma injection velocities are not equal – such situations are clearly highlighted in the text.

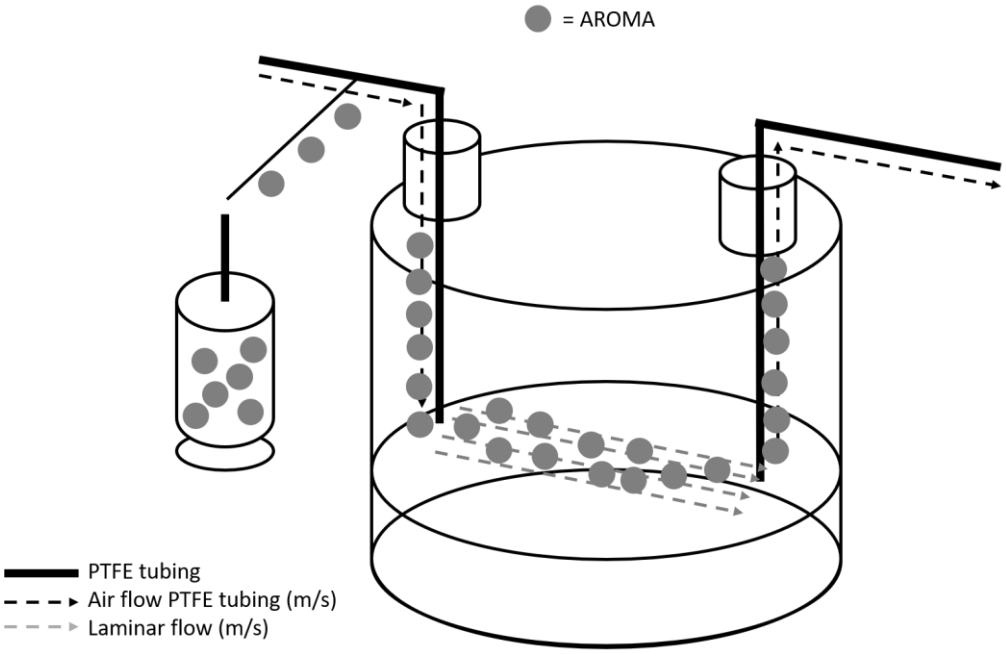

Figure 17 Air/Aroma flow through the reaction vessel

The second addition is the volatile delivery system, which consists of an automated syringe dispenser directly hyphenated to the headspace diluting stream. A switch valve isolates the injection sub-system pre-and-post aroma infusion. The syringe dispenser is then used to inject the headspace contained within the syringe to the dilution stream, which transports the volatiles to the interface housed within the reaction vessel. Aroma not lost to the system is detected by the APCI-MSMS.

3.3.1 Effects of infusion rate, dilution flow volumetric flow rate and interface temperature on aroma persistence

Aroma release from dilute aqueous solutions under dynamic headspace systems are a function of the mass transport properties of aroma and the flow rate (mL/min) of the applied dilution stream (Marin and Taylor 1999). Calculated mass transport coefficients for the release of aroma from flavoured aqueous solutions were governed to the greatest extent by the dimensionless Henry's law constant also referred to as the air water partition coefficient, K_{aw}.

Marin & Taylor concluded that for aroma with $k_{aw} \geq 10^{-3}$, mass transport process governs headspace stability, whereas for aroma with $K_{aw} < 10^{-3}$ headspace stability is governed by the volumetric flow rate or in mass transfer terms, the Reynolds number, N_{re}. Sensory panel focused studies conducted by (Ferreria *et al* 2006), suggested that logarithm transformed K_{aw} values correlate well with the perception of aroma persistence.

Computational fluid dynamic models of restful breathing and sniffing breathing regimes were characterised by laminar and turbulent airflow respectively. The act of sniffing causes an increase in aroma uptake by increasing the resistance to mass transport of aroma from the mucosal phase to the air phase. Turbulent airflow in the oro-nasal cavity occurs at volumetric flow rates of ≥ 300 mL/s and showed no significant uptake of aroma with increases in volumetric flow rate of up to 1L/s (Zhao *et al* 2006).

Parameters identified in the literature that are pertinent to aroma uptake by the mucosal surfaces included volumetric flow rate and the physicochemical parameters of the aroma. In the dynamic headspace systems of Marin and Taylor (1999), behaviour of aroma is governed by the same parameters. The additional refinements the proposed system makes to the existing dynamic headspace systems are designed to mimic a situation closer to that experienced by the oro-nasal cavities. In the dynamic system aroma concentrations are effectively infinite over the time course of the experiment whilst aroma concentrations the new system (henceforth to be referred to as the infusion system) is finite, a similar situation to the oronasal mucosa when inhaling aroma laden air. Aroma concentrations in the dynamic system are, at t=0, in equilibrium whilst no aroma is present at t=0.

Whilst the previously discussed influence of volumetric flow on aroma headspace persistence is present in the literature, the refinements made by the infusion system to the dynamic systems requires an investigation into the effects on aroma absorbed and aroma released when a quantity of aroma is introduced to the headspace of an air-water interface. Factors hypothesised to affect the behaviour of aroma in the infusion system included the aroma infusion rate (mL/min), volumetric flow rate of the dilution stream (mL/min) and the air-water partition coefficient. The air-water partition coefficient is a temperature dependant parameter (equation 21) (Gorenyi *et al* 2002).

$$K_H = p_i x_{i,w} V_m RT \qquad (22a)$$

$$p_i = \gamma_{i,w} x_i, w P_i \qquad (22b)$$

Equation 22a describes Henry's law constant (K_H) for ideal solutions, where p_i is the saturated vapour pressure (atm) of compound i, $x_{i,w}$ is the molar fraction of i, V_m is the molar volume of water, R is the universal gas constant (atm $mol^{-1}K^{-1}$) and T is temperature (K). For non-ideal solutions, p_i is given by equation 22b, where $\gamma_{i,w}$ is the activity coefficient (K) of compound i, and P_i is the saturated vapour of the pure compound.

Temperature dependence of the air-water partition coefficient is considered by factoring in changes in operating temperatures on the observed absorption of aroma during the infusion process and the post infusion persistence of the aroma.

3.4.1 Method and Materials

Ethyl butyrate (≥ 99%) and 2-heptanone (≥ 98%, FCC, FG)) were obtained from Sigma Aldritch (Gillingham, U.K). Solution preparation entailed dilution of compounds with deionised water to concentrations sufficiently low so as to minimise the probability of volatile-volatile interactions and ionisation suppression. Diluted concentrations totalled 1ppm for ethyl butyrate and 5ppm 2-heptanone.

A volatile solution is left to equilibrate in a syringe, with several mL of headspace. A PTFE cylindrical container modified with gas tight inlet and outlet ports was repurposed as a reaction vessel. Outlet port B joined with the MS NOSE attachment of a prototype TDQ APCI-MSMS (Waters, Elstree, U.K.). Through port A, a continuous flow of $N_{2(g)}$ at a rate of 16, 32 and 50ml/min was passed through the reaction vessel. Headspace volume was 16ml.

Contained within a 100ml Luer lock gas tight syringe was a 2ml quantity of equilibrated dilute aroma solution. An automated syringe dispenser injected a defined amount of the headspace above the equilibrated aroma solutions contained within each syringe. Automated syringe was arranged so that no solution was injected into the diluting stream.

APCI-MSMS running in multiple reaction-monitoring mode, monitored specific precursor–product ion transitions indicative of each aroma. Cone voltages (V) and Collison energies (eV) were optimised for each compound using an iterative approach to ascertain best signal quality. Corona pin potential of 4kV and ion dwell times of 0.05s were used throughout.

Aroma acquisition lasted until signal decayed to 5% of a maximum peak value or for 400s. Interfaces were heated by a hotplate under

the reaction vessel. Three independent infusions of 2-heptanone and ethyl butyrate were performed for three interface temperatures 20, 30 and 40°C and three different dilution rates 50, 32 and 16 ml/min.

APCI-MSMS settings were as follows: sampling rate 5 ml/min, positive ion mode, 24V cone voltage, MRM (multiple reaction monitoring) operating mode monitoring the molecular transition 115 > 55 m/z every 0.05 s

3.4.2 Data handling - Characterising aroma persistence under a diluting stream post infusion

The change in headspace aroma concentration over time post infusion produces a non-linear curve characterised by equation 23:

$$Y = (Y_0 - \text{plateau})\exp^{(-kx)} + \text{plateau} \quad (23)$$

Where Y_o is the concentration of Imax – the point of aroma infusion termination, plateau refers to the value at which concentration ceases to change – in this case plateaus are constrained to 0, negative aroma concentration in the headspace is not possible. Concentration is generally quoted relative to the Imax as a fraction or percentage. –k is the rate of aroma concentration change (s^{-1}) and x is time (s).

Values for k are automatically generated by Prism 7 Graphpad (Graphpad software, USA) curve fitting software.

3.4.3 Preliminary results and discussion – Repeatability of the method

If aroma concentration, infusion rate and quantity of aroma infused is kept constant between repeats, then the system is highly

reputable. 5ppm of 2-heptanone injected at a rate 32ml/min into the headspace volume of 16ml above a water interface of 8.6 cm^2 was assessed for post infusion release kinetics and quantity of aroma absorbed (%). produced very similar results. Three independent repeats consisting of three separate volatile solutions and three separate water interfaces were performed. Mean rate of aroma concentration change in the headspace post infusion over a 250 (s) time course was 0.0014 ± 7.41e-5 mg/m^3 s^{-1}± and mean aroma absorption of 88 ± 1.2%.

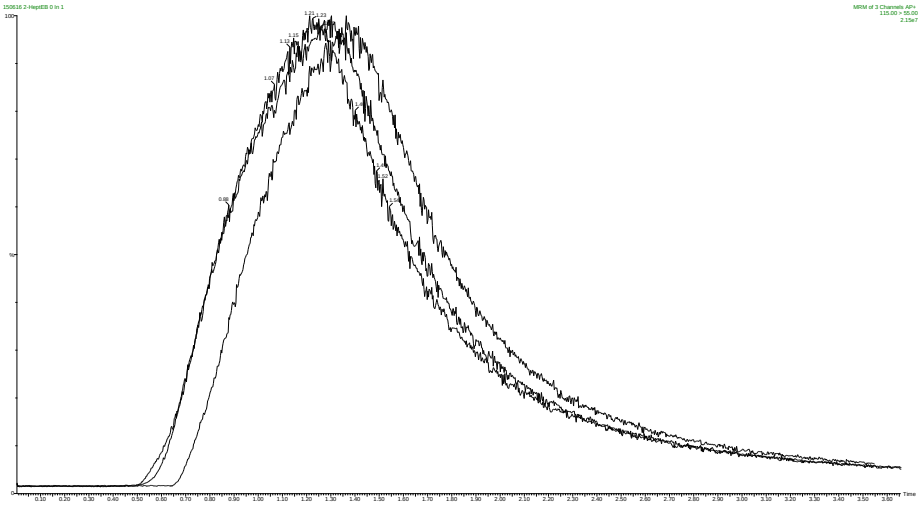

Figure 18 Overlay of 3 repeats of 300ppm 2-heptanone passed over a water interface at 0.83 mL/S

Three independent repeats consisting of three separate volatile solutions and three separate water interfaces were performed (figure 18). Peak shape, height and background levels are consistent between independent repeats.

The system allowed for highly reproducible results. The headspace above a 5ppm solution of 2-heptanone was introduced to a water interface using the described system. Area of the air-water interface was 8.55 cm^2 with a headspace of volume of 13cm^3, syringe injection

rate was set to 0.25 mL/s with a diluting flow of 0.83 mL/s. APCI-MSMS settings were as follows: sampling rate 0.5 mL/s, positive ion mode, 24V cone voltage, MRM (multiple reaction monitoring) operating mode monitoring the molecular transition 115 > 55 m/z every 0.05 s.

3.4.4 Behaviour of aroma in system A

At t = 0s, no aroma is present in the system. Assuming infusion begins between t = > 0 < 1s then for approximately 10s no aroma is detected. Post t = 10s aroma detection of aroma begins. Detected aroma levels in the headspace increases as infusion proceeds. At a designated time aroma infusion is terminated, for approximately 3s, detected aroma levels continues to increase before entering into a period of continual decrease in aroma detected in the headspace. Decrease in headspace aroma levels continues until the signal returns to the base level or the experiment is halted once a defined time is reached.

Figure 19 shows an infusion of 2-heptanone into the headspace above a solution of water. Period A, t = 0 to 30s, is the infusion period. Period B represents Imax approximately 3s after infusion ends. Period C, t = ~30 to >150s decay period where no new aroma is added to the system.

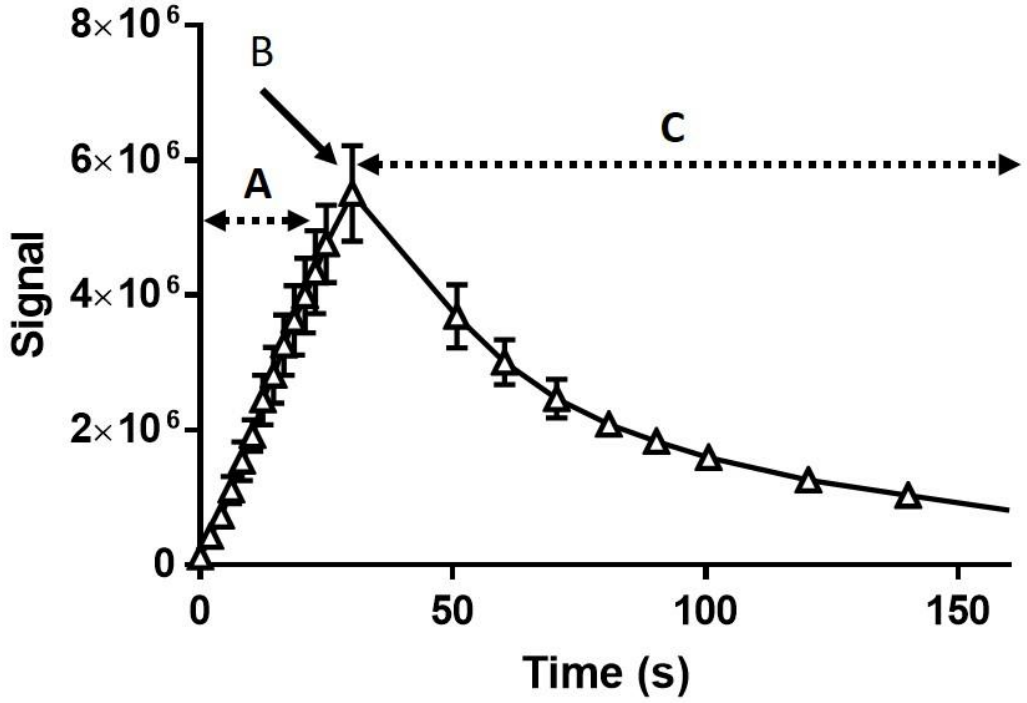

Figure 19 Peak generated by infusing a quantity of 2-heptanone into the headspace above a water solution. Data points are the mean of three independent repeats with standard deviations expressed by error bars.

Period C is analogous to traditional dynamic headspace studies but does differ in several key regards:

- Concentration cannot be assumed to be infinite
- Equilibrium is not established before headspace dilution begins i.e. at t = 0, $C_A \neq K_{aw}$

Change in headspace concentration with time represented by peak C, however, does display some with dynamic headspace studies – both represent the ability of an aroma to persevere in the headspace under dynamic conditions but under different circumstances.

3.4.5 Monitoring flow pre-and-post vessel

Pre-experimental assessment of air flow before the vessel and after existing the vessel was recorded with a volumetric flowmeter. Airflow at the exit port of the vessel was approximately 50% less

than flow at the entry port of the vessel. At the point of entry, the radius of the internal diameter of the PTFE tubing delivering airflow to the vessel is 0.0025m. The radius of the vessel is 0.02m. Expansion of the internal flow area in fluid dynamics results in a decrease in flow velocity and an increase in pressure.

3.5.1 Results and discussion

3.5.2 Aroma levels in the headspace above varied temperature water solutions under different dilution rates

50, 32 and 16 ml of 2-heptanone and ethyl butyrate infused into the headspace at a volumetric flow rate of 50, 32, 16 mL/min above a water solution heated to 20, 30 and 40°C produced a series of peaks describing the effects of dilution flow on the quantity and stability of an aroma in the headspace (figure 20).

Two-way ANOVA with Tukey multiple comparison test (Prism 7 graphpad), calculated the statistical significance ($P < 0.05$) in Imax values of ethyl butyrate and 2-heptanone at different interface temperatures and headspace dilution flows. Interaction between the effects of changing temperature and changing flow rate were significant for both compounds.

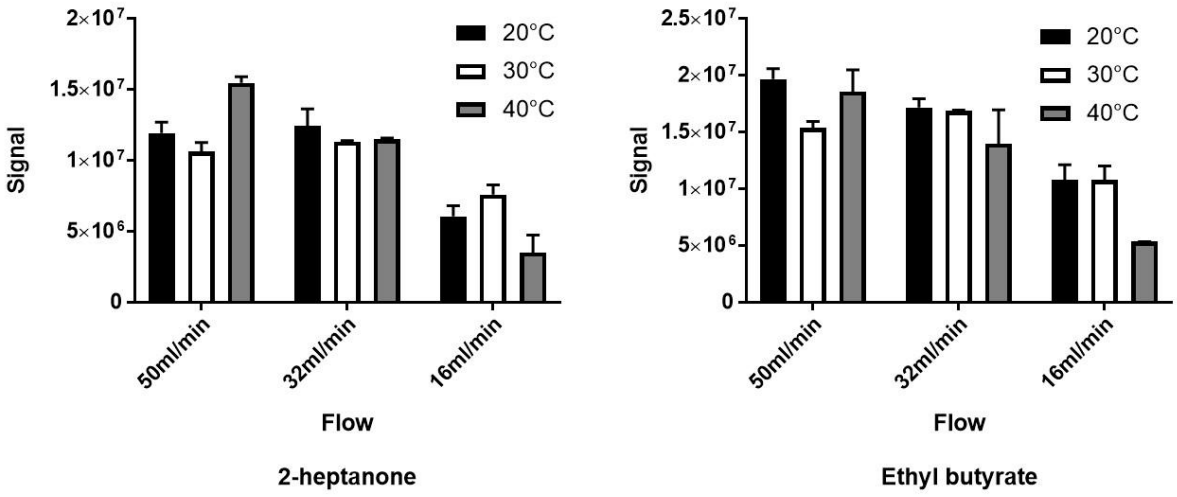

Figure 20 Maximum levels (Imax) of 2-heptanone (left) and ethyl butyrate (right) post infusion. Data presented is the mean of three independent repeats, error bars describe standard deviation between repeats.

3.5.3 Rates of aroma decay post infusion

Decay rates in this study refer to the period taking place from Imax to experiment end. Decay curves are normalised so that Imax achieved for each repeat is set to 1 and all other values expressed relative to 1. Decay rate is characterised by calculation of the rate constant k (s^{-1}) by non-linear regression one-phase decay models featured in Prism 7 (figure 21).

Two-way ANOVA with Tukey multiple comparison test (Prism 7 Graphpad), calculated the statistical significance ($P < 0.05$) in k values of ethyl butyrate and 2-heptanone at different interface temperatures and headspace dilution flows. Model factors consisted of dilution rate (ml/min), temperature (°C) and an interaction term between dilution rate and temperature. Interaction between the effects of changing temperature and changing flow rate were significant for both compounds.

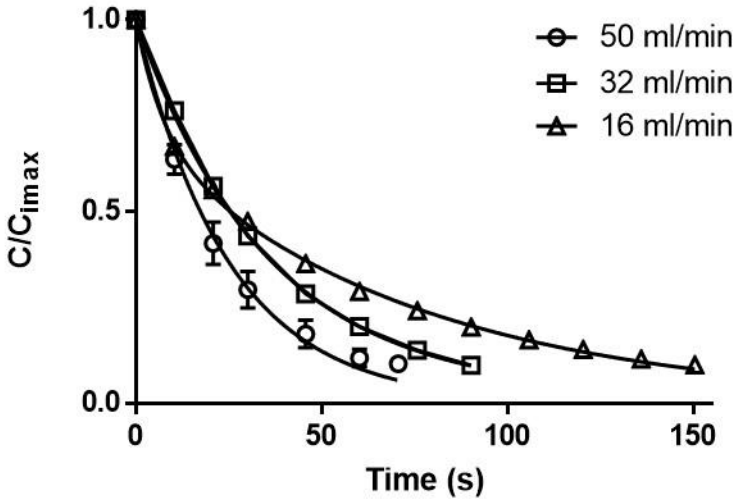

Figure 21 Change in ethyl butyrate levels in a headspace above a water solution subjected to diluting streams of 16, 32 and 50ml/min. At 50 ml ethyl butyrate loss in the headspace is characterised by one-phase decay whilst at 16 and 32ml/min, two-phase decay more accurately describes loss of aroma headspace. Data presented is the mean of three independent repeats, error bars describe standard deviation between repeats.

3.6.1 Conclusions

Results indicate that volumetric flow rate of the dilution stream, temperature of the interface and identity of an aroma are significant factors governing the partition behaviour under aroma headspace infusion. Partitioning of volatile compounds in equilibrium conditions is given by the air-water partition coefficient, K_{aw}, which is a temperature dependant factor. Whilst developing headspace dilution techniques for APCI, Marin and Taylor (1999) showed that release is a function Reynold's number and mass transfer process, for which K_{aw} was an important parameter in the calculation of mass transfer coefficients. The above described system behaves in line with the described dynamic headspace dilution system.

Chapter 4 - Improving detection sensitivity of APCI-MSMS through calibration and a dual mass spectrometer approach

4.1.1 Introduction

An attractive proposition of Atmospheric pressure chemical ionisation mass spectrometry (APCI-MSMS) is the ability to conduct rapid, non-destructive, direct, real-time assessment of gas phase samples (Davis *et al* 2011). APCI-MSMS is important tool in the fields off aroma chemistry and food science. Studies range from the quantitative assessment of volatile methylsiloxane release from landfill biogases (Badjagbo *et al* 2009), assessment of cheddar cheese maturation based on APCI detection of volatile biomarkers (Gan *et al* 2016) and breath-by-breath persistence of volatile compounds after consumption of aqueous solutions (Linforth and Taylor, 2000).

Optimisation of volatile detection by increasing the signal generated through modulation of cone voltages (also known as declustering potential) are documented in the literature (Avison, 2013). Increasing declustering potential by altering cone voltage settings alters energy imparted to the ions, facilitating decluttering. Generally increasing the cone voltage increase the energy imparted to ions with an associated increase in ion declustering. Increased declustering potentials can positively impact signal to noise ratios and or signal intensity by reducing chemical noise from ion clustering (Niessen, 2006).

Tandem mass spectrometry features a dual mass spectrometer with a collision induced dissociation (CID) chamber separating each mass spectrometer and has seen deployment in a variety of fields such as proteomics (Nesvizhskii *et al* 2003), steroid hormone analysis (Soldin and Soldin 2009) and genomics (Alghatani *et al* 2015). Dual mass spectrometer analysis allows for structural identification of molecular ions by mass filtering for specific precursor ion to product ion transitions unique to a molecule. In quadrupole mass spectrometers, a pre-defined precursor ions trajectory is stabilised through manipulation of applied RF (radio frequency) and magnetic field to the quadrupoles of the initial mass analyser. The trajectory of undesired ions collide with the quadruple and do not proceed to the detection phase. Selected ions proceed to a CID chamber for fragmentation to product ions, which in turn receive safe passage through the second mass analyser to the detector (Chong *et al* 2018). The premise of this chapter is the application of dual mass filtering techniques to increase the accuracy and detection sensitivity of APCI-MSMS detection of volatiles.

4.2.1 Method and materials

A static headspace sampling protocol was used to measure the signal intensity of the volatiles of interest. 100ml Schott bottles (Fisher Scientific, Loughborough, UK) were modified to include a sealable sampling port approximately equal to the diameter of the APCI-MSMS sampling line. Aqueous solutions of volatile compounds of interest were equilibrated for a minimum of 3h at 25°C in 100ml modified Schott bottles before introduction to APCI-MSMS (Waters TQD prototype, Manchester, UK). Each aroma was diluted to prevent overwhelming the ionisation source and to minimise volatile-volatile interactions. Headspace was sampled at a rate of

10ml/min for approximately 1 min through the transfer line housing a silica gas chromatography column (Phenomenex, Macclesfield, UK). Silica dimensions were a film thickness of 0.25μm and an internal diameter of 0.25mm. Uniform operating conditions for corona pin voltage (4 kV, positive ion mode), ion dwell time (0.1s) and transfer line temperature (120ºC) were used throughout.

An initial full mass scan ranging from 0-200 m/z was performed to identify volatile adduct ions in preparation for SIR. Signal intensity was initially assessed for all volatiles with the cone voltage parameter set to 20V with the APCI-MSMS operating in SIR mode. Volatiles were then sampled at cone voltages ranging from 10 to 50V in 5V increments generating an approximate optimal cone voltage. Optimisation of operating cone voltages was finalised by assessing signal intensity at 1V increments at a 5-10V range around the highest signal intensity identified in the previous step.

Optimisation of MRM operating parameters required the identification of appropriate precursor ion to product ion transitions and the optimal collision energy facilitating this transition. Product ions were subjected to collision energies of 5-30 eV in 5 eV increments. Argon was the neutral collision gas used throughout. A series of mass spectra of product ions was generated for each eV increment. Precursor-product ion transitions were selected based on the uniqueness of ion identity and signal strength. Transition information along with optimal collision energy were used to create MRM optimisation files.

Solutions of 2-pentanone (≥98%, FCC, FG), isoamyl acetate (≥95%, FCC, FG), 2,5-dimethyl pyrazine (98%), methyl butyrate (99%), 2-octanone (≥95%, FCC, FG), anisole (99%), Ethyl butyrate (99%), ethyl acetate (99%) and butyl formate (97%) obtained from Sigma

Aldritch (Aldershot, UK). Concentrations used to generate sample headspace are shown in table 4.

Ethical considerations when involving panellists were considered. All experiments involving panellists remained in the constraints of the precedents set in similar APCI-MSMS breath-by-breath measurement outlined in the literature (Heng Hui *et al* 2014, Linforth 2000, Rabe *et al* 2003, Rabe *et al* 2004, Heng Hui *et al* 2014, Sánchez-López *et al 2016)*

4.2.2 Gas phase *in vivo* aroma persistence

50 mL of volatilised aroma was directly injected into the panellist nasal cavity with a Luer lock syringe during inhalation. Panellists maintained normal breathing through their nostrils directly into a MS Nose interface of the APCI-MSMS during the injection period. Breath-by-breath intensity of select aromas were monitored after aroma injection by with a sampling rate pf 30 ml/min. A timed breathing protocol was applied through out to facilitate the ease of representing independent repeats at defined time points.

Volatilised aroma samples for inhalation were prepared by dilution of aroma compounds in deionised water, 150 ppm for 2,5-dimethyl pyrazine and 50ppm for anisole. 50 ml of dilute aroma samples contained within a modified 123ml Schott glass that allowed for extraction of a quantity of headspace by a Luer lock gas tight syringe. Samples were equilibrated at 70˚C for 3 h in 120ml Schott bottles modified with an access port.

4.3.1 Results and discussion

4.3.2 Static headspace analysis of equilibrium headspace

By sampling the headspace concentrations of 1 ppm solution of ethyl butyrate at cone voltages of 20 and 40V, the effects of cone voltage induced fragmentation of volatiles can be observed (Figure 22).

When operating in MS Scan mode, all detected ions in the ranges of 0 to 200 m/z are reported. The MS Scan at cone voltages of 20V shows the ethyl butyrate adduct ion 117m/z (116 + $[H]^+$), is the most abundant ion. An additional ion, 89 m/z, is also observable with approximately 20% the signal intensity of the ethyl butyrate adduct ion. Increasing the cone voltage from to 20 to 40V alters the observable ions detected by MS Scan. The ethyl butyrate adduct ion (117 m/z) signal intensity reduces and the signal intensity of ion 89 m/z. The formation of 89 m/z from 117 m/z corresponds to the loss of 28 Da, corresponding to 2 carbon atoms and associated hydrogen atoms.

Assessing gains in signal intensity by optimisation of the cone voltage was performed by comparison of a signal at a voltage of 20V to the optimal volatile cone voltage (Table 4).

Cone voltage optimisation strategies entailed sampling the headspace above dilute volatile solutions from 10 to 50V in 5V increments. A second round of sampling in increments of 1V was performed in a 5 to 10V range around the cone voltage generating the greatest signal intensity in the preliminary stage.

At a cone voltage of 20V signal intensity of 2-octanone was 53% of the optimal cone voltage of 30V (Table 4, figure 23). At 20V the signal intensity of 2,5-DMP was 75% of the optimal cone voltage of 48V. At 20V signal intensity of methyl butyrate was 34% of the optimal cone voltage of 29V. At 20V signal intensity of anisole was approximately 86% of the signal intensity at the optimised cone voltage of 32V.

One-way ANOVA performed in Graphpad Prism 7 (Graphpad software, California, USA) calculated the differences between signals

generated under optimal conditions versus non-optimal conditions as statistically significant, with P values < 0.05.

Table 4: Volatile precursor and product ion information and the optimal cone voltage and collision energy values.

Compound	Cone voltage (V)	Precursor ion (m/z)	Collision energy (eV)	Product ion (m/z)	Solution concentration (ppm)
2-Pentanone	20	87	15	45	20
Isoamyl acetate	15	131	10	70	1
2,5-Dimethyl pyrazine	48	109	20	82	50
2-Octanone	29	129	15	44	1
Methyl butyrate	29	102	10	71	5
Anisole	32	109	20	94	2
Ethyl butyrate	25	117	10	89	1
Ethyl acetate	20	89	20	61	1
Butyl formate	10	103	10	57	20

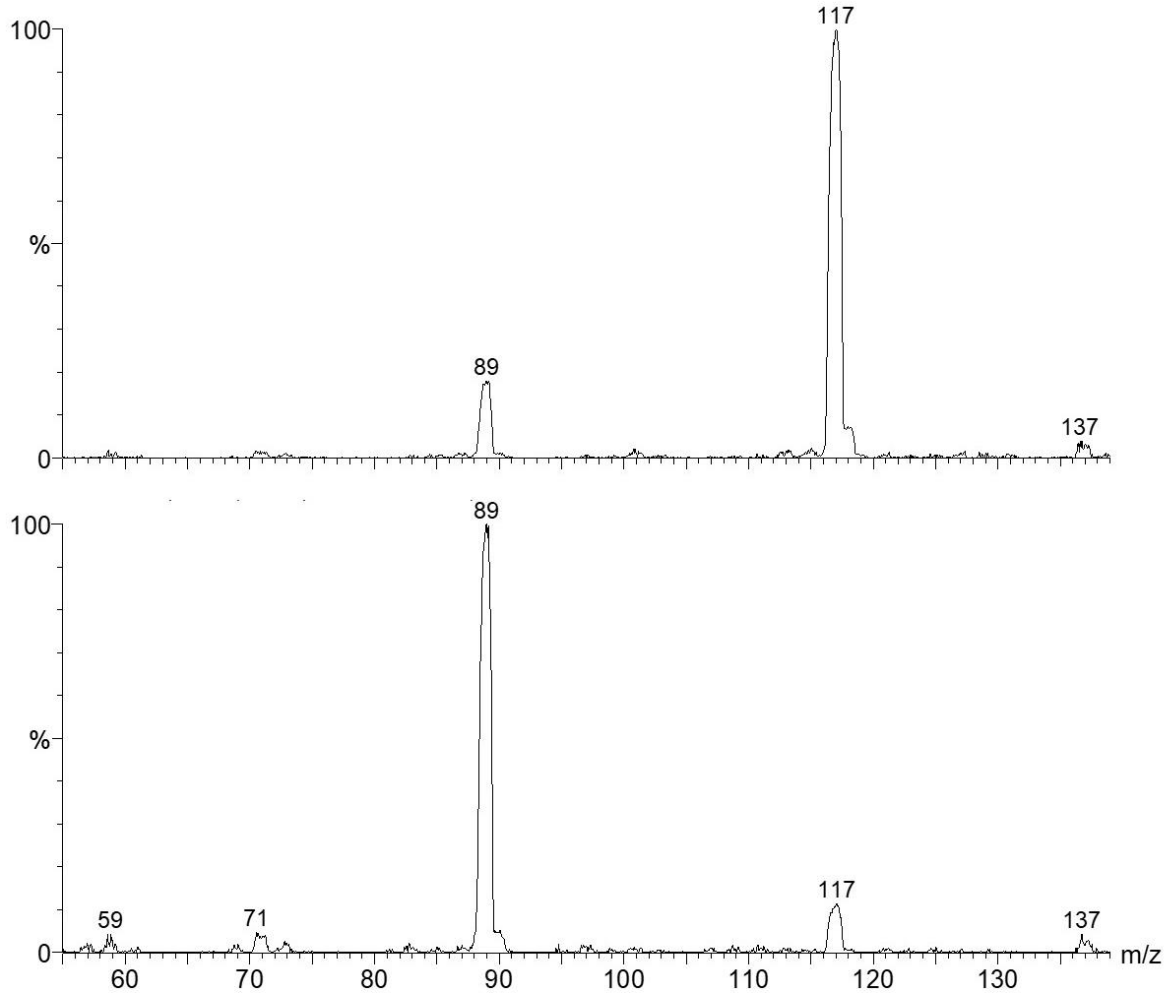

Figure 22 (Top) MS Scan spectra of ethyl butyrate with cone voltage set to 20V and (bottom) MS Scan of spectra of ethyl butyrate with cone voltage set to 40V. Optimisation of APCI-MSMS cone voltage for increased signal generation. Ion 137 results from cluster complexes formed of ethyl butyrate ions and hydronium ions (m/z = 19)

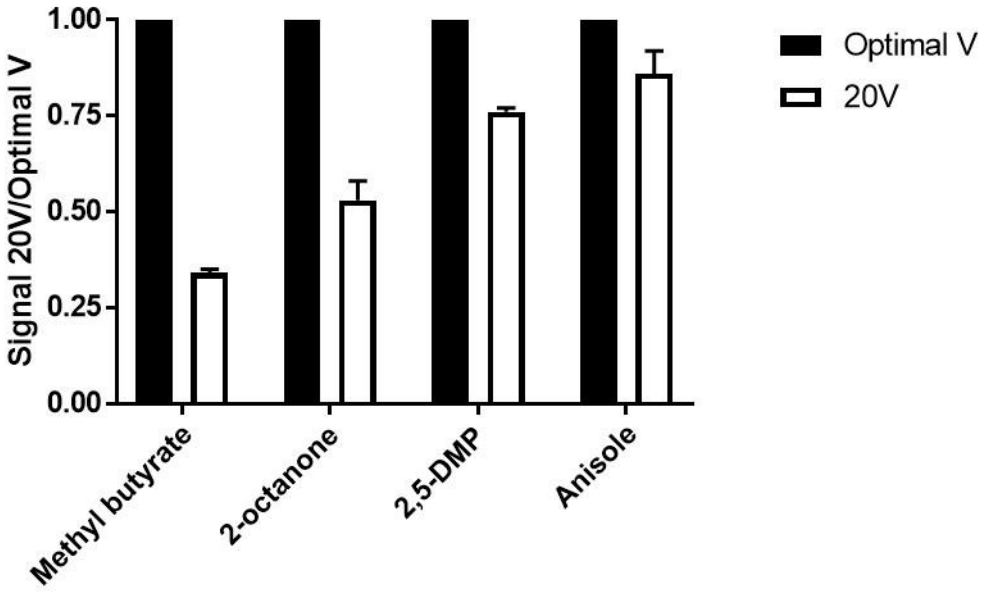

Figure 23 Signal intensity generated by sampling the headspace above solutions of methyl butyrate, 2-octanone, 2,5-DMP and anisole. Each presented value is an average of three independent replicates. Error bars express standard deviation between three independent repeats. Signal intensities normalised to optimal cone voltage

The amount of energy required to fragment a molecule is generally, a function of molecular weight and structure such as resonance stabilisation of aromatic rings (Naylor 1989, de Marque *et al* 2016). Lower molecular weight species require less energy to induce fragmentation. However, structural components can impart additional stability as well a decrease stability. Resonance stabilised structures such as aromatic rings will require greater energy to induce fragmentation than a non-resonance stabilised structure of a similar molecular weight. From table 1, anisole and 2,5-DMP both with ring structures, are able to withstand higher energy inputs in the form of cone voltage with nominal fragmentation, hence the greater cone voltage optima. Electric dipole constants describe the distribution of electrons within the two compounds.

4.3.3 Optimising multiple reaction monitoring processes

SIR makes use of a single filtering step at quadrupole 1 by stabilising the pathway of specified m/z. Volatiles that are of the m/z set to be detected by SIR pass unhindered by quadrupoles whereas volatiles with other m/z ratios are attracted to the quadruples and are eliminated in the collision. MRM mode makes use of two filtering steps after ionisation. The first quadrupole is set to detect ions of a particular m/z, this is the known as precursor ion. These ions then graduate to the second quadrupole (Q2) for collision-induced dissociation (CID). The third quadrupole is set to detect the ions from Q2 – known as the product ion (also referred to as a daughter ions). Ions that meet criteria of dictated at the third quadrupole pass through to the detector generating signal, the abundance of the product ion.

Additional optimisation steps are required for the use of MRM for detection of specific volatiles namely the assessment of the electron voltage (eV) applied to the CID chamber and identification of an appropriate product ion that is present in sufficient abundance post fragmentation. When considering a potential product ion candidate, complete fragmentation of the precursor ion has to be balanced with the need to produce a product ion that is sufficiently abundant. Product selection is achieved by operating the APCI-MSMS in product scan mode. Collision energy is varied in 5 eV increments over a range of 5 to 40 eV followed by comparison of the ion spectra at different eV allows the selection of the optimum transition.

Figure 24 shows a representation of spectra generated by a product scan of isoamyl acetate and 2,5-DMP at collision cell energies of 10, 15 and 20 eV. The adduct ion of isoamyl acetate precursor (131 m/z) is present in an approximate equal low abundance at 10, 15 and 20 eV. The presence of the precursor ion indicates an

incomplete fragmentation, however, relative to the generation of product ions, the presence of the product ion in the spectra is negligible at approximately 1%. Ion m/z 71 is present in a greater abundance at a collision energy of 10 eV relative to 15 or 20 eV. Increasing collision energy increases the fragmentation of isoamyl acetate precursor ions but decrease overall signal. It would, therefore, be practical to use a low collision energy when using MRM procedures for detecting isoamyl acetate by monitoring transitions from m/z 131 to m/z 71.

The adduct ion of 2,5-DMP is more resistant to CID than that of isoamyl acetate. Collision energies of 20eV are required to fragment the precursor ions of 2,5-DMP, however, the generation of product ions remains similar for ions 67 and 82 m/z. Selection of an appropriate precursor ion and collision energy level is less clear in these circumstances. The transition from m/z 109, to m/z 91 at a collision energy of 20 eV was arbitrarily selected.

4.3.4 Multiple reaction monitoring enhancement of limits of detection compared to single ion recording.

Signal to noise ratios provide a measure of sensitivity of an analysis and is determined by the ratio between the maximum signal level and the depth of the background noise (the signal present before headspace sampling). Ratios above 1:1 indicate more signal than noise, increased values of which are desirable. Increasing s/n ratios has the benefits of increasing the likelihood of detecting low abundance species extending the concentration range detectable.

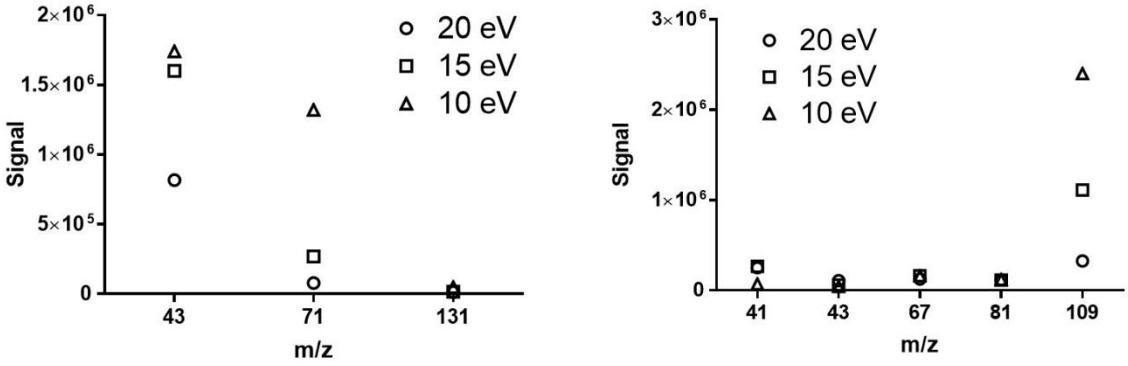

Figure 24 Ions generated by CID of isoamyl acetate (right) and 2,5-DMP (left) at 10, 15 and 20 eV.

Assessing the potential of MRM detection to increase the s/n relative to SIR detection was carried out by comparison of s/n ratios of SIR and MRM operating modes for 9 volatiles (figure 25). Compounds tested included, 2-pentanone, isoamyl acetate, 2,5-DMP, 2-octanone, anisole, ethyl butyrate, ethyl acetate, butyl formate and methyl butyrate. Molecular precursor-product ions, cone voltage and collision energy settings were optimised as detailed in table 1. All other operating parameters were as described in the method

In all instances MRM produced a greater s/n when compared to SIR (figure 25). Increases in s/n ranged from 1.5 to 25 times greater for MRM over SIR. Isoamyl acetate saw the greatest gain in detection sensitivity anisole saw the least.

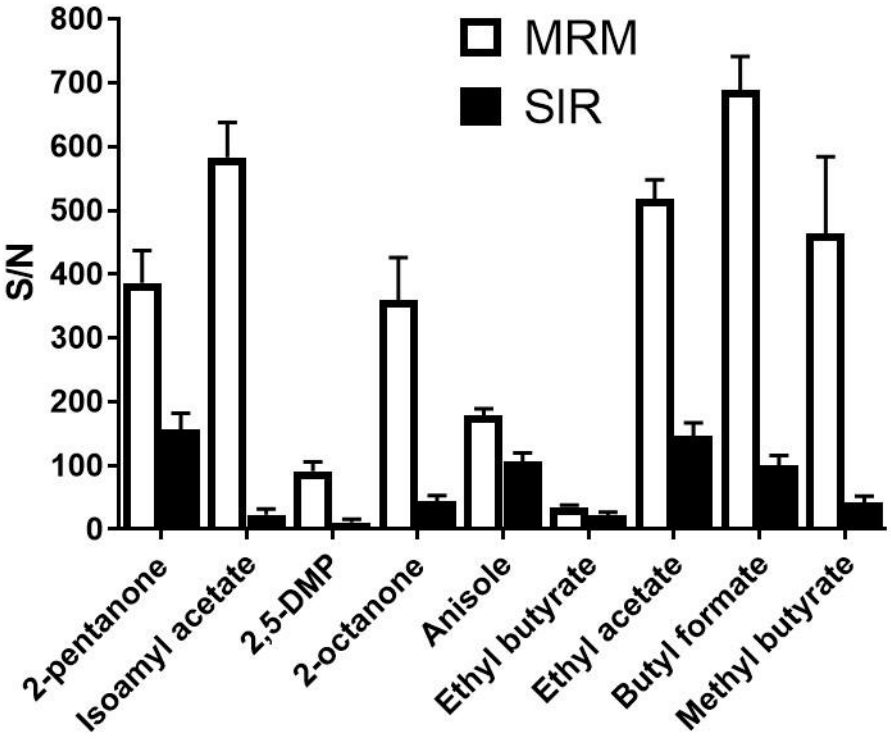

Figure 25 Comparison of signal to noise (s/n) ratios for several volatile compounds when detected in SIR and MRM operating modes. Each presented value is an average of three independent replicates. Error bars are the standard deviation.

Optimised MRM enhancing sensitivity of Liquid Chromatography-MSMS (LC-MSMS) procedures has been reported in the literature. Increased sensitivity through optimisation to a peptide specific cone voltage, and collision energy along with identification of appropriate molecular transitions was reported by researchers in the field of proteomics. Ultra-Pure Liquid Chromatography-MSMS (HPLC-MSMS) operating MRM with optimal parameters reported significant gains in signal intensity of optimised detection in comparison to default operating parameters (Sherwood *et al* 2009). Additionally, optimised MRM cone voltage and collision energy parameters increased detection sensitivity for stimulants and metabolites in human urine by LC-MSMS (Dong *et al* 2015).

4.3.5 MRM – resolving isobaric conflicts

MRM operating protocols features the potential to differentiate between isobaric compounds. Anisole and 2,5-DMP are two volatile compounds with the same molecular weight of 108 g/mol, using SIR techniques, there is no discernible way for differentiating between the two. Upon soft ionisation anisole and 2,5-DMP form adducts with a proton with a m/z of 109. Fragmentation of anisole at optimal conditions produces m/z 77 and 94. Ion m/z 77 is 58% more abundant than m/z 94. 2,5-DMP fragments to different ions of m/z 41 and 82 with m/z 41 25% more abundant than ion 82 m/z. Validating the premise that MRM could resolve conflicts was performed by comparison of equilibrium headspace concentrations of solutions of anisole and 2,5-DMP to a solution comprising of both volatiles. APCI-MSMS was set to detect ions that transition from 109 to 77 m/z (Anisole) and 109 to 82 m/z (2,5-DMP). The signals generated by each volatile in isolation and as part of a mixture are summarised in figure 27. One-way ANOVA of differences between signals generated for each volatile in isolation as part of an anisole+2,5-DMP mixture as assessed by Graphpad Prism 7 were statistically non-significant with P values of > 0.05. Monitoring specific molecular transition i.e. precursor ion 109 to product ion 77, allows for the separation of Anisole and 2,5-DMP.

Ion stability and reactivity are important factors for hypothesising fragmentation pathways (Demarque *et al* 2015). For instance, charge retention fragmentation reactions informed the proposed fragmentation pathway of anisole (figure 26). Charge stability of the delocalised π electron cloud prevents migration of charge to the fragmentation reaction site and does not participate in the reaction (Tomer *et al* 1988). The m/z of the major product ions of anisole (77 and 94) are consistent with removal of the distal methyl group

and the removal of the methyl ether group. 2,5-DMP fragmentation produce 81 m/z which could potentially involve remote hydrogen rearrangement reactions to protonate imine groups (figure 26)

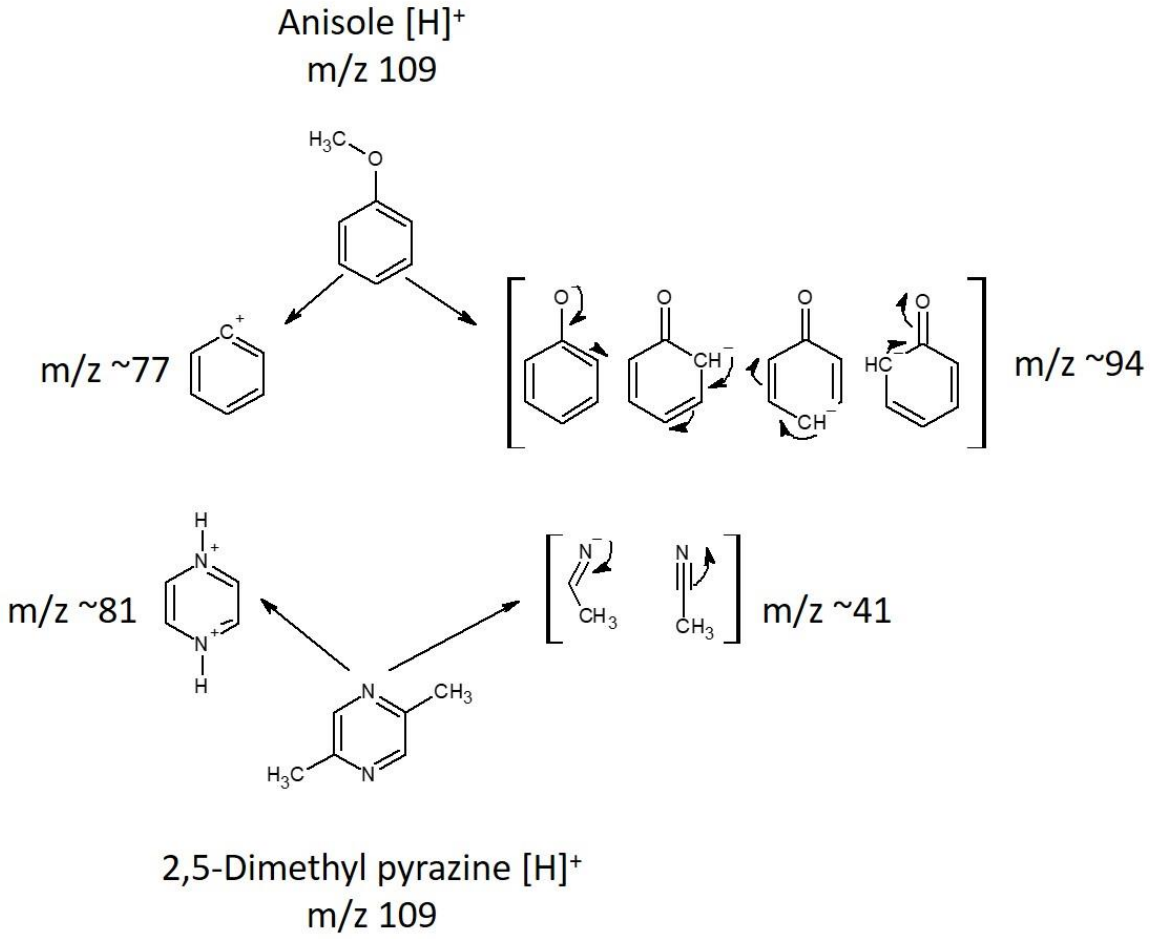

Figure 26 Figure 26: Proposed precursor fragmentation of 2,5– Dimethyl pyrazine and Anisole

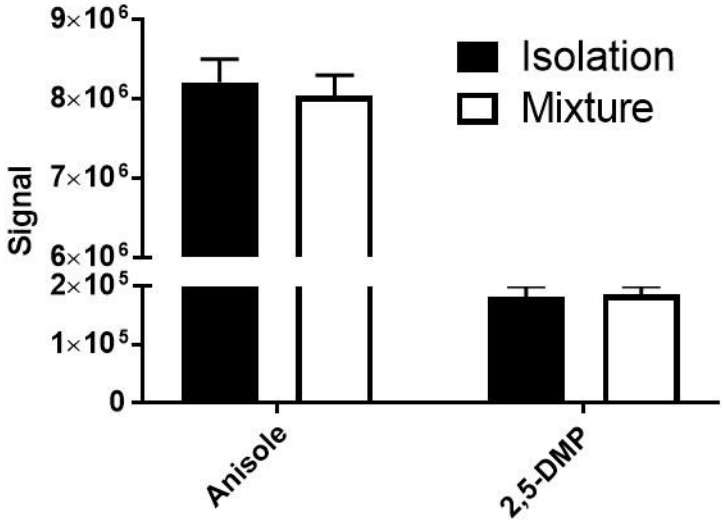

Figure 27 Comparisons of signals for the parent-daughter transitions of m/z 109.1 of 2,5-DMP and anisole when assessed individually or as part of an 2,5-DMP-anisole mixture. Each presented value is an average of three independent repeats. Error bars express standard deviation between repeats.

Energy imparted to molecules during the ionisation process can also result in fragmentation for certain molecules such as ethyl butyrate and is referred to as in-source fragmentation. In such situation, energy from the ionisation source is sufficient to induce fragmentation. In source fragmentation was generally observed for compounds with carbon skeletons with oxygen containing functional groups. The level of insource fragmentation was based upon compound type and the ionisation voltage.

Potential conflicts arise when analysing a sample where a volatile undergoes cone voltage-induced fragmentation with the resultant fragment produced is possesses the same m/z as another volatile in the sample. Such a situation can arise with in source fragmentation of ethyl butyrate and the ethyl acetate adduct ion. Figure 28 shows the spectra of ethyl butyrate analysed with cone voltage set to 40 m/z, ion 89 m/z features prominently. The ethyl acetate ion m/z is 89, a potential isobaric conflict can occur between ethyl butyrate

derived ion m/z 89 and the ethyl acetate ion m/z 89. Product ions of m/z 61 and 43 are produced by CID for the ethyl acetate ion, for the ethyl butyrate derived ion m/z 89 CID product ions are m/z 43 and 71. In each case a unique ion is generated by CID.

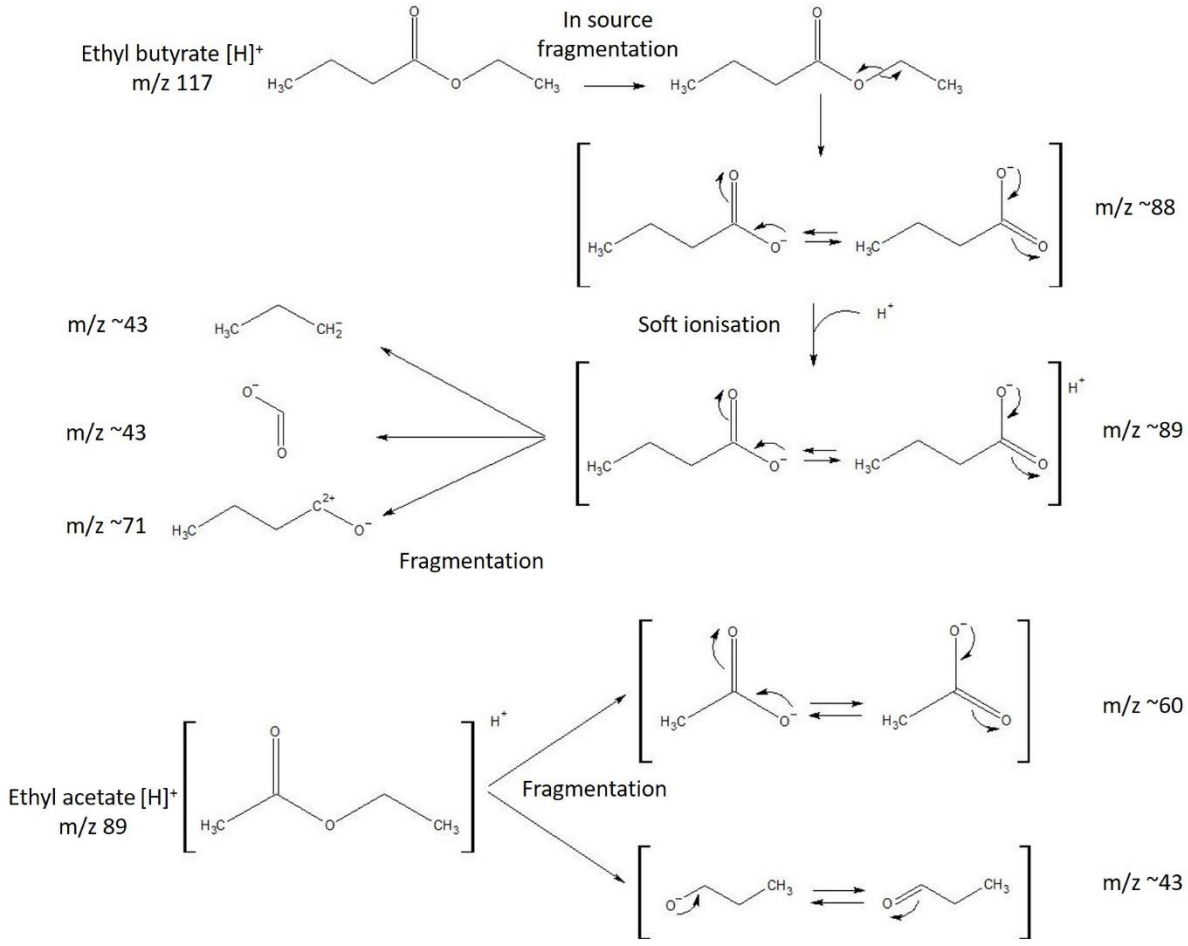

Figure 28 Proposed fragmentation patterns for the ethyl butyrate derive m/z 89.1 ion and ethyl acetate m/z 89.1 ion

Obtaining precursor-product transitions for ethyl butyrate fragment ion m/z 89 and ethyl acetate was performed in the same way as described earlier. The signal intensity of ions was assessed in isolation and as part of an ethyl butyrate-ethyl acetate mixture (figure 29). The transitions monitored were m/z 89 to 60 for ethyl acetate and m/z 89 to 71 for ethyl butyrate fragment ion m/z 89.

One-way ANOVA of differences between signals generated for each volatile in isolation or as part of an ethyl butyrate-ethyl acetate mixture as assessed by Graphpad Prism 7were statistically non-significant with P values of > 0.05. This shows that the use of molecular transition information can be used to independently monitor isobaric species that are present in the same sample.

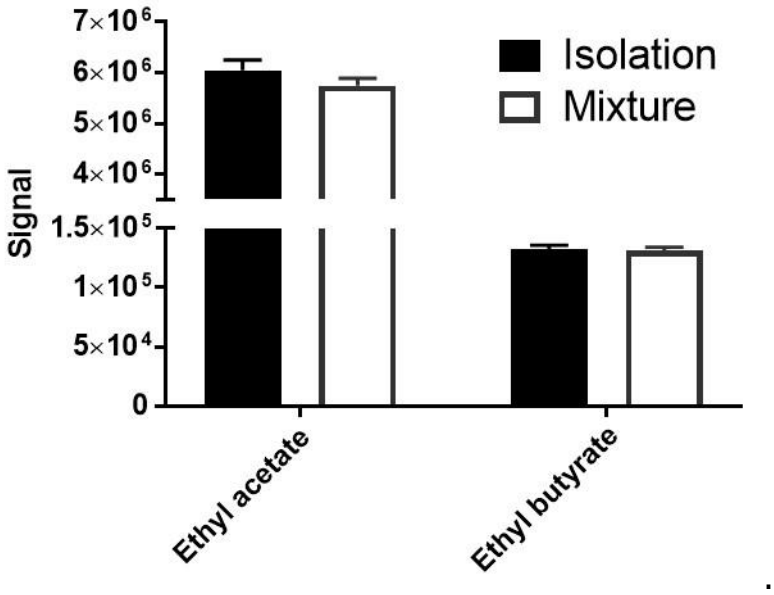

Figure 29 Comparisons of signals for the parent-daughter transitions of m/z 89.1 produced by in source fragmentation of ethyl butyrate and ethyl acetate. Isolation refers to each ion detected separately; mixture refers detection with both ions present. Each presented value is an average of three independent repeats. Error bars express standard deviation between repeats.

4.5.1 Post inhalation Breath-by-breath persistence of anisole, 2.5-dimethylpyrazine as a mixture and in isolation

Successful application of MRM based differentiation of compounds with identical m/z, anisole and 2,5-dimethyl pyrazine was validated by a breath-by-breath aroma persistence analysis. Two types of volatile samples were prepared, a mixture containing 50ppm anisole (m/z = 109) and 150ppm 2,5-dimethylpyrazine (m/z =109) and

separate samples of 50ppm anisole and 150 ppm 2,5-dimethylpyrazine. Breath-by-breath aroma intensity under a regimented breathing protocol for each sample was assessed by three panellists (figure 30). Decay curves and intensity levels for anisole and 2,5-dimethylpyrazine as part of a mixture or in isolation are similar in appearance, suggesting isobaric resolution was possible in real biological system.

Statistical assessment of decay in aroma intensity with time was achieved by first characterising the rate of aroma loss, k_d s^{-1}, by application of exponential one-phase decay non-linear regression models featured in line estimation software Prism 7 (Graphpad Software, California, USA). One-way ANOVA (Xlstat, Addinsoft, France) reported no significant difference ($P > 0.05$) between mixture and isolation k_d s^{-1} for anisole and 2,5-dimethylpyrazine. Statistically supporting the premise that separation of isobaric m/z compounds can also be conducted in *in vivo* systems

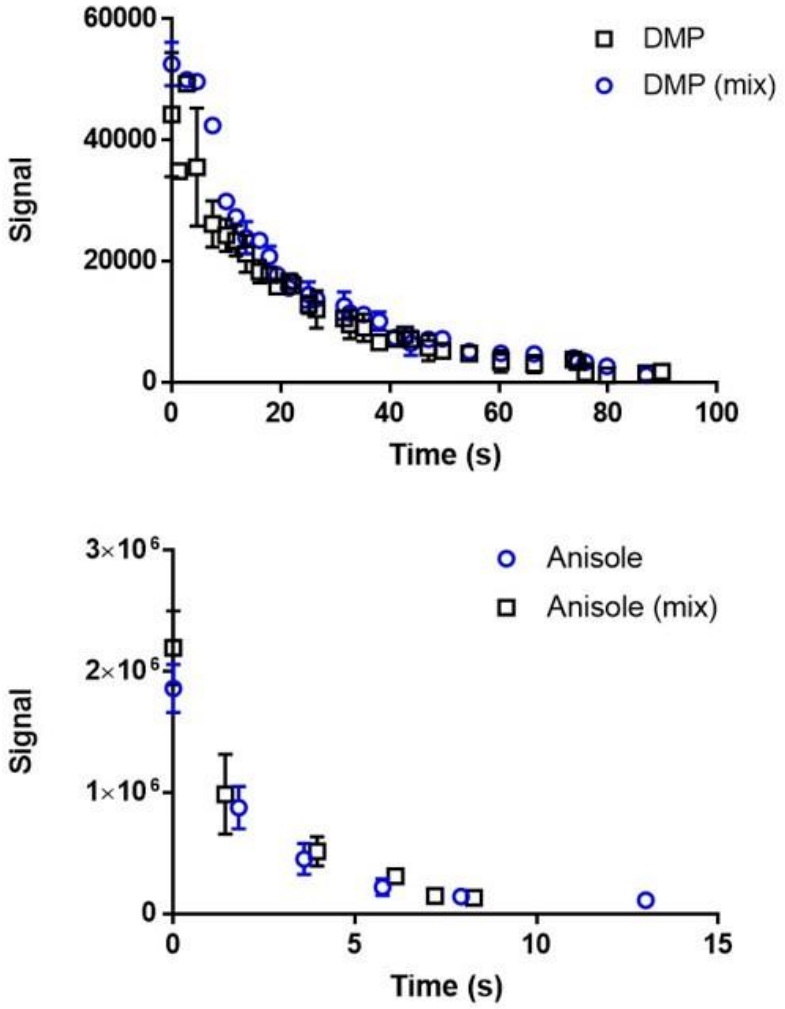

Figure 30 Nasal cavity persistence of 2,5-dimethyl pyrazine (top) and anisole (bottom) detected by APCI-MSMS where each aroma is monitored in isolation or as part of an anisole-2,5-dimethyl pyrazine mixture. Each data set represents the mean of 3 independent repeats for 2 panellists, error bars show standard deviation between repeats.

4.6.1 Conclusion

Enhanced signal gains are achievable by optimising cone voltages and adopting MRM detection protocols which make use of a dual mass filtering procedure allowing only the detection of compounds that fulfil the criteria of each mass analyser. MRM procedures also can differentiate between identical m/z compounds a particularly useful feature for analysis in biological systems such as oral cavity

persistence of specific aroma compounds after consumption of food matrices featuring complex aroma profiles such as wine.

Chapter 5 - Aroma Interactions with Lipids

5.1.1 Introduction

Oil-in-water emulsions are an important medium for investigating aroma compounds interactions with lipid systems (Doyen *et al* 2001, Miettinen *et al* 2002, *van* Ruth *et al* 2002, Ghosh *et al* 2008 and Doi *et al* 2019). Oil in water emulsions consist of a disperse phase of oil suspended in a continuous aqueous phase. Emulsifiers such as the anionic surfactants Tween 20 and Tween 80, types of polysorbate, coat the surfaces of oil droplets forming physical and energetic barriers (through repulsion) preventing oil droplets coalescing to form oil aggregates.

Determining the level of effect, a lipid system has on the volatilisation of aroma requires the observation of changes in headspace intensity of aroma when in the presence of lipids of various concentration. *In vitro* investigations into lipid-mediated changes in headspace aroma concentrations included GC-MS analysis of equilibrium (static) headspace concentrations. Similar APCI-MSMS measurements are also reported in the literature (Carey *et al* 2002). APCI-MSMS and GC-MSMS offer distinct advantages and disadvantages. Whilst GC-MS is limited to static headspace measurements, accurate calculation of headspace concentrations can be achieved with relative ease using appropriate internal standards (Heng Hui *et al* 2014). APCI-MSMS offers the advantage of real time analysis of headspace concentration change in the form of dynamic dilution headspace analysis by APCI-MSMS. Determination of headspace volatiles concentration by APCI-MSMS can be challenging owing to the variability of signal generated by similar samples depending upon operating conditions. Marin *et al* 1999 method for determining partition coefficients relied upon the direct injection of known quantities of hexane by automated syringe

into the APCI-MSMS source. Once injected into the source hexane rapidly and completely vaporises, if the rate of injection and concentration of hexane is known then the peak generated for hexane act as an internal standard. When using internal standards aroma release is reported as a partition coefficient, a ratio of volatile distribution between headspace and emulsion solution. Relative headspace intensity (RHI) provides a comparative measure between the headspace peak area of a water to control to that of an aroma solution of interest. RHI is useful when there are no internal controls to aide in concentration calculation. Chapters 6 and 7 discuss alternate methods of determining headspace concentrations.

Static headspace studies of lipid emulsions enable the determination and comparison of equilibrium headspace measurements of aroma in the presence of varying emulsion concentration, lipid type, emulsifier type, etc. Examples of the negative impact increasing lipid emulsion fraction on equilibrium headspace partitioning of aroma in lipid emulsion systems are present in the literature (Rabe *et al* 2003, Karaiskou *et al* 2008, Paravisini and Guichard et al 2017). A comprehensive analysis of equilibrium aroma headspace partitioning of 67 aroma at various low lipid concentration in cloud emulsions determined the influencing factors on the level of aroma contained within the equilibrium headspaces as the solubility of aroma in water, aroma hydrophobicity, aroma dipole vector and the lipid fraction (Carey et al 2001).

Dynamic headspace dilution analysis, through application of a continual renovating stream of nitrogen, recycles the headspace above a solution. Changes in headspace aroma intensity with time is a function of Reynolds number governed by the rate of renovation and the rate of mass transfer of aroma from the interfacial boundary

layer to the headspace. A persistent aroma relative to a less persistent aroma, maintains a stable aroma headspace concentration (Marin and Taylor 1999, Banavara *et al* 2002). Dynamic headspace dilution analysis of aroma in lipid emulsions reported a conferred stabilising effect of oil-in-water emulsions relative to water (Carey *et al* 2001). Flavoured water generally experiences an initial rate of rapid aroma loss followed by a decreased rate of aroma loss. Conversely, rate of headspace aroma loss proceeded at near homogenous rate for flavoured emulsion systems. Total rates of aroma headspace loss from emulsion systems decreased relative to aqueous systems indicating a stable release of aroma from lipid emulsion systems (Haahr *et al* 2000).

Complementary to previous studies, the present study is concerned with effects exerted by a system on the release of aroma from emulsion systems when the aroma is an intrinsic part of the system but also when aroma is introduced to the system via the headspace and is not an intrinsic component of the system at t = 0. Systems under consideration are as follows:

- The release of aroma after consumption of flavoured lipid emulsion and water.
- Interface loading and subsequent release of aroma after a quantity of aroma is infused into the headspace above water and emulsion interfaces under dynamic dilution conditions.
- The release of aroma from emulsion-aroma systems under dynamic dilution conditions.

Each system represents aroma in differing conditions. Dynamic headspace dilution features infinitely dilute concentrations of aroma with an aroma concentration large enough, that over the time course of each trial, concentration will effectively remain constant therefore, this type of system can be thought of as existing in a

steady state. The second *in vitro* system introduces aroma to the headspace of a 'clean' (i.e. no aroma present) air-solution interface and represents an unsteady state system where bulk solution concentrations of aroma are not present and unable to exert any effects on parameters such as mass transport. In-mouth release of aroma features aspects of steady state and unsteady state systems. Consumed solutions coat pharyngeal surfaces with a residue which contribute to *in vivo* aroma release. The remaining residue releases aroma to the oro-nasal cavities loading mucosal surfaces with aroma (Doyennette *et al* 2017), a situation the headspace infusion technique seeks to elucidate.

5.2.1 Materials and methods

2,5-dimethy pyrazine (≥ 98% FG), isoamyl acetate (≥95% FG), ethyl butyrate (≥98% FG), hexanal (≥95% FG), 2-heptanone (≥98% FG), p-anisaldehyde (≥97.5% FG), guaiacol (≥99% FG) and Tween20® obtained from Sigma Aldritch (Poole, UK). Sunflower oil obtained from KTC (Wednesbury, UK).

5.2.2 Aroma preparation

Aroma solutions were prepared by dilution in deionised water in 1L volumetric flasks. Dilution of aroma was required to prevent overwhelming the APCI-MSMS ionisation source which results in a suppression of signal and to minimise aroma-aroma interactions. Aroma dilutions for each experiment type are compiled in table 5.

5.2.3 Emulsion preparation

Tween20 was initially added to water and magnetically stirred at room temperature for ten minutes at a rate of 700rpm before the addition of sunflower oil. The resulting solution was then homogenised in a Silverson LSM homogeniser (Silverson Machines, Chesham, UK) for 2 minutes at 6000rpm. Oil droplet size and distribution was analysed by a particle size analyser (Malvern

Mastersizer S system, Malvern UK) to produce a mean oil droplet size of 6.1 μm – a size that falls within the range of typical cell sizes (1-100 μm). Emulsions droplet sizes were reassessed after 24 and 48hs. A drop in approximately 1.5 μm size was observed after 48hs. Emulsions were deemed stable for the short time period from production to use (<2 hours).

Dilution of 60% (v/v) emulsion solution with aroma flavoured deionised water to yield 5, 10 and 20% (weight %) aroma-emulsion mixtures along with a 0% emulsion aroma-water control. 40 mL of each solution were equilibrated in 123mL Scott bottles (Fisher Scientific, UK) for dynamic headspace analysis. All samples were equilibrated for 3h at room temperature before analysis.

40mL of deionised water and emulsion for headspace aroma injection analysis, which required no aroma to be present pre-headspace injection were housed in 123 mL Schott bottles and stored at room temperature.

5.3.4 APCI-MSMS settings

APCI optimisation and operation was performed in accordance with the method set out in chapter 4. Volatile headspace analysis was performed with MS NOSE APCI-MSMS (prototype TDQ; Waters, Manchester, UK). Ion detection was performed using Multiple Reaction Monitoring (MRM), a tandem mass spectrometry technique. Cone voltage, collision energy, concentration and monitored molecular transitions are catalogued in table 5. Silica dimensions of MS NOSE interface with a film thickness of 0.25μm and an internal diameter of 0.25mm were used throughout all experimental runs (Phenomenex, Macclesfield, UK). Uniform operating conditions for corona pin voltage (4 kV, positive ion mode), ion dwell time (0.1s) and transfer line temperature (120ºC) were used throughout.

5.3.1 Dynamic headspace dilution analysis

100 mL solutions of flavoured water (aroma concentrations listed in table 5) or flavoured oil-in-water emulsions were contained within 123 mL Schott bottles modified to include inlet and outlet ports as per Marin *et al* (1999) and Doyen *et al* (2001). Headspace volume in the vessel was kept constant at 20 mL and interface area was 6.2cm^2. Through the inlet ports PTFE tubing delivered a 70mL/min stream of nitrogen directly to the headspace, PTFE tubes terminated ~5mm from solution surfaces. The outlet port incorporated a stainless steel "T" junction joining the APCI-MSMS to the reaction vessel whilst allowing for an exhaust outlet for excess nitrogen. Samples were bought to equilibrium before the nitrogen-diluting stream was introduced. A short period of signal acquisition to establish base line signal was proceeded by release of a valve to begin the dilution process, signal acquisition was terminated after a period of ~300s.

5.3.2 *In vivo* aroma persistence analysis (solution consumption)

Four panellists were instructed to hold 10mL of solution in their mouth for ten seconds whilst maintaining restful breathing, exhaled breath was continuously sampled by APCI-MSMS through a modified transfer line to establish a signal baseline. After ~10 seconds panellists were instructed to swallow the solution and to continue normal restful breathing as sampling continued. Sampling terminated either when the signal decayed to 5% of the initial maximum value or until 1min expired. Aroma concentrations contained within each solution are shown in table 1. APCI-MSMS sampling rate was set to 30-50 mL/min. Normal breathing by panellists was monitored by intensity of acetone (m/z 59) in panellists' breath.

Ethical considerations when involving panellists were considered. All experiments involving panellists remained in the constraints of the precedents set in similar APCI-MSMS breath-by-breath measurement outlined in the literature (Heng Hui *et al* 2014, Linforth 2000, Rabe *et al* 2003, Rabe *et al* 2004, Heng Hui *et al* 2014, Sánchez-López *et al 2016).*

Table 5: Aroma APCI operating conditions and system dilutions

	Cone Voltage (V)	Collision Energy (eV)	Molecular Transition	DYN ppm	IV&INF ppm
p-anisaldehyde	40	20	137 > 77	50	100
Hexanal	10	15	101 > 55	2	50
Guaiacol	25	20	125>110	50	100
2,5-Dimethylpyrazine	48	20	109 > 82	50	150
2-heptanone	24	15	115 > 55	2	20
Isoamyl acetate	15	10	131 > 70	1	5
Ethyl Butyrate	25	15	117 > 89	1	5
Acetone	15	10	59 > 31	n/a	n/a

5.3.3 Headspace aroma injection analysis

Water and emulsion solutions housed within 123 mL Schott bottle, modified with the same inlet/outlet additions as featured in dynamic headspace analysis protocols, produced an air-water/emulsion interface for headspace aroma infusion analysis. Reaction vessel dimensions included a headspace volume of 20 ml and an interface

area of 6.2cm^2. A 70 ml/min dilution stream of N_2 was continually passed over the headspace through the inlet port to the outlet port with an appropriate exhaust. At t = 0 a 50 mL quantity of volatilised aroma was manually injected into the diluting stream pre-reaction vessel. Evolved aroma intensity was monitored by APCI-MSMS with a sampling rate of 10ml/min for approximately 300s or till signal decreased to baseline levels.

50 mL of dilute aqueous aroma solutions (concentrations listed in table 5) were equilibrated at 70˚C for 3h in 120ml Schott bottles modified with an access port for syringe extraction. With a Luer lock gas tight syringe, 10 ml of aroma solution headspace was extracted and manually injected immediately into the dilution stream. Method of aroma introduction were repeatable with minimal standard deviation (< 2%) between repeats.

5.4.1 Gas phase *in vivo* aroma persistence

Preparation of volatised aroma samples was conducted identically to the method used for headspace injection persistence. 50 mL of extracted volatilised aroma was directly injected into the panellist oral cavity with a Luer lock syringe during inhalation. Panellists maintained normal breathing through their nostrils directly into a MS Nose interface of the APCI-MSMS during the injection period. Breath-by-breath intensity of select aroma was monitored after aroma injection by APCI-MSMS at a sampling rate of 30mL/min.

5.5.1 Data treatment

Raw signal vs time data was imported to Microsoft Excel for processing. Background signal measurements were subtracted from overall signal before signal was normalised to fractions of signal I_{max} so that maximum signal read as 1 whilst all values lower than I_{max} are reported relative to 1. Normalised aroma loss curves were then imported into line fitting software, Prism 7 (Graphpad Software, UK)

for rate constant determination. Aroma concentrations are normalised to 1 to determine the relative effects of interface alteration on aroma persistence. A line of best fit for each decay curve was fitted based on one of two equations: one-phase decay or two-phase decay. One-phase decay model is given by equation 24:

$$\frac{N}{N_0} = exp^{-kt} \tag{24}$$

Where N is the level of aroma in the headspace at t = x, N_0 is the aroma level in the headspace at t = 0. Time is given by t (s) and k is the rate constant (s^{-1}). Two-phase decay models are given by equation 25:

$$N = P_f exp^{-k_{fast}t} + P_s exp^{-k_{slow}\,t} \tag{25}$$

$$P_f = N_0 \frac{k_{fast}}{100} \tag{26a}$$

$$P_s = N_0 \left(1 - \frac{k_{fast}}{100}\right) \tag{26b}$$

Where P_f is the percentage amount of time spent in fast decay whilst P_s is the remainder of the percentage amount of time spent in slow decay, k_{fast} is the rate constant for fast decay (s^{-1}) and k_{slow} is for the rate constant for slow decay (s^{-1}).

For the purposes of statistical analysis, a single descriptive term to describe two-phase rate decay was achieved by combination of rate

constant of the fast decay period, k_{fast} and the rate constant of the slow decay period (Cobelli *et al* 1980) equation (27).

$$k_d = \left(k_{fast}\frac{P_f}{100}\right) + \left(k_{slow}\frac{P_{slow}}{100}\right) \quad (27)$$

The term k_d is the sum of the k_{fast} and k_{slow} and the respective contribution of each period to the total decay period.

When calculating best lines of fit for two models, Prism 7 includes an option to statistically compare the fits of two models using Akaike's method to determine a percentage likelihood that a model for a set of data is correct. Prism reports a corrected AIC value as a percentage, for this study, simpler one-phase decay models were selected as the default option unless returned AIC values were 90% in favour of using the more complex two-phase decay model. This precautionary step was taken to avoid over fitting of data.

The application of two-phase and one-phase decay in the assessment of aroma release is discussed to a greater extent in chapter 6, where the methods and reasoning were originally developed. Software derived two-phase decay model fits were introduced after it became apparent that two common methods of data linearization (natural logarithms of y for one-phase and reciprocals of y for two-phase) produced disparate plot types. Reciprocal transformation plots increase linearly with time whilst natural logarithm transformations decrease linearly with time. Two-phase models were used so that comparison of one-phase and two-phase decay was possible. Two-phase decay models were retroactively applied to the work discussed in this chapter.

5.6.1 Analytical strategy

Analytical strategy for assessing aroma release under dynamic conditions from different solutions in different systems included expressing release curves in a uniform manner to enable statistical conformation of differences between aroma, interface and systems and finally, an assessment on the applicability of mass transfer models in the explanation of aroma release kinetics.

5.7.1 Results

5.7.2 Headspace dilution kinetics

Differences in aroma loss with changes in solution composition is taken to be a measure of a solutions influence on aroma release to the gas phase. An aroma displaying an increased persistence from one solution relative to another can be observed by the decrease in the rate of aroma loss from the headspace with time. Release of seven aroma compounds as a function of time with exposure to different forms of dilution either through an applied flow of $N_{2(g)}$ or exhaled breath, were characterised.

Kinetics of aroma loss are described in terms of persistence, namely, the ability of an aroma to retain a presence in the headspace. The intensity of an aroma in the headspace or in exhaled breath of a persistent aroma is greater than a less persistent aroma. For instance, if at t = 20s, the levels of aroma X have decreased to 20% of the levels experienced at t = 0s whilst aroma Y levels at t = 20s have decreased to 45% of the levels experienced at t= 0 then aroma X is less persistent than aroma Y.

The systems can be broadly separated into two groups based upon the state of aroma in the system at t = 0. The first group describes a situation where aroma is initially in equilibrium between gas and liquid phases, systems of this nature include dynamic headspace (DYN) and to a lesser extent solution *in vivo* (IV). The second group

contains gas phase *in vivo* (GIV) and headspace injection (IF) and describes systems where no aroma is present at t=0.

5.7.3 Dynamic headspace dilution

Headspace persistence of aroma is represented by k_d (s^{-1}) a measure calculated from decay curves generated by the loss of aroma intensity as a function of time. Normalisation parameters and method of k_d determination are covered in chapters 3, 4 and in the method of this chapter. The headspace persistence of seven aroma compounds varied significantly between solutions of 0, 5, 10 and 20% oil in water emulsions. One-way ANOVA procedures performed in R (The R Foundation, USA) identified aroma specific significant differences ($P < 0.0001$) between different lipid content. Honest significant difference tests featured in the R package "agricolae", separated significant k_d period-lipid content differences. Letters above each column of Figure 31 communicates significant differences in inter-aroma k_d values, if X = X then differences in k_d between lipid solutions for that aroma are non-significant, if X ≠ X then differences are significant ($P<0.05$). Aroma headspace persistence was lowest for aqueous systems as evidenced by the uniformly high rates of decay, k_d. Persistence was greatest for compounds with k_H values < 10^{-5}, for aroma with K_H values exceeding 10^{-5}, release of aroma was more pronounced as shown by the higher rates of decay. The behaviour aroma in aqueous dynamic headspace systems of this study in aqueous systems conformed to the behaviour outlined in the literature where governing factors for aroma loss are the applied dilution stream for compounds with K_H values < 10^{-5} or governed by mass transport for aroma with $K_H > 10^{-5}$ (Marin and Taylor 1999). Mass transport measures calculated for the aqueous dynamic headspace persistence models introduced by

Marin & Taylor (1999) were primarily driven by k_H. Thus, parity between the two investigations can be observed.

Lipid emulsion solutions stabilised headspace persistence relative to aqueous solutions resulting in reduced k_d values for all tested aroma. A reduction of ~90-94% in k_d was experienced by aromatic ring containing compounds guaiacol, 2,5-dimethylpyrazine and p-anisaldehyde when comparing aqueous solutions to 5% emulsion solutions. Hexanal k_d reduced by ~55%, whilst k_d reductions of ~60-70% was observed for saturated carbon skeleton compounds 2-heptanone, isoamyl acetate and ethyl butyrate. Isoamyl acetate headspace stability was further increased with 17% reductions in k_d with increases in lipid content from 5 to 10 and 20%. Altering lipid content from 10 to 20% resulted in no significant change in k_d for all other tested aroma under dynamic headspace conditions suggesting a lipid emulsion concentration limit on the stabilising effect. Such a situation may occur when the interfacial region between air and solution reaches a maximum emulsion saturation.

Conferred aroma headspace stability by the presence of lipid emulsions is well characterised in the literature. Ethyl esters, ethyl hexanoate, ethyl butyrate and ethyl octanoate under dynamic dilution conditions experience increases in headspace stability with addition of increasing concentrations of tricaprylin (C8) lipid emulsion. Increasing saturated carbon chain length increased the effect of lipid emulsion enhanced headspace stability (Doyen *et al* 2001).

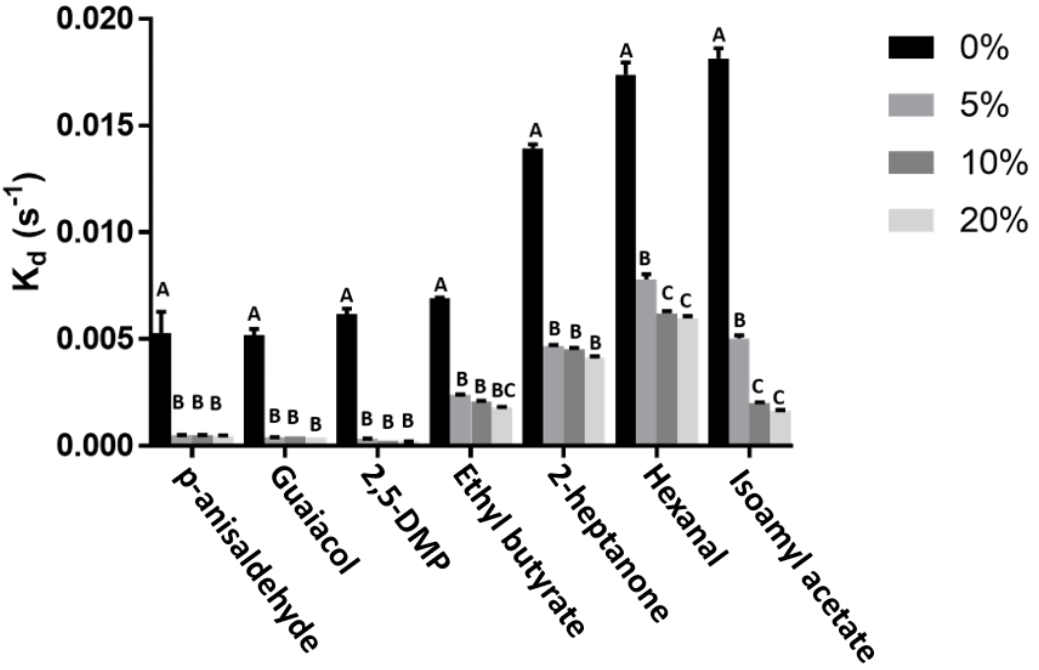

** 2,5-DMP = 2,5-dimethyl pyrazine*

Figure 31 Dynamic headspace dilution rates of aroma loss, k_d for solutions of 0, 5, 10 and 20% lipid emulsion containing one of seven aroma compounds. Letters above each column signify inter-aroma significant differences where X = X then P > 0.05 and if X ≠X then P < 0.05. Each column represents mean of three independent repeats with the standard deviations given by error bars.

Under non-equilibrium conditions compounds with Henry's law constant $<10^{-5}$ are generally able to successfully replenish lost headspace aroma concentrations relative to compounds with a Henry's law constant $\geq 10^{-5}$ values. For instance, two compounds, A and B in equilibrium between a continuous phase of water and air with k_H values of 0.1 (A) and 0.001 (B) and with the same aqueous concentration of 150 ppm then equilibrium concentrations of volatile A are 15 ppm and volatile B are 0.015ppm. When exposed to a diluting stream, maintenance of headspace concentrations of aroma B requires less movement of aroma from liquid to gas phase than aroma A, which requires increased net mass transfer to maintain

headspace concentration (Fisk 2015). The inclusion of lipid alters partition coefficients along with the disruption of continuous water phase and increases systems complexity, introducing partitioning mechanics between aroma and lipid droplet and potentially aroma and emulsion surfactant (Relkin *et al* 2004).

Inclusion of lipid to a system alters partitioning behaviour of aroma between solution and air (k_{ae}, the air-emulsion partition coefficient) phases is affected in one of three ways.

1) The air partition coefficient K_{aw} is greater than k_{ae}. With the inclusion of lipid, aroma released to the headspace is decreased. With application of a dilution stream less aroma release from emulsion phase is required to maintain the decreased headspace levels, observed k_d decrease to reflect increased headspace stability.

2) If K_{aw} is approximately equal to k_{ae} then aroma persistence remains unchanged between water and lipid solutions with application of a dilution stream.

3) If K_{aw} is less than k_{ae} then aroma persistence is negatively affected resulting in observable k_d increases.

For all compounds tested, the inclusion of lipid relative to water results in situation 1, where persistence is increased through the changing solution composition and therefore the change in air-solution partition coefficient. When comparing k_d values of 5 to 10%, the non-significant change in k_d is observed for all compounds except for the most hydrophobic compound Isoamyl acetate. Situation 2 applies in such circumstances where there is no perceivable change in partition coefficients, therefore only the lipophilic compounds are further affected by increases in lipid content. Further changes in persistence with increases in lipid content for hexanal are less difficult to attribute to changes in

partition coefficient, hexanal has previously been described as a volatile biomarker of lipid oxidation in vegetable oils (Ha *et al,* 2011 and Elisia and Kitts, 2011).

When considering the initial rate of headspace aroma loss under dilution of aqueous systems Haahr *et al* (2000) observed a rapid decline of aroma followed by a decrease in the rate of aroma loss whilst emulsion systems experienced an increase in aroma release resulting in a headspace stabilising effect.

To understand the difference between initial and late phase decay, aroma decay curves were separated in to two periods; initial (0-60s) and late (60-120s) for each lipid solution to assess any significant differences in aroma loss between decay periods (Figure 32). One-way ANOVA procedures performed in R identified aroma specific significant differences ($P < 0.0001$) between different solution lipid content and period of decay.

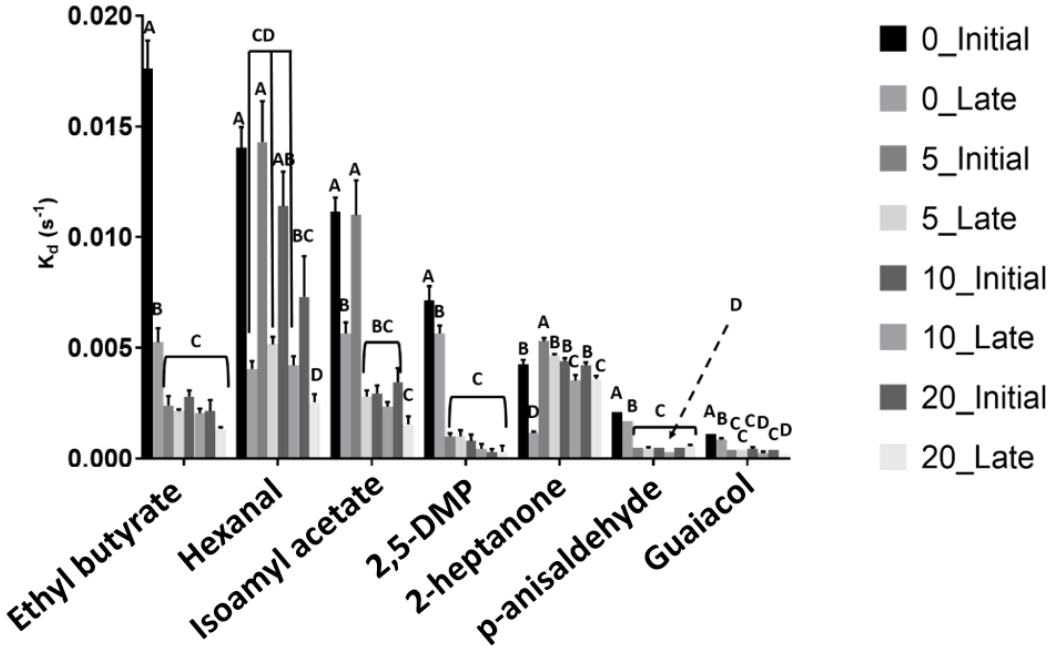

**2,5-DMP = 2,5-Dimethyl pyrazine*

Figure 32a: ANOVA results for initial (0-60s) and late (60-120s) dynamic headspace dilution rates of aroma loss, k_d for solutions of 0, 5, 10 and 20% lipid emulsion containing one of seven aroma compounds. Letters above each column signify inter-aroma significant differences where X = X then P > 0.05 and if X ≠X then P < 0.05. Each column represents the mean of three independent repeats with the standard deviations given by error bars.

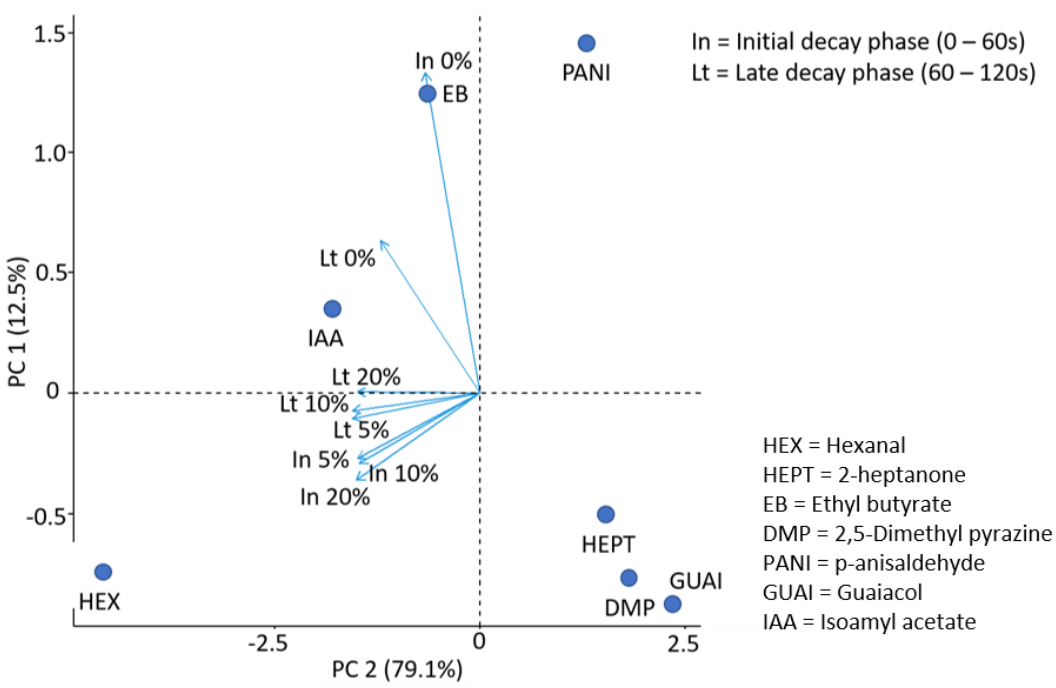

Figure 32b: PCA for initial (0-60s) and late (60-120s) dynamic headspace dilution rates of aroma loss

Isoamyl acetate, 2-heptanone and hexanal experienced significant differences between initial and late phase aroma decay with the inclusion of lipid emulsions. Isoamyl acetate, features a substantial increase in aroma persistence for aqueous systems between initial and late phase decay. For lipid systems, initial and late phase decay tended towards an emulsion concentration consensus, indicating the mechanics of aroma release are generally stable and likely linear. The change in aroma headspace per unit time for such systems does not change suggesting that either concentration has little effect on release or release of aroma is dependent on a second limiting factor, in this instance, likely the movement between aroma from emulsion micelles to the aqueous surroundings.

Large changes in Initial decay relative to late period decay are experienced by hydrophobic compounds 2-heptanone, isoamyl acetate and hexanal. Ease of movement through hydrophobic

domains likely results in enhanced initial release resulting in an initial low persistence. Once headspace levels have sufficiently diluted a decreased, stable level of persistence is reached.

Principal component analysis (PCA) enabled a visualization of the differences between the aroma, system type and decay period (figure 32b). PCA component 1 (PC1) accounts for ~12.5% of total observed variation whilst PCA component 2 (PC2) accounts for ~79.1% of total observed variation. From figure 32b, projection of aroma compounds along PC2 suggests the majority of the variation observed is based on aroma differences. Emulsion concentration and time phase are projected into a similar space along PC2, variation between lipid concentration and time phase is associated with PC2, which accounts for a relatively small amount of the variation.

Headspace persistence of low K_H, aromatic compounds, guaiacol, p-anisaldehyde and 2,5-dimethyl pyrazine generally did not significantly vary with increases in lipid concentration from 5 through to 20%. However, a significant change was observed between aqueous solutions and lipid solutions for the same compounds. Changes in 2,5-dimethyl pyrazines persistence are more pronounced between aqueous and lipid phases than guaiacol and p-anisaldehyde.

Table 6: Physicochemical parameters of select aroma obtained from EPA (Environment protection agency, USA) T.E.S.T 4.1 software.

	Log P	Water Solubility Mol/L	Molar volume cm^3	Polarizability $Å^3$	K_H	Vapour pressure, mmHg at 25°C
p-anisaldehyde	1.76	0.032	125	15.7	$9.30E^{-06}$	0.03
Guaiacol	1.23	0.12	112	13.8	$5.29E^{-05}$	0.1
2,5-dimethylpyrazine	0.63	0.74	108	12.7	$1.37E^{-04}$	4.33
2-heptanone	1.96	0.04	141	13.7	$6.93E^{-03}$	3.85
Hexanal	1.78	0.056	125	11.9	$8.73E^{-03}$	11.3
Ethyl butyrate	1.8	0.047	131	12.5	$1.25E^{-02}$	12.8
Isoamyl acetate	2.25	0.015	148	14.4	$2.00E^{-02}$	5.6

5.8.1 In vivo solution kinetics

Breath-by-breath persistence of aroma after consumption of 0, 5, 10 and 20% emulsion solutions containing one of seven aroma compounds was measured by APCI-MSMS.

Aroma persistence is greatly reduced in in-mouth systems relative to dynamic headspace persistence. Differences in k_d ranging from 800-fold increases for ethyl butyrate to 3-fold increases for p-anisaldehyde when compared with dynamic headspace persistence. One-way ANOVA procedures in R identified a minimum of one significant difference in breath persistence of guaiacol, 2,5-dimethylpyrazine, hexanal and isoamyl acetate (figure 33). Honest significant differences multiple comparisons classified and grouped inter-aroma significant differences with changes in lipid concentration. Significant differences between 5, 10 and 20% lipid emulsions were observed only for the k_d of hexanal and isoamyl acetate under dynamic headspace dilution protocols whilst

significant differences were observed in k_d for a broader range of compounds for the same lipid concentrations in-mouth. All aroma experienced increased persistence under dynamic headspace dilution conditions when comparing aqueous solutions relative to emulsion solutions. Under in-mouth conditions persistence was significantly decreased or unchanged when comparing aqueous systems to emulsion systems for hexanal, isoamyl acetate, p-anisaldehyde and 2-heptanone.

As with dynamic headspace dilution PC analysis, aroma type accounted for the largest amount of observed variation with the solution type accounting for a smaller proportion of the variation. The distribution of aroma arrows along PC2, with the exception of Hexenal), suggest a strong association with PC2, a statement confirmed by the uniformly high cos^2 values of 0.94 to 0.97. The large contribution of PC2 to the observed variation indicates release is mostly governed by aroma type (88.3%).

Previously, a precedent in the literature reported dynamic headspace dilution underestimation of in-mouth breath persistence of three ethyl esters after consumption of flavour laden water and emulsion systems (Doyen *et al* 2001), an observation the presented work supports. In mouth systems represent an increase in the complexity of interactions aroma experience, such as dilution by saliva (van Ruth *et al*, 2002), interactions with salivary components (van Ruth et al, 1999, Friel *et al* 2001) and increased velocity of dilution (chapter 3, Marin *et al*, 1999).

When considering *in vivo* breath-by-breath persistence, defining a uniform oro-nasal cavity volume and renovation rate is hampered by inter-individual variability. Other considerations as previously stated, include the dilution of lipid content by saliva (van Ruth *et al* 2002) and interactions of aroma with salivary constituents and

possible effects of salivary proteins on emulsion vesicles. The potential for change of emulsion properties in the presence of salivary components are a necessary consideration for *in vivo* breath-by-breath aroma persistence after consumption of oil-in water emulsions. Mucin interactions with oil in water emulsions described in the literature include observations of association of approximately 1 mg/m^2 of mucin to cationic emulsions stabilised by lactoferrin and approximately 0.6 mg/m^2 to anionic emulsions stabilised by β-lactoglobulin for 20%(wt) soy oil emulsions in a continuous phase of artificial saliva. Droplet size distribution was shown to be unaffected by the presence of mucins and salts (Sarkr *et al* 2009). The literature makes a case for necessary consideration of effects of salivary constituents in any systems seeking to replicate in-mouth release of aroma from emulsions.

For dynamic headspace dilution a simple side-by-side comparison of water and emulsion k_d at different periods was sufficiently able to highlight evolving rates of aroma loss through the time course of an experiment. The rapid rates of aroma loss experienced by in-mouth breath dilution hinder the ease of such a comparison. Instead, a comparison of one-phase and two-phase decay fits are used to highlight potential changes in aroma release kinetics with time for in-mouth systems (table 7).

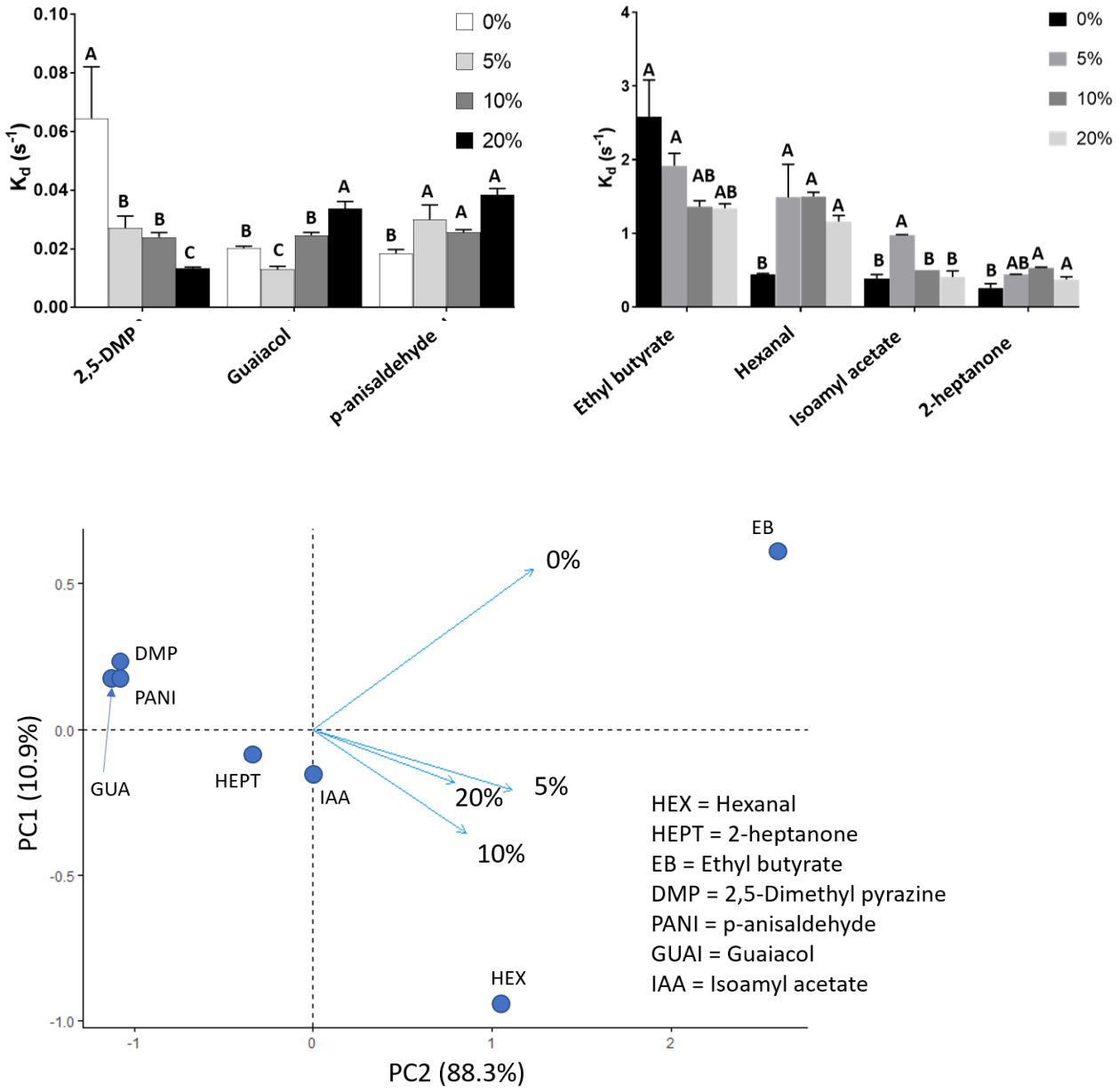

Figure 33 [Top] *In vivo* k_d of seven consumed aroma compounds featured as part of flavoured aqueous and emulsion solutions (0-20% lipid concentration). Each column represents means of independent repeats with the standard deviations given by error bars. [Bottom] PCA of *in vivo* breath-by-breath rates of aroma loss, k_d of seven consumed aroma compounds featured as part of flavoured aqueous and emulsion solutions

Table 7: Rates of breath-by-breath loss of seven aroma compounds after consumption of flavoured aqueous and oil-in-water emulsions. k_d in bold were calculated by the AiCc test to be better represented by two-phase decay models compared to one-phase decay models. Presented k_d are mean values of three independent repeats of four panellists, standard deviation values represented by column error bars

	0% Lipid		5% Lipid		10% Lipid		20% Lipid	
Aroma	k_d (s^{-1})	SD	k_d (s^{-1})	SD	k_d (s^{-1})	SD	k_d (s^{-1})	SD
2,5-dimethyl pyrazine	**0.065**	0.02	0.027	0.00	0.024	0.00	0.013	0.00
Ethyl butyrate	2.583	0.50	1.919	0.17	1.364	0.08	1.342	0.06
2-heptanone	0.259	0.06	**0.444**	0.00	**0.533**	0.01	**0.375**	0.04
Isoamyl acetate	0.390	0.05	**0.972**	0.01	**0.504**	0.00	**0.409**	0.08
Hexanal	0.444	0.01	1.488	0.45	1.502	0.06	1.160	0.08
Guaiacol	0.020	0.00	0.013	0.00	0.025	0.00	0.019	0.02
p-anisaldehyde	0.018	0.00	0.030	0.00	0.026	0.00	0.039	0.00

SD of 0 = <0.0001

Of the tested aroma, only 2, 5-dimethyl pyrazine was best described by a two-phase release model for aqueous solutions whilst 2-heptanone and isoamyl acetate aroma loss from emulsion systems were best described by two-phase decay models. All other aroma experienced a steady exponential decay of breath-to-breath aroma intensity. Dynamic, headspace dilution described rates of aroma loss from emulsion systems as generally homogenous across the time course of an experiment but was unable to predict the bi-phasic nature of isoamyl acetate and 2-heptanone. The Biphasic nature of dimethyl pyrazine, isoamyl acetate and 2-heptanone decay indicates the presence of 2 different forms of decay, indicating a direct interaction. For isoamyl acetate and 2-heptanone the effects of the

interaction(s) are only significantly observable with in-mouth persistence after consumption of flavoured lipid solutions. The reverse is true for 2, 5-dimethyl pyrazine indicating the addition of lipid supress the observed interaction whilst for 2-heptanone and isoamyl acetate the effect is enhanced with the addition of, and also the increase in lipid concentration.

5.9.1 Headspace injection

Persistence of seven aroma compounds after infusion of a quantity of aroma into the headspace at air-solution interfaces was characterised for four types of interface, water (0%), 5, 10 and 20% lipid emulsions. Changes occurring in k_d for an aroma exposed to different air-solution interface types describe the ability of solution composition to govern the dynamic persistence of an aroma. The rate of Ethyl butyrate headspace loss when exposed to air-water interfaces increases from ~0.03 s^{-1} relative to the rate of ethyl butyrate headspace loss observed at 5% lipid interfaces (~0.11 s^{-1}). Therefore, the headspace persistence of 2-heptanone is decreased with the inclusion of 5% lipid emulsions when compared to water.

Inclusion of lipids resulted in a reversal of behaviour experienced by several aroma compounds when compared to dynamic headspace trials. Rather than increasing headspace stability, inclusion of lipids significantly reduced dynamic persistence of ethyl butyrate, 2-heptanone, guaiacol and 2, 5-dimethylpyrazine. For the described system equilibrium conditions are not present, manual injection of aroma, results in a rapid surge in detected aroma followed by a period decay. Aroma partitioning behaviour is driven by the increased pressure in the headspace caused by the action of the syringe, as shown by the increases of oxygen dissolution into water when pressurising headspaces at air-water interface (Fung 2002). Manual syringe injection favours movement of aroma across the

interface due to pressurisation of the headspace. The effect of increased gas phase compound uptake by a surface can be observed when considering the action of sniffing. The sniff response results in an increase in pressure arising from increases in air flow, consequently, an increased up-take of aroma by an interface is observed owing to the increase in resistance to mass transfer of absorbed aroma from the surface to the air phase (Zhao 2006).

Deriving an expression to describe the quantity of aroma detected in the headspace for the first few seconds after injection of aroma was achieved through taking the ratio of the area under the curves of lipid emulsions relative to water providing a measure of relative headspace intensity (RHI) of an aroma at a lipid interface. RHI can be interpreted as differences in aroma absorbance during the injection event, when RHI is equal to 1, then lipid interfaces absorbed an equal amount of infused aroma to that of water, if RHI is less than 1 then more aroma was absorbed leaving less aroma in the headspace for detection. Finally, if RHI is greater than 1 then less aroma was absorbed by the lipid interface than by water (figure 34). Significant differences in RHI between emulsion only systems were identified by One-way ANOVA and HSD tests for ethyl butyrate, 2-heptanone and 2,5-dimethylpyrazine. RHI significantly increased over the base level of 1 set for water, indicating a decrease in overall aroma absorption (figure 34).

When considering rate of headspace loss, a minimum of one significant difference in k_d exists for each aroma with changes in interface composition, as identified by one-way ANOVA. Honest significant difference test identified and grouped specific inter-aroma differences in k_d (figure 5). Ethyl butyrate persistence decreased significantly when exposed to lipid solutions relative to water solutions as evidenced by the increases in k_d. Ethyl butyrate k_d

increased linearly (R^2 0.91) with increases in lipid concentration from 0 to 20%. Similarly, 2-heptanone experienced a linear increase in k_d (R^2 0.91) with the same increases in lipid content. Effects of lipid increase for 2-heptanone differed to ethyl butyrate with less pronounced changes in rate, with a decreased overall magnitude of change with a maximum rate of 0.01 s^{-1} compared to 0.257s^{-1} for ethyl butyrate. Additionally, 2-heptanone required larger changes in lipid concentration to effect rate significantly after the initial increase in rate observed between 0 and 5% lipid solutions.

No significant correlation was observed between rates of headspace loss and the difference in initial RHI indicating rates of release for is independent of the headspace concentration. Without quantification of overall aroma added to the system it is difficult to ascertain aroma absorbed to the interface during the injection event. The aroma that showed significant different RHI with between different lipid concentrations also displayed two-phase rate behaviour indicating two separate rate events such as rate release from water and a slower rate release from lipid to water before release to the headspace (table 8).

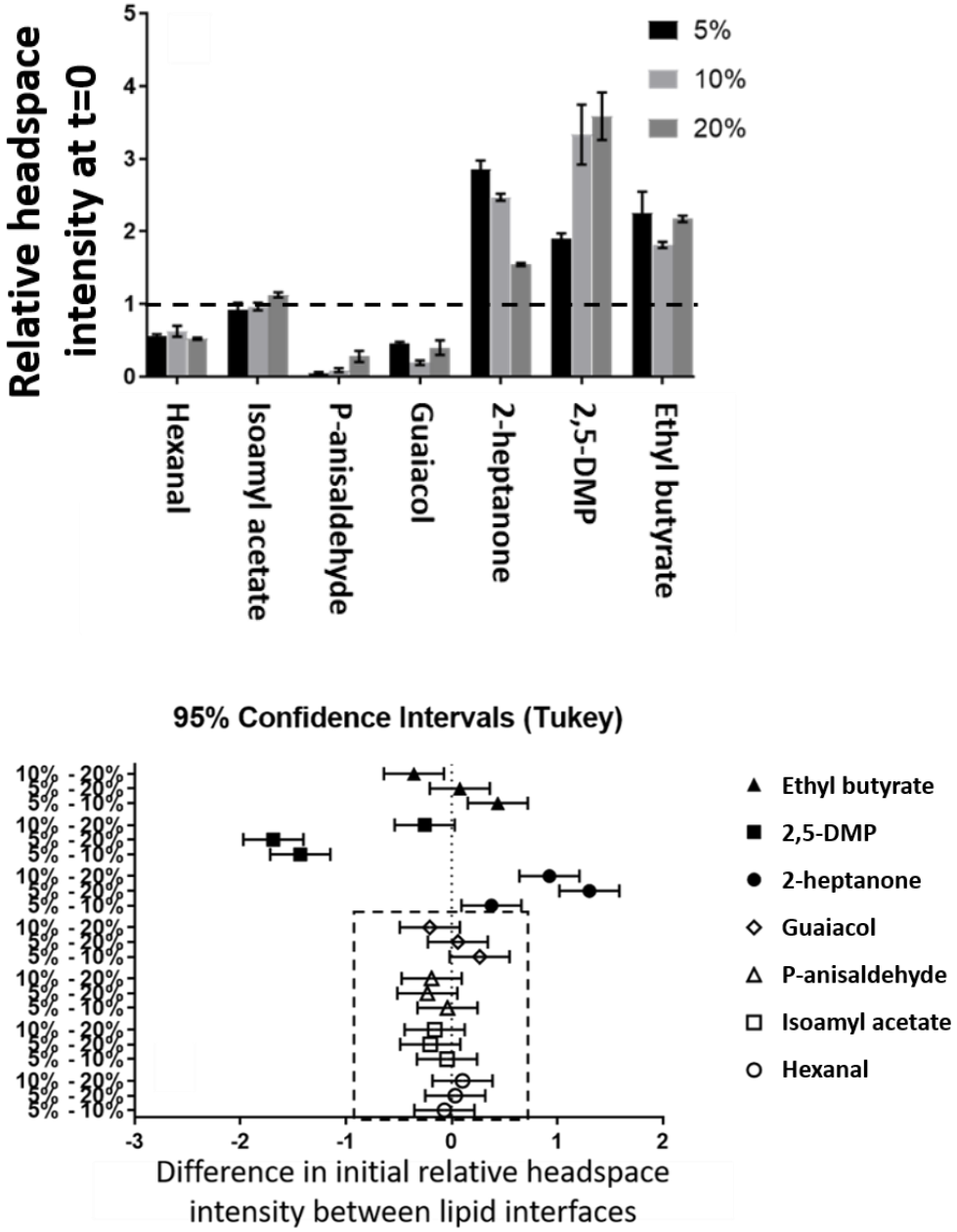

Figure 34 Relative headspace intensities for the initial 3s after infusion into the headspace at 5, 10 and 20% emulsion. Tukey test derived confidence intervals (95%) highlighting significant differences in RHI between interface lipid concentrations. Aroma cosseted by a dotted line are non-significant (P<0.05).

Table 8: Rates of headspace loss of seven aroma compounds after infusion into the headspace of water and oil-in-water emulsions. k_d in bold were calculated by the AiCc test to be better represented by two-phase decay models compared to one-phase decay models. Presented k_d are mean values of three independent repeats of four panellists, standard deviation values represented by column error bars

	0% lipid		5% lipid		10% lipid		20% lipid	
Aroma	AVG k_d s^{-1}	SD	AVG k_d s^{-1}	SD	AVG k_d s^{-1}	SD	AVG k_d s^{-1}	SD
2,5-DMP*	0.009	1.78E-04	0.020	6.92E-04	0.032	6.98E-04	0.042	1.05E-03
Ethyl butyrate	0.034	9.97E-04	0.107	1.00E-02	0.203	1.33E-02	0.250	1.42E-02
Guaiacol	0.033	9.72E-03	0.05	1.52E-04	0.054	2.40E-04	0.043	1.76E-03
2-heptanone	0.024	5.78E-04	0.061	2.77E-03	0.069	2.22E-03	0.096	5.66E-03
Hexanal	0.042	3.78E-03	0.040	6.73E-04	0.030	1.31E-03	0.030	1.53E-03
Isoamyl acetate	0.040	2.67E-03	0.042	2.09E-03	0.039	7.25E-04	0.043	7.39E-04
p-anisaldehyde	0.031	7.51E-04	0.003	9.19E-05	0.004	1.53E-04	0.002	8.50E-05

Significant changes in 2, 5-dimethyl pyrazine persistence relative to a water control required a lipid concentration of 10%. Further increase in lipid concentration to 20% resulted in significant decreases in persistence relative to 10% lipid solutions

Hexanal experienced a significant increase in persistence with increases in lipid concentrations, however, hexanal as a by-product of lipid oxidation is identified in the literature. Likely, the increase in hexanal headspace presence at high lipid concentration interfaces can be attributed to increased lipid oxidation.

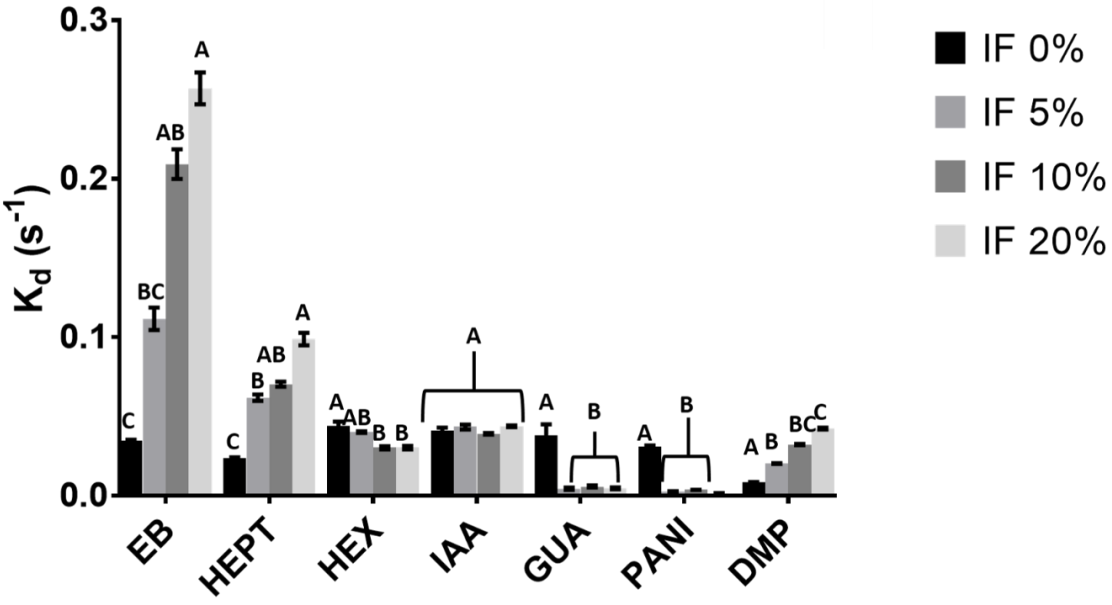

Figure 35 Rate of aroma loss, k_d, for 200s after injection of a quantity of aroma into the headspace of interface ranging from 0 – 20% lipid emulsion. Letters above each column signify inter-aroma significant differences where X = X then P > 0.05 and if X ≠X then P < 0.05. Each column represents means of independent repeats with the standard deviations given by error bars.

PCA accounted for 99.2% of total variation with 97.6% of variation contributed by PC 1 alone. Results confirmed aroma compounds were strongly associated with PC1 suggesting the majority of release is governed by aroma with medium type accounting for a smaller portion of variability. The use of near instantaneous manual injection and the subsequent high pressurisation of the reaction vessel likely lead to the low contribution of surface type to the release behaviour. Subsequent studies (chapter 6 and 7) made use of controlled, automated injection to counter the high pressurisation of experienced by the reaction vessel under manual injection conditions. The minor contribution of surface type on decay rate is not reflected by RHI measurements, where several compounds headspace intensity is significantly greater when lipids are present relative to when no lipids are present.

Investigations into the kinetics of aroma release from a variety of matrices and situations make use of first order model fits to describe initial rates of aroma release (Bylaite *et al* 2005, Ly *et al* 2008, Samavati *et al* 2012). For Investigations into the kinetics of aroma release from water and model custards under simulated mouth conditions (application of a shear rate of 100 s^{-1}), rate of releases was determined to be the initial linear portion of a decay curve, and as such did not factor late stage aroma release (Lubbers and Butler 2010). Second order (two-phase decay) equations have been used in the characterisation of yoghurt retention of saliva, which eschewed initial rate kinetics in favour of a holistic approach which required the incorporation of two rate factors (Marin *et al* 2004).

5.10.1 Relevance of *in vitro* systems to in mouth aroma persistence

Pearson r, correlation analysis of in-mouth k_d and headspace infusion k_d produced several significant correlations. Correlation of in-mouth release of tested aroma from water solutions produced significant correlation between headspace infusion release from 5, 10 and 20% emulsion interfaces, with r values of 0.89 (P = 0.01) for 5%, 0.96 (P = 0.0005) for 10% and 0.95 (P = 0.0013) for 20%.

In mouth aroma release from 5% emulsion solutions significantly correlated with in-mouth release of 10 and 20% emulsion concentrations with r values of 0.95 - 0.98 (P = 0.0001). From table 7, generally, in-mouth release k_d changes little when increasing concentration from 5 to 20%, hence the significant correlation. In-mouth aroma release from 5% emulsions correlated significantly with release from headspace infusion from 5% emulsion interfaces (r = 0.082, P = 0.03). Aroma release from in-mouth 10 and 20 lipid emulsions also correlate significantly with release from headspace infusion 5% systems to a lesser extent with, a marginally r values

of 0.74 (P = 0.05) for 10% and r value of 0.8 (P = 0.03) for 20% interfaces. System correlations are show by a PCA plot in fig 36. PCA procedures performed with in R with visualisation tools from 'factoextra' R packagae. A total of 89.3% of total variation in aroma release in mouth and after headspace infusion for water and emulsion systems. PC1 accounted for the majority of variation k_d, 76.1%. Low concentration emulsion and aqueous in-mouth release are projection along PC1.

Release behaviour of aroma injected into the headspace above 5% emulsion strongly correlates with aroma release from 5, 10 and 20% in mouth release of the same aroma, albeit to a lesser extent for 10 and 20% emulsion interfaces. Headspace injection systems negate any effects of aroma in bulk solution, whilst also mimicking pressured induced dissolution of gas phase molecules into a liquid surface. Interface loading of aroma potentially represents in-mouth phenomena. Consumed water-soluble compounds will experience an increased likelihood of solubilisation into the saliva, the same compound after movement across the air-solution interface after headspace injection in the describe headspace infusion system will show an increased likelihood to solubilise into continuous water phases. Consumed lipophilic compounds will show an increased tendency to interact with hydrophobic regions of the oral mucosa and salivary constituents, the same is true for the infusion system, after partitioning to the liquid phase lipophilic compounds are likely to interact with hydrophobic domains of an interface. Comparison of post infusion release of aroma from water interface with in-mouth aroma releases yielded no significant correlations, only after the inclusion of hydrophobic domains was significant relationship observed. The use of anionic emulsions used in the correct manner

show potential as a low cost, easy preparation mimetic for some in-mouth aroma release processes.

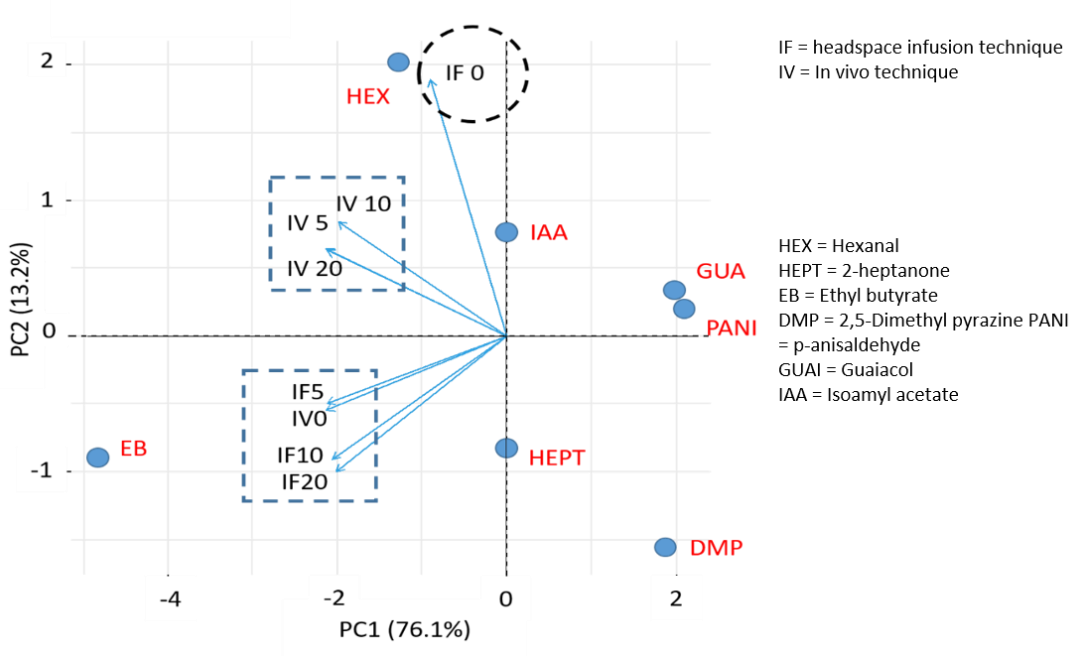

Figure 36 Principle component analysis biplot of k_d for seven aroma and eight interfaces including aroma headspace infusion to water and 5, 10 and 20 emulsions and in-mouth consumption of flavoured water and 5,10 and 20% emulsions. Like surfaces, as identified by correlation, are enclosed in dotted line squares.

5.10.2 Factors effecting headspace stability

Headspace dilution analysis of volatile compound release based upon mass transfer theory features in the literature where the ability to of aroma to replace lost headspace intensity is governed by partitioning affinity of aroma and the hydrodynamic regime aroma is subjected to (Marin & Taylor 1999, Dattatreya *et al* 2002, Marti *et al* 2014 and Bruneel *et al* 2018). If operating parameters are fixed, then mass transfer coefficients can be determined using predicted physicochemical parameters and thus, calculate headspace persistence. This study makes use of the mass transfer models described by Marti and colleagues (2014) who suggest a volatilisation factor (V_f) parameter to characterise the extent of

volatile compound release from an aqueous system in a variety of situations such as aroma release free fall water droplets and polluted ponds. Volatilisation factor equations are of the form (equation 28):

$$V_f = \frac{1000}{\left(\frac{1}{k_H}\right) + \left(\frac{f_r V}{A k_m}\right)} \quad (28)$$

Where V_f is the volatilisation factor (kg/m^3), A is the interface area (m^2), k_m is the mass transfer coefficient (m/s), f_r is the headspace renovation rate (s^{-1}) and V is the headspace volume m^3. Overall, mass transfer coefficients for each aroma are calculable using a two-phase boundary model, where a constant gradient exists at a thin zone near the interface:

$$k_m = \frac{1}{{k_l}^{-1} + \left(k_g k_H\right)^{-1}} \quad (29)$$

Where k_l is the mass transfer coefficient of aroma in water, k_g is the mass transfer coefficient of aroma in air and k_H is the dimensionless Henry's law coefficient.

Estimation of mass transfer coefficient is possible using the following relationship (equation 30):

$$k = k_{ref} \frac{D}{D_{ref}}^{0.67} \quad (30)$$

Where k and k_{ref} are the mass transfer coefficient of interest and k_{ref} is a known reference mass transfer coefficient, such as water in air and D and D_{ref} are diffusion coefficients m^2s.

Theoretical models for the calculation of air-emulsion partition coefficients developed by Buttery *et al* 1997 describe the partition behaviour of aroma between air and emulsion phases as:

$$k_{ae} = \frac{1}{K_{aw}/F_w + F_o/k_{ao}} \qquad (31)$$

Where k_{ae} is the air-emulsion partition coefficient, F_w is the water fraction, K_{aw} is the air-water partition coefficient, F_o is the oil is the lipid fraction and k_{ao} is the air-oil coefficient. Replacing k_H with equation 7 and replacing k with V_f in one-phase degenerated predictive decay curves for the loss of aroma headspace intensity under dynamic dilution conditions at lipid emulsion solution of 5, 10 and 20%. A selection of model fits compared to actual data are shown in figure (figure 37).

One-phase decay fits proved to have limited predictive capability for lipid system under dynamic headspace dilution conditions (figure 37). Further refinements to the model were made to accommodate two forms of aroma headspace intensity decay with time. A semi empirical two-phase decay model, which separates V_f into a component driven by the dilution stream and component driven by mass transfer:

$$\frac{N}{N_0} = (0.5 - f_0)\exp^{(-f_r\, t)} + (0.5 + f_o)\exp^{(-V_{fe}\, t)} \qquad (32)$$

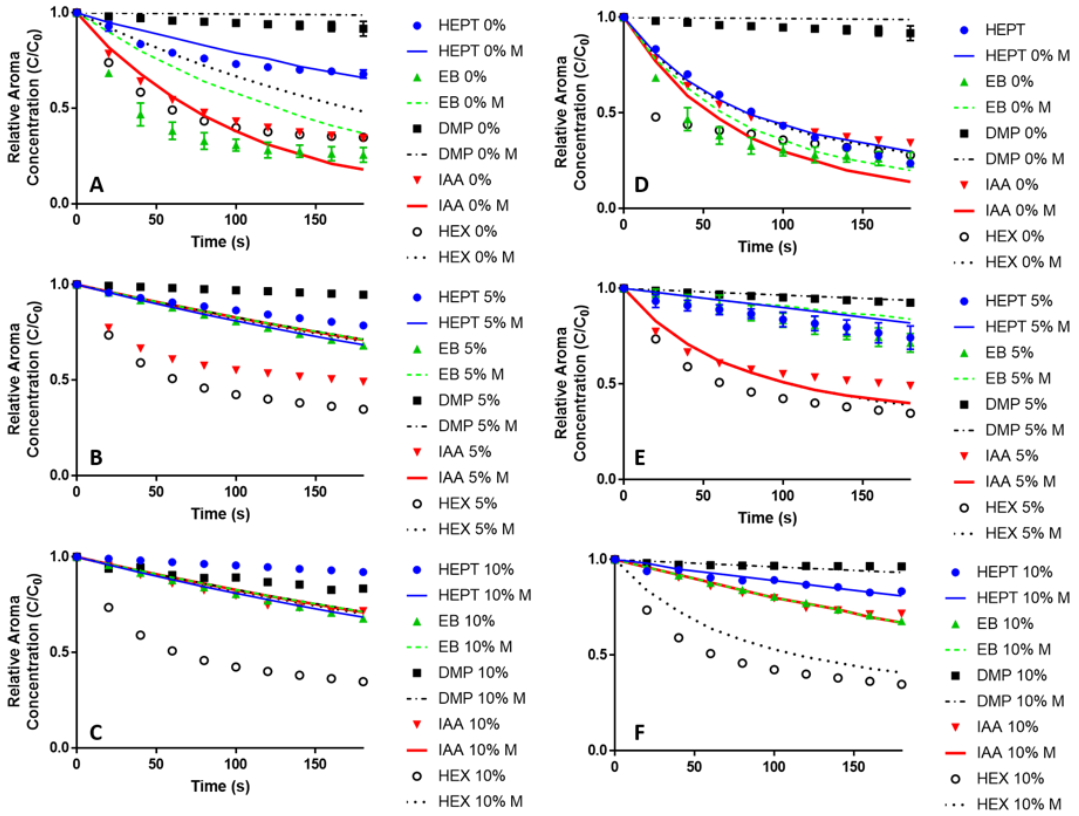

** IAA = Isoamyl acetate, HEPT = 2-heptanone, HEX = Hexanal, DMP = 2,5-dimethyl pyrazine and EB = Ethyl butyrate*

Figure 37 A, B and C: Experimental (symbol) and calculate one-phase decay (line) release curves from different emulsion concentrations under headspace dilution conditions for a selection of aroma compounds. D, E and F: Experimental (symbol) and calculate two-phase decay (line) release curves from different emulsion concentrations under headspace dilution conditions for a selection of aroma compounds. Each data point equates to the mean of three independent repeats with SD represented by error bars.

Where V_{fe} is the volatilisation factor for each solution. The prior knowledge of which aroma decay is two-phase in nature is required hence the model status as semi empirical and are only used for predictive models for aroma already confirmed to be two-phase in nature. The semi-empirical nature of the model limits the predictive nature of the model. However, the model is justified in attempting differentiate between sources of decay types within the systems

under investigation, R^2 fits in excess of 0.97 are promising indicators that the two types of decay present are based upon headspace refresh rates and medium specific partitioning tendency of each aroma (figure 38). Present findings are in line with assertions made in previously cited works on headspace dilution, where air-solution partitioning and headspace refresh rate are the determining factors in aroma headspace persistence.

Predictive models for headspace decay of aroma injected into the headspace of air-water interfaces took the form of either one- or two-phase exponential decay equations. Like dynamic headspace dilution predictive models, empirical identification of decay type (one or two-phase) is required. Interface specific volatilisation factors can predict k and k_{slow}, but currently are unable to predict $\%_{fast}$. Predicted one-phase decay rate constants for aroma headspace persistence after aroma is injected into a 'clean' system are identical to V_f models, with the addendum that aroma total mass transfer coefficient $k_{m,}$ are replaced by aroma in air mass transfer coefficient k_a. Relative headspace concentration at t = x can be calculated with equation 24. Two-phase decay models require additional information for effectively predicting relative headspace concentrations at the above described conditions. Where, for dynamic headspace conditions an approximation of decay components was possible with the rate constant ratios equating to approximately half of the decay component each for aqueous aroma, ratios were then modified for emulsions according to equation 31. Two-phase decay models make use of empirically derived $\%_{fast}$ values for each aroma and system, models are the form (33):

$$k_d = \frac{\%_{fast}}{100} \exp^{(-f_r\, t)} + \left(1 - \frac{\%_{fast}}{100}\right) \exp^{(-V_{fe}\, t)} \quad (33)$$

Quality of model fit for water interfaces given by R^2 values ranged from 0.99 for 2-heptanone to 0.95 for 2, 5-dimethylpyrazine. Similar R^2 ranges were identified for 5% emulsion interfaces (R^2 0.99 for 2-heptanone to 0.95 for p-anisaldehyde) and 10% emulsion interfaces (R^2 0.99 ethyl butyrate to 0.96 for guaiacol)

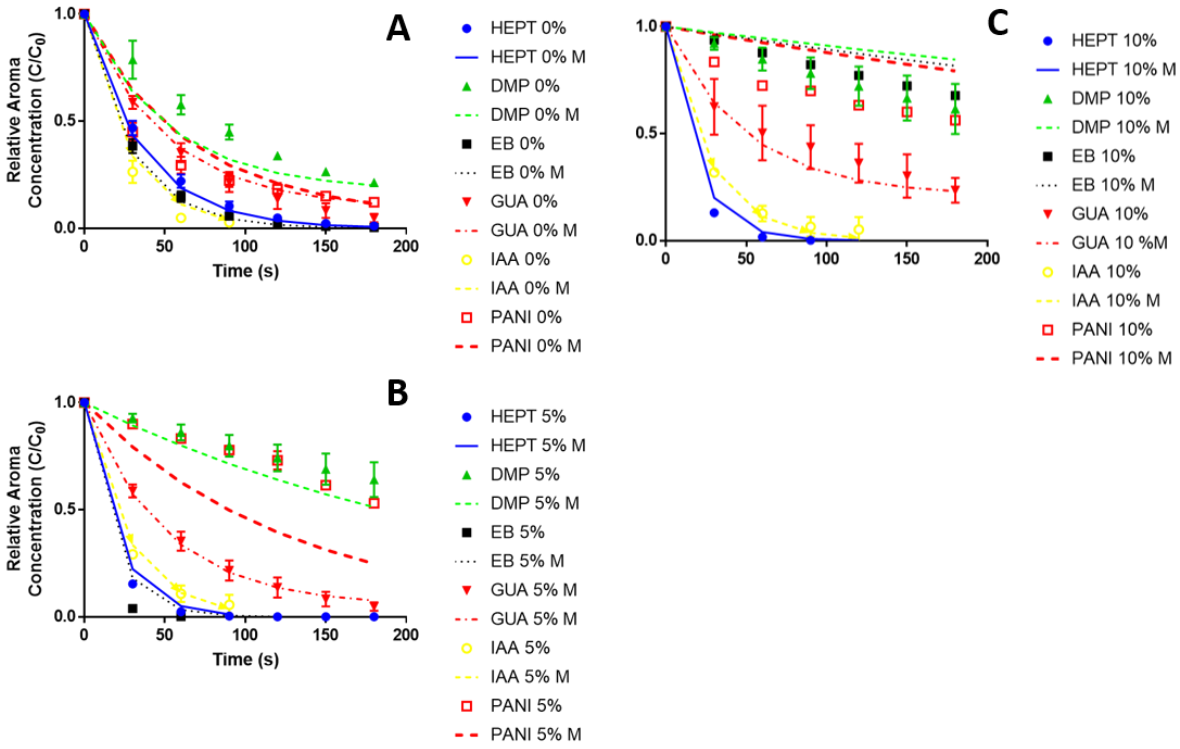

** IAA = Isoamyl acetate, HEPT = 2-heptanone, HEX = Hexanal, DMP = 2,5-dimethyl pyrazine and EB = Ethyl butyrate*

Figure 38 Experimental (symbol) and calculated (line) release curves for a selection of aroma after injection to [A] air-water [B] air-5% emulsion and [C] air-10% emulsion interfaces. Each data point equates to the mean of three independent repeats with SD represented by error bars.

Whilst some success can be claimed in the ability of mass transfer models for establishing rates of aroma loss in one-phase decay system along with the identification of the likely governing factors in two-phase decay systems (refresh rate and solution specific partition coefficients), factors governing percentage of decay period remain obfuscated. Initially, $\%_{fast}$ was thought to be related to k_H but no significant means for determining a relationship was found. Also, model relevance appears to decline when increasing lipid concentration of emulsion solutions beyond 10%.

5.11.1 Conclusions

Presented is the change in aroma persistence when exposed to some form of dilution, either through applied nitrogen flow or exhaled breath. Persistence mechanics of dynamic dilution headspace analysis was unable to estimate, to a significant extent, in-mouth release of aroma after consumption of flavoured water and lipid emulsions.

A novel headspace aroma infusion at water/emulsion interfaces significantly correlated with in-mouth aroma release kinetics after consumption of 5% water and 5% emulsion solutions. Headspace infusion techniques with appropriate interfaces show some promises in contributing to the wider discussion of in-mouth aroma release. Future refinements require consideration of biological factor such as salivary constituents, surface type and oral micro-fauna. Issues related to the manual infusion technique related to the potential of high pressurisation of the reaction vessel were also identified. Over pressurisation of the reaction cell was linked to previous studies related to the increase in volatile compounds movement from the air phase to the solution phase when the headspace is subjected to high pressures.

Attempts to quantify the aroma absorbed/released through RHI highlighted the need for an accurate means of quantifying aroma absorbed and released by future systems.

Chapter 6 - Effects of mucin and shear stress on the absorption and release of volatilised aroma compounds

6.1.1 Introduction

When considering the application of *in vitro* experimental data to the understanding of biological phenomena, *in vitro* ideally should approximate biological conditions. Modelling aroma flux into the surfaces of the oro-nasal cavity (saliva and nasal mucus), need to consider encounters with the biopolymer. Mucin has previously been identified as the key salivary component that is able to significantly effect in-mouth aroma release (van Ruth *et al* 1998).

Mucus layers coating mucosal surfaces such as the oro-nasal cavity, gastrointestinal tracts and respiratory systems perform several roles including lubrication, defence, hydration and access gating to the epithelium (Perez-Vilar and Hill 1999). Of interest to this study is nasal mucus and saliva, which coat the surfaces of the nasal and oral cavities respectively.

Approximately 90% of nasal mucus is water, the remaining component consist of glycoproteins mucins, immunoglobulins, lipids, cellular debris and salts; sodium, potassium, calcium, magnesium, bicarbonate, phosphate and chloride (Bansil and Turner 2006) (Burke 2014). Saliva is a more dilute substance than nasal mucus, comprising of 99% water along with a similar suite of glycoproteins, salts and immunoglobulins (de Almeida *et al* 2008) to that of nasal mucus.

The most abundant proteins present in human saliva include; mucins and acidic PRPs (proline-rich proteins), followed by α-amylase, basic

PRPs and basic proteoglycan. Less abundant levels of antibodies immunoglobulin (Ig) G, secretory IgA and IgM are present along with the enzymes lactoperoxidase and lysozyme and antimicrobial histatins. Nasal mucus protein profiles feature increased levels of lactoferrin, lysozomes and secretory IgA over saliva (Brandão *et al* 2014).

In human saliva, two types of mucin are present, MUC5B and MUC7. The molecular weight of MUC7 (200-250 kDa) is lower than that of MUC5B (>1MDa) and account for up to 26% of saliva protein content (Zalewska *et al* 2000). In human nasal mucus, mucins accounted for approximately 28% of total protein weight. Proteomic analysis of nasal secretions of ten human subjects identified the mucin types MUC5A/C (~640 kDa) and MUC5B (Casado *et al* 2005) (Schomig *et al* 2016).

Nasal mucus layers consist of a periciliary liquid layer approximately 6μm thick covering the nasal mucosa and a mucus layer covering the periciliary layer (Fahy and Dickey 2014). The sum total thickness of both layers is approximately 10-15 μm (Beule 2010).

Rheology describes the flow and deformation of matter. Important to the characterisation of mucus consistency are the rheological properties viscosity and elasticity. Viscosity describes the ability of a substance to resist flow whilst elasticity describes the ability of a gel to return to original dimensions following some form of stress induced change (Lai *et al* 2010). Integration of large biopolymers such as mucins, impart a gel-like structure to mucus which displays heterogeneous viscoelastic properties. Mucus is a non-Newtonian fluid, physical behaviour of non-Newtonian fluids is dependent upon the application of sheer stresses. With increases in shear rates, viscosity decreases in a log linear fashion.

Rheological properties viscosity and spinnbarkeit (a measure of a viscoelastic substances ability to be drawn apart) of 51 subject's unstimulated and chew-stimulated whole saliva content varied according to MUC5B and MUC7 content. With increased levels of MUC5B in unstimulated whole saliva, viscosity increased whilst increased levels of MUC7 in unstimulated whole saliva increased spinnbarkeit levels. Viscosity and spinnbarkeit levels were significantly increased ($P<0.05$) in unstimulated whole saliva over chew-stimulated whole saliva, whilst flow rate were significantly increased in chew-stimulated ($P<0.0001$) whole saliva over that of the unstimulated variety (Inoue *et al* 2008). The action of chew stimulation and the abundance of a mucin type notably affects the rheological properties of saliva, and is therefore, an important consideration when investigating the impact of mucin content on aroma retention.

Interactions between mucin and aroma and the resultant effects on partitioning behaviour has also received attention in the literature. Increased hydrophobic character of ketones and esters with increases in aliphatic chain length were purported to be the reason for reductions in equilibrium partitioning of aroma when in the presence of mucins (Pagès-Hélary *et al* 2014). Aldehydes and ketones experienced reduction in equilibrium partitioning when mixed with artificial saliva systems (van Ruth *et al* 1995, van Ruth *et al* 1999 and Friel and Taylor 2000). The effects of artificial saliva on non-model food systems such as coffee and raw cabbage are significantly modified when each food system meets artificial and ex vivo saliva (Genovese *et al* 2014 and Frank *et al* 2018)

This work differs from previous studies by characterising real time absorption of volatilised aroma compounds by air/water-mucin interfaces, to understand time sensitive aroma partitioning

behaviour of aroma exposed to biological relevant interfaces. The effects of chewing is simulated by the application a mechanical stirrer. Interface undergoing stirring are termed mobile interfaces, whilst un-stirred interfaces are referred to as stagnant interfaces.

The route taken by aroma in this study is analogous to considered retronasal and orthonasal olfaction, where odorant-laden air is transported to the olfactory region.

6.2.1 Materials

Bovine submaxillary mucin, benzaldehyde (≥ 99%), (R)-(+)-Limonene (97%), cis-3-hexenal (≥98%), isoamyl acetate (≥95%), 2-heptanone (≥98%), menthone 90% and ethyl octanoate (≥99%) obtained from Sigma Aldritch (Aldershot, UK).

6.3.1 Method

Interfaces were housed within 200mL PTFE reaction vessels modified with inlet and outlet ports and an additional port for a mechanical stirrer. Headspace volume in the vessel was kept constant at 150mL, the air/water-mucin interfaces area was 7.1cm^2 and solution volume was 50 ml. The mechanical stirrer was present for both stagnant and mobile runs. For mobile runs, mechanical stirrer was in operation pre, post and during aroma infusion, running at 60rpm. Pre trials identified no significant difference in aroma behaviour for 60, 80, 100 and 120 rpm. Stirring rate was kept low as to minimise solution volume increases and alteration of interface surface area through vortex generation.

The following procedure was identical for mobile and stagnant interfaces. A 50 ml/min dilution stream of N_2 was continually passed over the headspace through the inlet port to the outlet port. The outlet port was connected to a Waters prototype APCI-MSMS with an appropriate exhaust for excess N_2. At t = 0 a 50 ml of

equilibrated volatilised aroma was injected by an automated syringe dispenser into the diluting stream pre-reaction vessel at a rate of 50 ml/min for 60s. Aroma passing through the headspace of the reaction vessel was detected by APCI-MSMS operating in multiple reaction monitoring (MRM) mode at aroma specific optimal conditions for collision energy, cone voltage and molecular transitions as outlined in chapter 4. APCI-MSMS sampling rate was 10ml/min and mediated through a heated transfer line housing a silica gas chromatography tube (Phenomenex, Macclesfield, UK). Silica film thickness was 6µm with an internal diameter of 0.32mm. Uniform operating conditions for corona pin voltage (4 kV, positive ion mode), ion dwell time (0.1s) and transfer line temperature (120ºC) were used throughout.

Gas phase aroma samples were prepared by pipetting a quantity of liquid aroma (µl) into 1 litre of distilled water, producing dilute aqueous aroma solutions where 1 µl/L is equal to 1 ppm. 40 ml of dilute aqueous aroma solutions were equilibrated at 70˚C for 3 h in 120ml Schott bottles (Fisher Scientific, Loughborough, UK) modified with an access port. With a Luer lock gas tight syringe, the headspace above the aroma solution was extracted and injected immediately into the dilution stream. Method of aroma introduction was repeatable with minimal standard deviation (< 2%) between repeats.

For each aroma a series of quantification peaks were generated by injection of defined amounts of volatilised aroma directly into the APCI-MSMS source, providing a measure of the signal generated by a known amount of aroma.

Solutions forming the interfaces to be investigated were produced through the addition of defined amounts of mucin to deionised water undergoing magnetic stirring (750 rpm), stirring continued for 30

min after solute addition. 50 mL of solutions were directly decanted into reaction vessels and immediately exposed to testing before discarding. Each individual run used a new interface. In total, four mucin concentrations were considered in this study, a 0% mucin control (deionised water) along with 0.25, 0.5 and 0.75% (w/w) mucin.

6.3.2 Statistical analysis

Triplicate repeats underwent statistical analysis to characterise differences between total aroma released (%) and the rate at which aroma is lost. Significant differences are identified through two-way analysis of variance (ANOVA) procedures and Tukey (HSD) multiple comparisons with a significance value of $P < 0.05$. Principal component analysis (PCA) provided a visualisation of the data to assist with the identification and description of relationships identified by ANOVA. All statistical procedures were conducted in R Studio, scripts are included in appendices.

6.4.1 Results and discussion

6.4.2 Peak characterization

Aroma detection peaks generated by injecting aroma into the headspace of air-solution interfaces consist of several distinct periods. Pre-aroma injection; where no aroma is present in the gas or liquid phase of an interface of interest. After a brief period of base line signal acquisition, a 30mL of volatilised aroma was infused into the headspace above a surface at a constant rate of 30ml/min. At $t = 60$, infusion is halted, dilution of the headspace continues at a rate commensurate with the infusion rate. A lag period of approximately 10s occurs once injection starts before signal increases above baseline levels. Proceeding termination of aroma injection, a second lag period of 1-5 seconds occurs depending upon aroma and surface type.

The decay period is characterised as either, when signal intensity decreases to 10% of Imax or after 300s has elapsed. The infusion period is characterised as time taken for the signal to achieve Imax from a starting point defined as 5% of Imax. Defining the decay period as 300s was taken as a preventive measure against potential machine drift.

For each aroma, a quantification peak (Q_p) is generated by, injecting a defined quantity of aroma at controlled rate into the APCI-MSMS source (figure 39). Quantification peaks produced a measure of the amount of aroma infused into a system and were used to calculate percentage quantity of aroma released by a system, termed REL% (equation 34)

$$\mathrm{REL\%} = \frac{\mathrm{E_p}}{\mathrm{Q_p}} * 100 \qquad (34)$$

Where E_p is the area under the curve for an experimental peak and Q_p is the area under the curve for the quantification peak.

6.4.3 Aroma release percentage

Aroma release percentages from stagnant interfaces are summarised in table 9, aroma release percentages from mobile interfaces are summarised in table 10.

Details of two-way ANOVA with Tukey multiple comparisons are presented in figure 40. Tukey test results are summarised with column annotation indicating inter-aroma variation by group with changes in solution mobility (stagnant and mobile) and mucin concentration (from 0 to 0.75%). When a significant difference is

observed between two columns the letters above each column will be different (i.e. A ≠ A), columns with non-significant difference (P

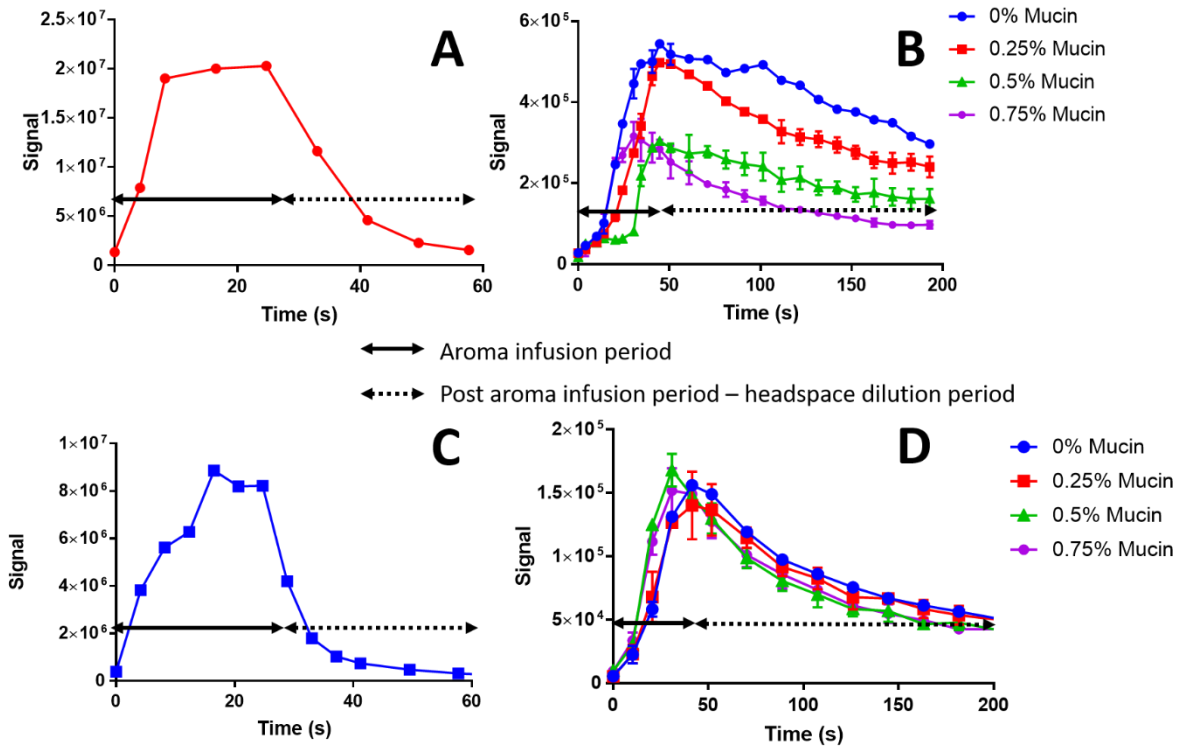

Figure 39 Examples of quantification peaks and experimental peaks for several aroma. [A] (benzaldehyde) and [C] (3-hexenal) quantification peaks. [B] (benzaldehyde) and [D] (3-hexenal) peaks generated by injection of aroma into the headspace above surfaces of 0, 0.25, 0.5 and 0.75% mucin. Injection period and post injection period are annotated with solid and dashed lines. Error bars represent standard deviation between independent repeats.

>0.05) will feature the same letter (i.e. A = A). The letter A is assigned to the highest value.

A minimum of one significant difference was observable for each aroma with differences in exposure conditions, with a general decline in release percentage occurring with increases in mucin concentration under stagnant conditions. Visualisation of aroma and

Table 9: Aroma release percentages from interface containing 0, 0.25, 0.5 or 0.75% mucin. Values are mean of triplicate independent repeats, standard deviation (SD), provides a measure of data spread

	0% Mucin	SD	0.25% Mucin	SD	0.5% Mucin	SD	0.75% Mucin	SD
Ethyl octanoate	56.7	1.0	46.3	4.0	37.3	3.8	19.6	0.5
Isoamyl acetate	24.8	0.2	28.9	5.8	17.6	0.8	18.6	0.9
3-hexenal	10.5	0.1	10.1	0.7	9.4	0.5	9.4	0.6
Menthone	19.9	1.1	14.8	1.4	24.6	0.4	17.8	0.6
Benzaldehyde	21.1	5.5	13.1	0.1	7.9	0.0	6.4	0.2
2-heptanone	21.6	0.8	14.5	3.0	19.5	1.2	13.8	2.1
Limonene	58.3	2.4	53.7	9.7	26.6	0.6	20.2	1.9

Table 10: Aroma release percentages from mechanically stimulated interfaces containing 0, 0.25, 0.5 or 0.75% mucin. Values are mean of triplicate independent repeats, standard deviation (SD), provides a measure of data spread

	0% Mucin	SD	0.25% Mucin	SD	0.5% Mucin	SD	0.75% Mucin	SD
Ethyl octanoate	55.2	6.6	65.8	2.2	35.5	0.7	24.2	2.8
Isoamyl acetate	23.1	0.8	14.4	1.3	19.3	0.1	22.8	4.1
3-hexenal	7.3	1.4	3.7	0.2	5.6	0.0	7.5	0.5
Menthone	12.5	0.1	12.3	0.2	14.4	0.8	15.0	1.0
Benzaldehyde	9.6	0.3	11.3	0.5	6.2	3.9	4.3	0.1
2-heptanone	12.8	0.6	6.4	0.0	8.8	0.6	7.3	2.1
Limonene	96.8	3.2	69.2	4.0	45.3	11.4	19.9	6.8

system differences were aided by PCA of aroma release, which was able to account for 94.7 % of total variation (figure 41). PC 1 accounted for most of the observed variation (~85%). Aroma compounds distribution along PC 1 generally followed a trend of decreasing log P when reading the biplot from left to right. All

interfaces types project into a similar region of PC1 indicating that differences in compound type is the key driver of variation in the percentage amount of aroma released, an observation supported by the significant differences in aroma percentage ($P < 0.05$) as assessed by ANOVA.

Inspection of ANOVA results and the associated Tukey tests for multiple comparisons show that for several compounds, little change is observed between mobile and stagnant interfaces.

Global REL% differences between stagnant and mobile interface were only significant for 2-heptanone and 3-hexenal as described by one-way ANOVA. However, two-way ANOVA procedures indicated a high significance ($P < 0.00001$) of a mucin*mobility interaction term (a term collecting together the four levels of mucin concentration and two levels of solution mobility), meaning a true statistical interpretation of main effects is not possible due to the significance of the interaction term. The significance of the interaction term indicates that aroma persistence is affected by mucin concentration and the mobility the interface.

PC 2 accounted for a total of 10% of observed REL% variation. Aroma release from stagnant interfaces after exposure to 0 and 0.25% mucin concentrations are projected into the same PC space indicating a strong correlation. Interfaces of mucin concentration 0.5 and 0.75% under stagnant conditions project into a similar space along PC 2 indicating a strong correlation. No correlation can be observed between low (0 and 0.25%) and high (0.5 and 0.75%) mucin concentration interfaces under stagnant conditions.

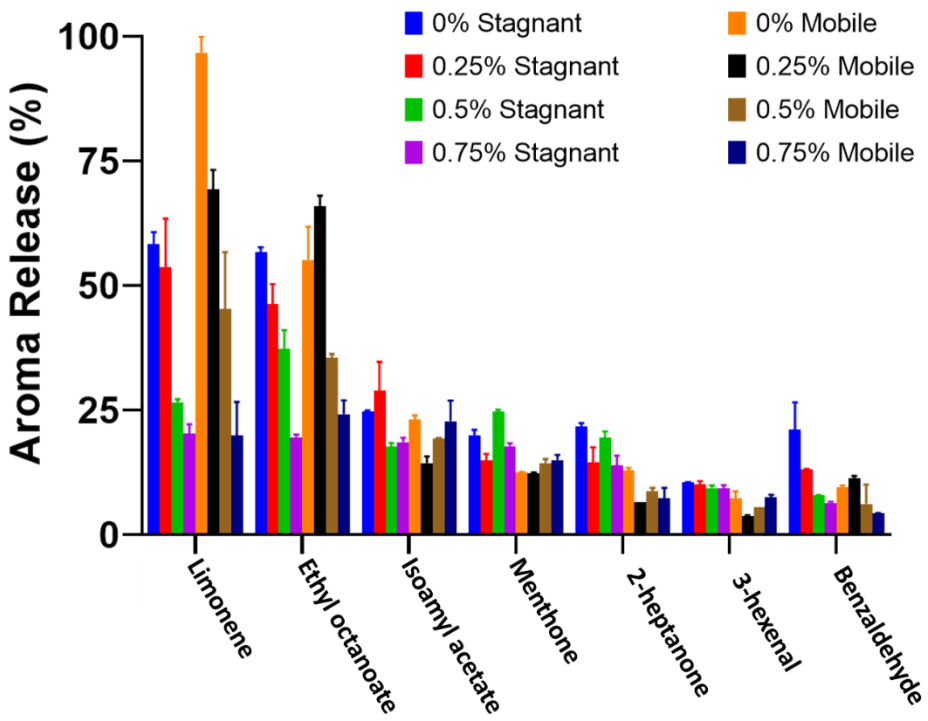

Figure 40 Total percentage of aroma released post aroma infusion into the headspace of interfaces of differing mucin composition and solution mobility. Data presented is the mean of triplicated independent repeats, standard deviations is expressed by column error bars.

For mobile interfaces, 0, 0.25 and 0.5% are correlated well as evidenced by similar projection into PC space, whilst 0.75% mobile interfaces are poorly correlated to other mobile interfaces, indicating distinct aroma release behaviour for this interface. Unique behaviour of aroma at 0.75 mucin interfaces are accounted for by ANOVA results where REL% is statistically distinct for most compounds after exposure to 0.75% mucin interfaces relative to REL% after exposure to other mobile interfaces. For instance, 3-hexenal, limonene and benzaldehyde significantly alter relative to the statistically indistinct REL% between 0.25 and 0.5% mucin mobile interfaces.

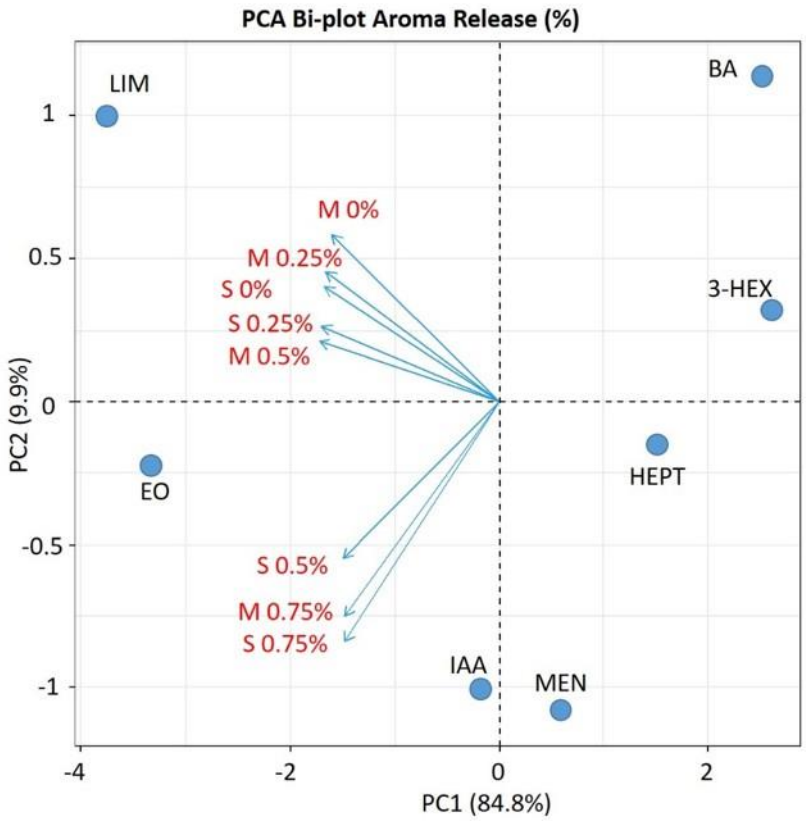

M = Mobile interface, mechanically stirred at 60 rpm

S = Stagnant interface, no applied mechanical stirring

Figure 41 PCA of aroma REL% from mobile and stagnant interface composed of 0, 0.25, 0.5 and 0.75% mucin

Overall, release percentage of hydrophobic compounds ethyl octanoate and limonene (Log P 3.8 and 4) are most affected by inclusion of mucin with the greatest observed change in REL% with change in mucin concentration. Large changes in REL% for the hydrophobic compounds occurred at both mobile and stagnant interfaces. The influence of mucin retention on hydrophobic compounds in dynamic systems conforms to similar findings observed by previous researchers in static systems. Non-polar molecular interactions between aroma and mucin are identified in the literature by (Friel *et al* 2001) where strong interactions were assumed between hydrophobic compounds such as decanal and

cymene resulting in significant reductions in headspace aroma concentrations under equilibrium conditions. Reductions in air-liquid partition coefficients of hydrophobic compounds were also observed by van Ruth and colleagues (2001) when assessing aroma partitioning differences between artificial saliva and water systems.

Retention of aldehydes by interaction with proteins is described in the literature (Hansen and Heinis 1999, Fares *et al* 1998, Kora *et al* 2004), for instance, Weel and colleagues (2011) observed a decrease in aldehyde release under static and dynamic headspace conditions of aqueous solutions containing whey protein relative to water. Benzaldehyde REL% decreased significantly for high (0.5 and 0.75%) mucin concentrations relative to water regardless of solution mobility. Overall REL% of 3-hexenal was decreased significantly under mobile conditions relative to stagnant conditions indicating a weak interaction with mucin when stimulated by an applied force. Under mobile conditions a minor decrease in REL% of 3-hexenal is observed, with the addition of mucin, significant decreases in REL% are observed. If a weak interaction occurs between mucin and 3-hexenal, the increased solubility induced by the mechanical stirrer could relocate mucin-3-hexenal complexes to the bulk solution, 3-hexenal after dissociation will no longer be a constituent of the interfacial boundary layer and, thus, unable to participate in headspace regeneration. Changes in aldehyde REL% with the introduction and increase of mucin to an interface indicates aldehyde-mucin interactions are significant enough to impact on overall aldehyde release when exposed to mucin containing surfaces.

Interactions within aqueous protein solutions have also been shown to reduce release of volatile ketones (Androit *et al* 2000). Ketones menthone and 2-heptanone displayed significant changes in REL%

with exposure to mucin containing interfaces. 2-heptanone, behaved as expected based upon previous studies by Androit and colleagues (2000), inclusion of mucin decreased the headspace presence of 2-heptanone, a situation that was exacerbated by stirring. Menthone behaviour under stagnant conditions appeared to show preferential interactions with 0.25 and 0.75% mucin. Menthone log P of 3 indicates potential for hydrophobic interactions along with ketones suspected ability to interact with mucin however it remains unclear as to why menthone REL% is increased in the mid-tier mucin concentration.

With the application of mixing, possible fates for aroma bound mucin increase; aroma-mucin complexes are moved to the bulk solution whilst the interfacial region is continuously recycling with fresh mucin molecules, mixing also results in increased protein solubilisation and increased protein precipitation to the surface effectively increasing interfacial concentration. An additional consideration of increased proteins solubilisation is an increase in aggregation, potentially leads to increases in viscosity and a movement towards gel like properties (Iyer and Pryzbycien 1994, Biddecombe *et al* 2007, Biddecombe *et al* 2009, Thomas and Greer 2010). This study agrees with static and dynamic headspace findings on hydrophobic interactions between aroma and mucin. Limonene and ethyl octanoate REL% are significantly modified when exposed to increasing concentrations of mucin. Such observations could be interpreted shear rate induced changes in partitioning behaviour. Limonene and ethyl octanoate experienced significant increases in REL% after exposure to mixed surfaces. Aroma forced into the interface by action of the automated syringe were in turn forced out by the mechanical stirrer post infusion as indicated by the increase in REL% for ethyl octanoate and limonene when comparing

identical interface types under differing rates of solution mobility. Interestingly, increasing mucin concentration beyond 0.25% reduced the ability of the mechanical stirrer to induce release of ethyl octanoate and limonene release. Only small differences in REL% for 0.5 (ethyl octanoate) and 0.75% mucin (ethyl octanoate and limonene) were observed.

The physicochemical parameters of limonene and ethyl octanoate describe water insoluble hydrophobic compounds with relatively high air-water partition coefficients. Such compounds would show a tendency to rapidly exit the water phase with application of driving force. The inclusion of mucin reduced REL% under stagnant conditions. With the increase in mucin solution concentration and the increase in mechanically driven solubility of mucin likelihood of limonene and ethyl octanoate encountering mucin significantly reducing the REL%.

6.5.1 Aroma releases kinetics

6.5.2 Aroma release rate

Accessing the release kinetics of aroma from mucin containing interfaces provides additional information to aroma release behaviour. Rate of Loss of aroma for 300s post aroma injection is given by the variable k. Aroma concentrations are expressed relative to normalised Imax values, where Imax = to 1. All other values are expressed relative to the normalised Imax.

Aroma releases curves follow the form of an exponential decay curve. When assessing rates of release, data can be linearized either by logarithmic transformation or by taking the reciprocal of the y-axis data. Line fit quality, as expressed by the regression coefficient (R^2), varied in quality depending upon the interface, applied transformation and aroma. R^2 values ranged between 0.75 to 0.99. Line estimation software Prism 7 (Graphpad Software, California,

USA) automatically calculated line of best fit based on one-phase and two-phase decay equations. One-phase decay models are of the form (equation 35):

$$\frac{N}{N_0} = \exp^{-kt} \tag{35}$$

Where N is the level of aroma in the headspace at t = x, N_0 is the aroma level in the headspace at t = 0. Time is given by t (s) and k is the rate constant (s^{-1}). Two-phase decay models are given by (equation 36):

$$k_d = P_f \exp^{(-k_{fast}\, t)} + P_s \exp^{(-k_{slow}\, t)} \tag{36}$$

$$P_f = N_0 \frac{P_f}{100} \tag{36a}$$

$$P_s = N_0 \left(1 - \frac{P_f}{100}\right) \tag{36b}$$

Where P_f is the percentage amount of time spent in fast decay whilst P_s is the remainder of the percentage amount of time spent in slow decay, k_{fast} is the rate constant for fast decay (s^{-1}) and k_{slow} is for the rate constant for slow decay (s^{-1}).

Two-phase decay equation are based up the principle that two distinct decay processes are occurring simultaneously. In context of the system, physical process effecting the presence of an aroma in a headspace can be postulated.

For the purposes of statistical comparison between two methods, a single descriptive term to describe two-phase rate decay was

achieved by combination of rate constant of the fast decay period, k_{fast} and the rate constant of the slow decay period (equation 37)

$$k = (k_{fast} * \frac{P_f}{100}) + (k_{slow} * \frac{P_s}{100}) \quad (37)$$

The term k is the sum of the k_{fast} and k_{slow} and the respective contribution of each period to the total decay period. Rate decay constants were calculated encompassing Imax to 10% of total Imax (or 200s).

Table 11: Summary of Regression coefficient for data transformation and non-linear model fits for ethyl octanoate and benzaldehyde

Aroma/Interface	Fit type	Stagnant				Mobile			
		Mucin 0%	Mucin 0.25%	Mucin 0.5%	Mucin 0.75%	Mucin 0%	Mucin 0.25%	Mucin 0.5%	Mucin 0.75%
		R2							
	log10(A)	0.97	0.97	0.99	0.93	0.96	0.98	0.97	0.97
Ethyl octanoate	1/(A)	0.96	0.96	0.95	0.93	0.9	0.92	0.94	0.92
	One-phase	0.97	0.98	0.97	0.97	0.96	0.96	0.98	0.97
	Two-phase	0.99	0.99	0.99	0.99	0.99	0.99	0.99	0.99
	log10(A)	0.95	0.95	0.94	0.96	0.95	0.88	0.88	0.84
Benzaldehyde	1/(A)	0.98	0.99	0.96	0.95	0.98	0.97	0.98	0.98
	One-phase	0.97	0.96	0.95	0.94	0.98	0.94	0.93	0.9
	Two-phase	0.99	0.98	0.97	0.99	0.99	0.99	0.99	0.99

Bold values indicate candidate decay curves where two-phase decay models were the preferred analysis

When calculating best lines of fit of different models, Prism 7 includes an option to statistically compare the fits of two models using Akaike's method to determine a percentage likelihood that a model for a set of data is correct. Prism reports corrected AIC value

as a percentage, for this study, simpler one-phase decay models were selected as the default option unless returned AIC values were ≥90% in favour of using the more complex two-phase decay model. This precautionary step was taken to avoid over fitting of data by needlessly using complex models when simpler models were sufficient.

Small values of k maintain a greater presence in the headspace whilst large k values decline at increased rates. Calculated k_d provides a measure of aroma persistence when presented with interfaces composed of differing mucin concentrations. For example, Menthone k (-0.0044 s^{-1}) from 0% mucin systems relative to menthone k (-0.0048 s^{-1}) from 0.5% mucin systems results in a difference of 18% less aroma lost from the headspace after 90s.

Two rate constants are considered in this study, k, where aroma concentrations are expressed as percentages relative to a quantification peak and k_d where concentrations are normalised to 1.

Rate constant k was expected to highlight system to system differences such as significant differences in rate kinetics between aromas. Concentration dependant k_d was expected to highlight inter-aroma differences with changes in interface type.

A two-way ANOVA was carried out on k and k_d of headspace aroma post infusion for each tested compound. Significant differences with changes in solution mobility and composition were identified for all aroma for both rate calculation methods (table 12). For both methods of determining rate constant, interaction terms were only significant for isoamyl acetate (k and k_d) and 3-hexenal (k) and ethyl octanoate (k_d).

Table 12: Statistical analysis ANOVA two factor with interaction

Aroma	Model factor	k_d		k	
		F	Pr(>F)	F	Pr(>F)
3-hexenal	Mucin	18.1	**0.001**	7.8	**0.016**
	State	9.7	**0.009**	5.2	**0.042**
	Mucin:State	8	**0.015**	2.9	0.116
benzaldehyde	Mucin	2	0.181	3	0.109
	State	7.2	**0.02**	16.2	**0.002**
	Mucin:State	0.7	0.404	1.7	0.212
Ethyl octanoate	Mucin	22.9	**0.0004**	11.8	**0.005**
	State	41.8	**<0.00001**	7.9	**0.016**
	Mucin:State	7.5	**0.018**	0.6	0.455
2-heptanone	Mucin	6.6	**0.025**	3	0.108
	State	3.13	0.102	55.5	**<0.00001**
	Mucin:State	0.61	0.449	0.1	0.754
Isoamyl acetate	Mucin	28.8	**<0.00001**	25.8	**0.001**
	State	7.8	**0.017**	11.5	**0.005**
	Mucin:State	9	**0.011**	5.5	**0.037**
Limonene	Mucin	13.78	**0.003**	7.2	**0.02**
	State	0.94	0.352	4.8	**0.049**
	Mucin:State	0.31	0.586	0.3	0.622
Menthone	Mucin	9.6	**0.009**	10.1	**0.008**
	State	67.4	**<0.00001**	89.2	**<0.00001**
	Mucin:State	1.4	0.25	1	0.337

Significant P values are in bold

Assessing decay curves provides information on the behaviour of an aroma in different systems. Ethyl octanoate is a lipophilic aroma (log P 3.8), during the infusion process, ethyl octanoate favourably absorbs to stagnant high mucin concentration (0.75%) interfaces, as evidenced by the low concentration of aroma in the headspace after the infusion process (approximately 6%) relative to water

interfaces under stagnant conditions (approximately 11%) (Figure 42a). As discussed in chapter 5 and as seen in the findings of steady state dynamic headspace studies (Carey *et al* 2002, Weel *et al* 2004, Muñoz-Gonzalez *et al* 2014), maintenance of a large headspace concentration under dilution requires a large movement of aroma from interface to headspace. With inspection of normalised headspace rates of decay, ethyl octanoate differences in persistence between stagnant water and 0.75% mucin interfaces are non-significant, loss of aroma is equal in rate but with a difference in intensity. The decrease in headspace intensity of ethyl octanoate indicates an interaction with mucin, less ethyl octanoate is released to the headspace. The statistically identical rate kinetics of ethyl octanoate at water and mucin 0.75% (stagnant) interfaces indicate, that mucin interactions are non-reversible (for the experimental time course) and released ethyl octanoate detected in the headspace is released from water, with the only difference being that ethyl octanoate interactions with mucin reduce ethyl octanoate in water available for release.

Applying mechanical shear rate to water and mucin 0.75% solutions results in increased ethyl octanoate initial concentration in the headspace, with headspace concentrations of ~20% at water interfaces and ~12% at 0.75% mucin interfaces. In each case, initial headspace concentration is increased twofold relative to stagnant interfaces. Under mechanical stirring, increased mucin solubility increases aroma-protein encounters, this situation is reflected in the different decay rates observed for ethyl octanoate at 0% and 0.75% mucin under mobile conditions. Increased mucin mobility results in a significant increase in rate of ethyl octanoate decay at 0.75% mucin interfaces relative to water interfaces under mobile conditions. Ethyl octanoate is driven out of solution by

mechanical stirrer but when high concentrations of mucin are present, loss of aroma is to the headspace is mitigated by increased mucin mobility. If mucin-ethyl octanoate encounters were not increased, rate of decay would be identical between water and mucin as is observed for the same aroma and interfaces under stagnant conditions. ANOVA confirms a statistically significant interaction between mucin and solution mobility for ethyl octanoate. Similar situations are observable for isoamyl acetate which also featured a statistically significant interaction between mucin concentration and solution mobility.

For menthone, a clear distinction can be observed in the decay rates at low (0 and 0.25%) and high (0.5 and 0.75%) mucin concentrations, (figure 42b). At low mucin concentrations under stagnant conditions release behaviour of menthone appears to be more sensitive to effects of concentration with rapid rates of decay observed at high mucin concentration because mass transfer rates are insufficient to maintain the initial higher concentrations of menthone. Conversely, persistence of menthone at low mucin concertation is increased albeit with reduced headspace concentration. Menthone post infusion release behaviour appears to be modulated by the air-solution partition coefficient rather than direct interactions with mucin.

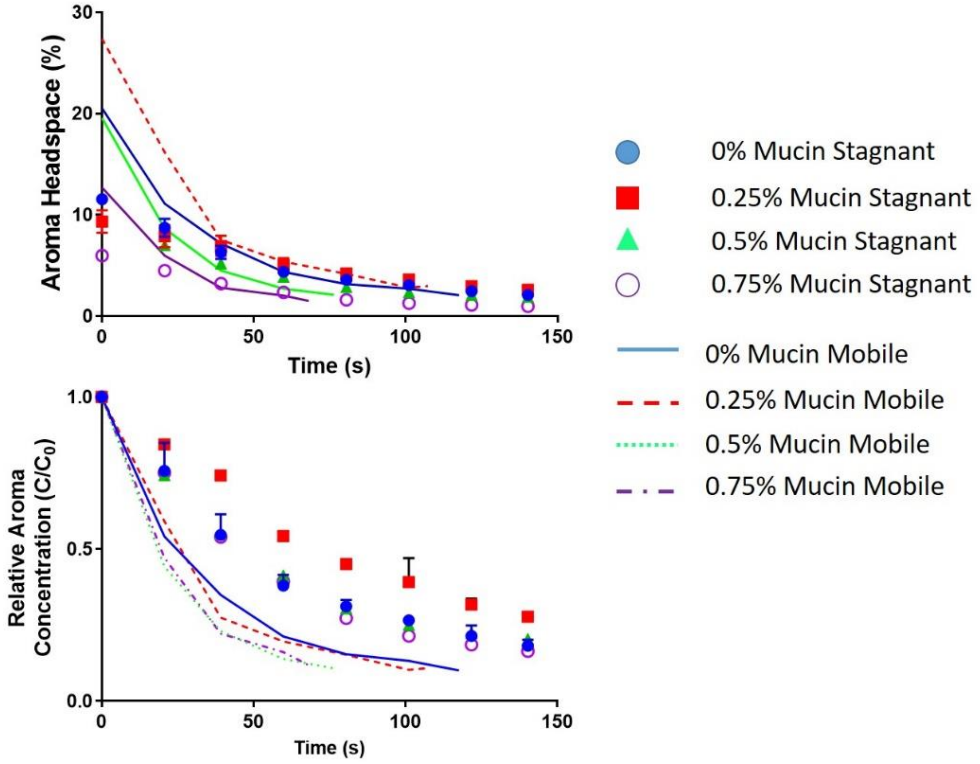

Figure 42 Ethyl octanoate release curves from stagnant and mobile solutions containing 0, 0.25, 0.5 and 0.75% mucin. [Top], concentration expressed relative to a quantification peak and [Bottom] concentration normalised to a maximum of 1. Mean data presented from three independent repeats; error bars correspond to standard deviation between repeats

From inspection of the decay curves it becomes apparent that the absorption and release of aroma with inclusion of mucin produces variable aroma specific behaviour, what follows is an attempt to conflate aroma behaviour with physicochemical parameters.

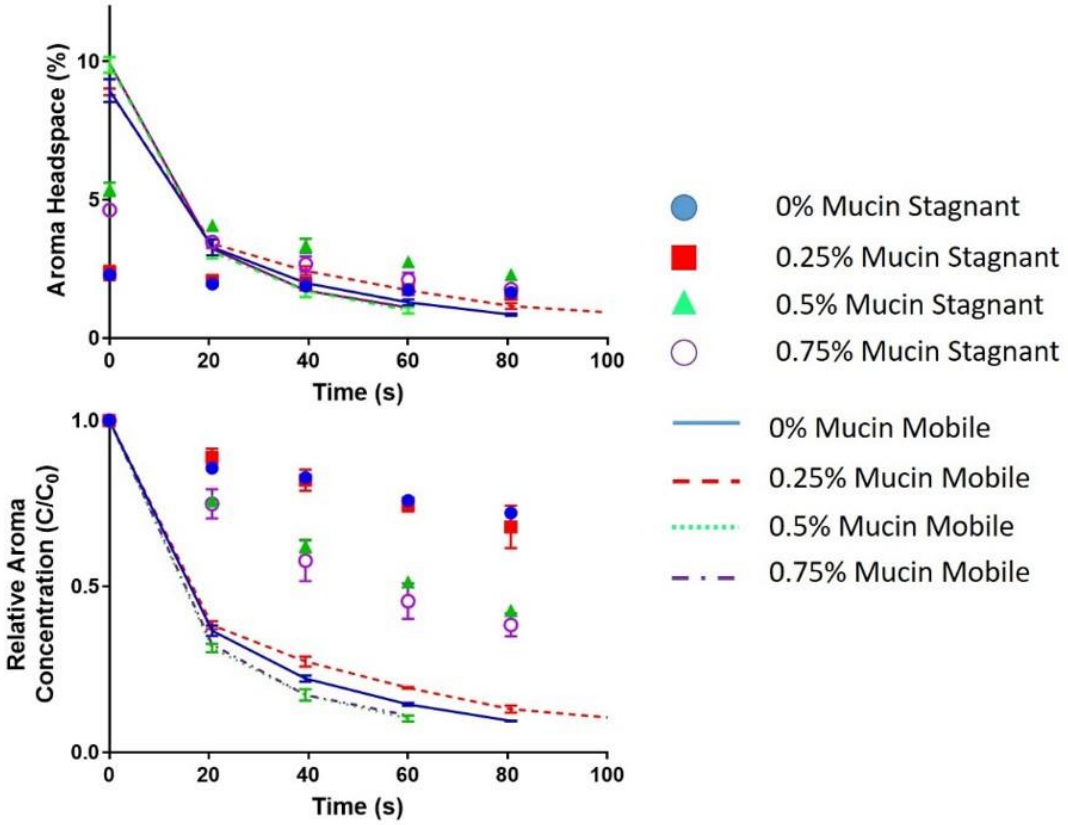

Figure 43 Menthone release curves from stagnant and mobile solutions containing 0, 0.25, 0.5 and 0.75% mucin. [Top], concentration expressed relative to a quantification peak and [Bottom] concentration normalised to a maximum of 1. Mean data presented from three independent repeats; error bars correspond to standard deviation between repeats

6.5.3 Factors governing headspace persistence

Pearson r analysis calculated significant correlations between aroma REL% and aroma Log P for all interfaces. Mobile 0.5% mucin interfaces featured the strongest correlation with an r value 0.96 and R^2 of 0.92 (P = 0.0007), whilst the weakest correlation of 0.83 was observed for mobile 0.75% mucin interfaces with r value of 0.8 and R^2 0.7 (P = 0.02). Significant correlation of aroma REL% with log P indicates that hydrophobic interactions govern most of the release behaviour of aroma at water-mucin interfaces (Figure 43).

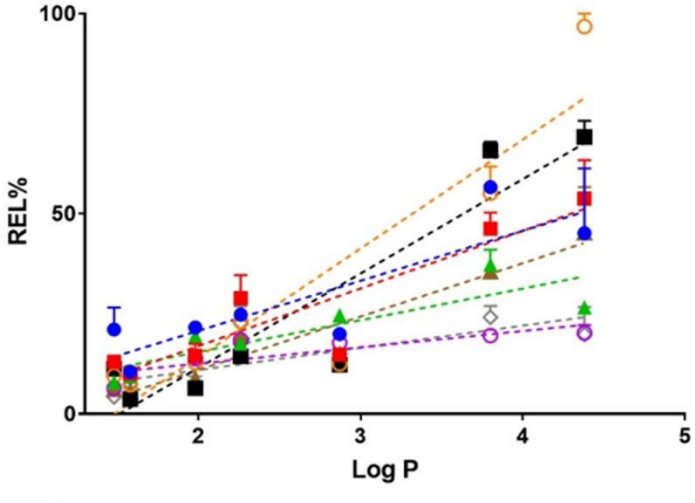

	r	R^2	P
0% Mucin Stagnant	0.86	0.74	0.0135
0.25% Mucin Stagnant	0.91	0.83	0.0043
0.5% Mucin Stagnant	0.86	0.75	0.0121
0.75% Mucin Stagnant	0.84	0.71	0.0179
0% Mucin Mobile	0.91	0.83	0.0044
0.25% Mucin Mobile	0.92	0.85	0.0029
0.5% Mucin Mobile	0.96	0.93	0.0005
0.75% Mucin Mobile	0.76	0.58	0.0464

Figure 44 Pearson r correlation of Log P with aroma REL% for water and mucin interfaces under stagnant and mobile conditions. Means of three independent repeats presented with variation indicated by error bars

The literature states that the ability to of aroma to replace lost headspace intensity is governed by partitioning affinity of aroma and the hydrodynamic regime aroma is subjected to. Mass transfer models have seen some success in describing loss of aroma in isolated, dynamic systems. (Marin & Taylor 1999, Dattatreya *et al* 2002, Marti *et al* 2014 and Bruneel *et al* 2018). If operating parameters are fixed, then mass transfer coefficients can be determined using predicted physicochemical parameters and thus,

calculate headspace persistence. This study makes use of the mass transfer models described by Marti and colleagues (2014) who suggest a volatilisation factor (V_f) parameter to characterise the extent of volatile compound release from an aqueous system in a variety of situations such as aroma release free fall water droplets and polluted ponds. Volatilisation factor equations are of the form (equation 38):

$$V_f = \frac{1000}{\left(\frac{1}{k_H}\right) + \left(\frac{f_r V}{A k_m}\right)} \quad (38)$$

Were V_f is the volatilisation factor (kg/m^3), A is the interface area (m^2), k_m is the mass transfer coefficient (m/s), f_r is the headspace renovation rate (s^{-1}) and V is the headspace volume m^3. Overall mass transfer coefficients for each aroma are calculable using two-phase boundary models (Welty *et al* 2015), where a constant gradient of mass transfer exists at a thin zone near the interface (equation 39):

$$k_m = \frac{1}{{k_l}^{-1} + \left(k_g k_H\right)^{-1}} \quad (39)$$

Where k_l is the mass transfer coefficient of aroma in water, k_g is the mass transfer coefficient of aroma in air and k_H is the dimensionless Henry's law coefficient.

Estimation of mass transfer coefficient is possible using the following relationship (equation 40):

$$k_m = k_{ref} \frac{D}{D_{ref}}^{0.67} \quad (40)$$

Where k_m and k_{ref} are the mass transfer coefficient of interest and k_{ref} is a known reference mass transfer coefficient, such as water in air and D and D_{ref} are diffusion coefficients m^2s.

An alternative calculation of mass transfer coefficient was proposed by Banavara and colleagues (2002) based aroma permeability to an air-water interface (equation 41):

$$P_b = D_{air} \frac{\alpha^2}{V_f} \sqrt{\frac{VP}{S}} \quad (41)$$

Where P_b is permeability, D_{air} is aroma diffusivity in air (m^2/s), V_f is the volumetric flow rate of dilution stream (m^3/s), VP is aroma vapour pressure (mm Hg at 25°C), S is aroma water solubility (mg/L) and α is calculated from film theory of mass transfer, this study makes use of the value α = 0.67, quoted by Marti and colleagues (2014). Mass transfer coefficient can then be calculated using dimensionless Reynold's number and Schofield number (equation 42):

$$k_m = \frac{0.026\ Re^{0.5} Sc^{0.34}}{P_b} \quad (42)$$

Significant correlation ($r = -0.9$, $R^2 = 0.81$, $P = 0.006$)was achieved between $k_{\%}$ and k_N of mobile water interface with k_m (equation 38) where k_m is calculated by equations 41 and 42.

Significant correlation between $k_{\%}$ and V_f for stagnant water interface was achieved $k_{\%}$ and V_f with Pearson r values of -0.9 and R^2 of 0.81 ($P = 0.006$). When correlating K_m with k% for mobile water interfaces (again, k_m is calculated from equations 41 and 42) correlation were less significant with Pearson r values of 0.8 and R^2 values of 0.6 ($P = 0.035$).

Correlation between k_N (where aroma concentrations are normalised to a maximum of 1) for stagnant water interfaces with the V_f produced significant correlations with Pearson r values of -0.95 and R^2 of 0.89 ($P = 0.002$). Mobile water interface $k_{\%}$ were not significantly correlated with V_f. However significant correlations between k_n of mobile water interface are significant if k_m is calculated using equation 39, Pearson r values of -0.98 and R^2 of 0.96 ($P < 0.0001$).

Significant correlation between mucin and stagnant k_N interfaces of 0.5 and 0.75% mucin interfaces with P_b Pearson r values of 0.89 (0.5%) and 0.89 (0.75%) and R^2 of 0.79 (0.5%, $P = 0.007$) and 0.77 (0.75%, $P = 0.008$).

Significant correlation between mucin and stagnant $k_{\%}$ interfaces of 0.25, 0.5 and 0.75% mucin interfaces with P_b Pearson r values of 0.78 (0.25%), 0.89 (0.5%) and 0.85 (0.75%) and R^2 of 0.6 (0.25%, $P = 0.04$), 0.73 (0.5%, $P = 0.014$) and 0.81 (0.75%, $P = 0.03$).

6.6.1 Conclusion

Headspace concentrations infused aroma at t = 0 were greater at mobile interfaces relative to stagnant interface for the same aroma. Solution mixing by the action of a mechanical stirrer disrupts the ability of aroma to replenish the headspace resulting in large effluxes of aroma to the headspace positively affecting decay rates. The inclusion of mucin increased the headspace destabilisation by shear rate for hydrophobic compounds likely through increased mucin solubility increasing mucin-aroma interactions. Inclusion of mucin regardless of solution mobility generally, significantly affected the release rate of aroma and the quantity of aroma released to the headspace post infusion. Modified models describing release of volatiles from water through mass transfer process produced significant correlations with aroma release data for water interfaces of this study indicating mass transfer governs headspace persistence of aroma exposed to water surfaces.

Post infusion release of aroma from stagnant mucin interfaces are likely governed by ability to permeate the interface. Permeability is based upon volatility; thickness of the boundary layer and the solubility od an aroma compound in water (Log P derived model of solubility).

Aroma REL% for the majority of mucin containing interfaces correlated well with Log P values, indicating hydrophobic interactions were the main influencers on total aroma released during the aroma infusion and post aroma infusion.

Future work needs to consider the saturation behaviour to fully understand net movement of aroma exposed to air-solution interfaces.

Chapter 7 - Salt-induced modulation on mucin properties and the implications on aroma absorption and release

7.1.1 Introduction

This chapter represents an evolution of the foundational mucin work outlined in chapter 6 by moving towards a biologically relevant system with the introduction of salts.

Mucins of saliva and nasal mucus exist in the presence of a variety of salts, including sodium, potassium, calcium, magnesium, bicarbonate, and phosphates. Bicarbonates and phosphates function as buffers, maintaining pH levels whilst calcium and phosphates work collaboratively with proteins as an anti-solubility factor preventing the demineralization of teeth (Humphery *et al* 2001).

Bile salts, such as tetrachlorate, binding with bovine submaxillary mucin (BSM), porcine gastric mucin (PGM) and rat intestinal mucin (RIM) as identified by a centrifuge/HPLC method, is theorised to be an interaction between bile salt micelles and hydrophobic mucin domains and through interactions with carbohydrate side chains. PGM bound less of the three tested bile salts, taurocholate, taurodeoxycholate, taurochenodeoxycholate, than either BSM or RIM. Amino acid analysis characterised PGM as possessing 2-3 times less hydrophilic amino acid content to that of BSM and RIM. The increase in hydrophobicity through reduction of hydrophilic content, is the suspected reason for increases in the level of bile salt-mucin binding (Weidmann *et al* 2004). The observable increased affinity of submaxillary mucin for non-polar compounds informed the choice of BSM over the PGM used in artificial saliva compositions in other studies (van Ruth *et al* 2009).

Potential salt binding/interactions sites of bovine gallbladder mucin (BGM) are evident in the literature BGM binds Ca^{2+} to a high affinity at a neutral pH, binding affinity is reduced when pH is reduced. The usual calcium bindings sites (likely carbonyl groups) become protonated as hydronium ion concentration increase with decreases in pH. Calcium bound BGM display an increased affinity for bilary lipids than non-calcium bound BGM. Increasing the hydrophobic character BGM promoted non-polar interactions between hydrophobic bilary lipids (Nui *et al* 1990a).

A study performed in the same laboratory as the current study, using similar APCI-MSMS techniques, described the effects salt-mucin complexes have on the equilibrium headspace of several aroma compounds. Aqueous solutions consisting of mucin-salivary salt complexes aroma partitioning behaviour significantly differed for the same aroma compounds when compared to water and water-mucin solutions. Hydrophobic compounds were affected to a greater extent than hydrophilic aroma compounds (Friel and Taylor, 2001).

Comparative studies of artificial and human saliva showed no significant differences when assessing the differences in partitioning behaviour of several tested aroma compounds (van Ruth and Roozen, 2000; Friel and Taylor, 2001). Artificial saliva formulations consisted of salivary salts, mucin and amylase, non-significance in the partitioning behaviour between artificial saliva and human saliva essentially eliminated other salivary constituents as contributing to significantly to the modulation of aroma headspace release.

Discussed studies have shown the ability of calcium and other salivary salts ability to affect the availability of binding sites of various forms of mucin and in turn, affecting mucin specificities, even affecting functions of mucin. Calcium bound mucin provides a

seeding area for the crystallisation of cholesterol by providing a stable hydrophobic area (Nui *et al* 1990b)

This study makes use of an ultra-analytical centrifuge to understand the effects caused by addition of salt whilst APCI-MSMS is used to characterise the real-time impact of mucin, salt and mucin-complexes have on the absorption and release of aroma.

7.2.1 Materials and methods

Interface preparation was based upon the artificial saliva recipes of van Ruth (2001) and Friel (2001). Solutions composed of either bovine submaxillary mucin (henceforth referred to as mucin) and or salivary salts; calcium chloride dehydrate (2.99 mmol); sodium chloride (15.00 mmol); sodium bicarbonate (61.9 mmol); potassium phosphate dibasic trihydrate (5.99 mmol); and potassium chloride (6.39 mmol). Sodium azide (7.69 mmol) was added to prevent microbial growth. Mucin concentration was kept within the biologically relevant levels quoted in the above study of 0.25%. Solution creation entailed the addition of mucin or salt to diluted water undergoing magnetic stirring (750 rpm). Stirring continued for 30 min after solute addition. When mucin and salt were required, salt was added before mucin. 10ml of solutions were directly decanted into modified reaction vessels and immediately tested before discarding. Each individual run used a new interface.

Interfaces are assigned a code based upon the constituents contained, M_X indicates mucin dissolved in water, S_X indicates salivary salts dissolved in water and MS_X:X, indicates a mixture of salivary salts and mucin dissolved in water. X can be 0, 0.5 or 1 depending on the concentration of constituent present, 0 equals control water interface, 0.5 indicates half of the maximum concentration of components (concentrations used detailed in method) and 1 indicates full concentration present. For example,

MS _0.5:1 refers to a mucin-salt mixture where mucin is present at half maximum concentration whilst the maximum concentration of salivary salts is present as indicated by 1. All products were obtained from Sigma Aldrich (Aldershot, U.K), unless stated otherwise.

Interfaces were housed within PTFE reaction vessels modified with inlet and outlet ports. Headspace volume in the vessel was kept constant at 200 ml, interface area was 6.2cm^2 and solution volume was 10 ml. A 50 ml/min dilution stream of N_2 was continually passed over the headspace through the inlet port to the outlet port. The outlet port was connected to a Waters prototype APCI-MSMS with an appropriate exhaust for excess N_2. At t = 0, 50 ml of equilibrated volatilised aroma was injected into the diluting stream leading to the vessel input port at a rate of 50 ml/min for 60s. Aroma passing through the headspace of the reaction vessel was detected by APCI-MSMS operating in multiple reaction monitoring (MRM) mode at aroma specific optimal conditions for collision energy, cone voltage and molecular transitions as outlined in chapter 4. APCI-MSMS sampling rate was 10ml/min. Sampled aroma proceeded through a heated transfer line housing a silica gas chromatography tube (Phenomenex, Macclesfield, UK). Silica film thickness was 6µm with an internal diameter of 0.32mm. Uniform operating conditions for corona pin voltage (4 kV, positive ion mode), ion dwell time (0.1s) and transfer line temperature (120ºC) were used throughout.

Gas phase aroma samples were prepared by pipetting of a quantity of liquid aroma (µl) into 1 litre of distilled water, producing dilute aqueous aroma solutions where 1 µl/L is equal to 1 ppm (Table 13).

Table 13: Physicochemical properties of aroma along with concentrations used

	Log $P_{(ow)}$	$K_{(H)}$	Vapour pressure (atm/mol)	Water solubility (mL/L)	Log $P_{(ao)}$	Polarizability Å^3	Molar volume cm^3	Conc. ppm
Benzaldehyde	1.46	2.67E-05	0.7	6.56E-02	3.9	13.1	101.1	20
3-hexenal	1.54	5.72E-05	9.8	1.09E-01	3.7	11.9	118.5	20
Isoamyl acetate	2.17	5.87E-04	7.0	1.54E-02	3.9	14.4	147.9	4
Ethyl benzoate	2.64	7.33E-05	0.6	4.79E-03	4.8	16.9	143.8	50
2-heptanone	1.95	1.69E-04	5.3	3.88E-02	4.0	13.7	141.2	20
Menthone	2.97	1.74E-04	0.2	3.49E-03	4.9	18.4	175.1	20

40 ml of dilute aqueous aroma solutions were equilibrated at 70˚C for 3h in 120ml Schott bottles (Fisher Scientific, Loughborough, UK) modified with an access port. With a Luer lock gas tight syringe, the headspace above the aroma solution was extracted and injected immediately into the dilution stream. Method of aroma introduction was repeatable with minimal standard deviation (< 2%) between repeats.

For each aroma a series of quantification peaks were generated by injection of volatilised aroma directly into the APCI-MSMS source, providing a measure of the signal generated by a known amount of aroma.

7.2.2 APCI-MSMS peak characterisation

Quantification peaks are produced by direct injection of 50 ml of aroma into the APCI source (Figure 44). Response time is immediate. Aroma is detected as soon as injection starts, similarly, halting aroma injection results in an immediate almost total decrease in aroma detection.

Behaviour of aroma in the system is assumed to be governed by system specific interactions according to the state of each system. At t = 0s, no aroma is present in the headspace, a continuous flow of N_2 purges the headspace at a rate of 50 ml/min above interfaces of water, salt and or mucin. At some time, t, 50ml of volatilised aroma is injected into the headspace. The N_2 dilution stream is halted during this process by the action of a switching valve. Aroma injection proceeds at a rate of 50 ml/min. No aroma is detected by APCI for the first 10s of aroma injection. After 10s aroma is detected in the headspace, the level of aroma detected increases with time. At t = 60s aroma injection is halted when the switching valve reintroduces the N_2 diluting stream to the headspace. From t = 60s aroma is flushed from the headspace until the experiment is terminated a t = ~300s. The level of aroma detected is based upon the specific solution-air interface and type of aroma.

Percentage of aroma absorbed during and after injection is expressed relative to the total amount of aroma injected into the system. The following equation was used to calculate the total aroma absorbed by the system, ABS% (equation 43):

$$\mathrm{ABS\%} = \frac{\mathrm{A_q} - \mathrm{A}}{\mathrm{A_q}} * 100 \qquad (43)$$

Where A_q is the area under the curve of the quantification peak and A is the area under the curve during an experimental run with an absorptive interface.

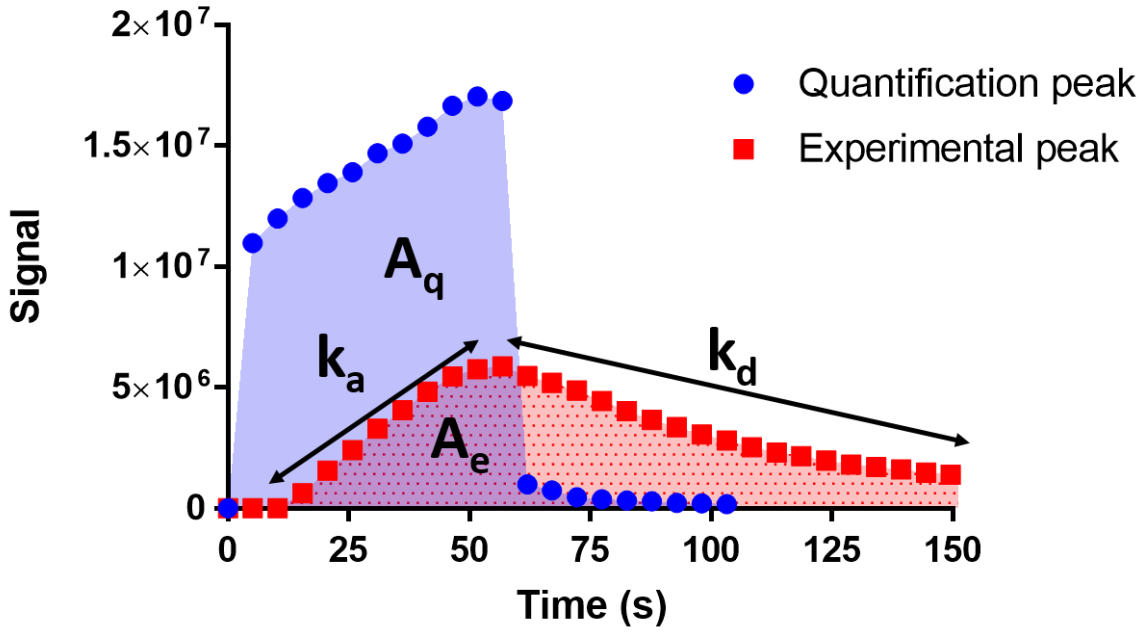

Figure 45 Representation of signal peaks as detected by APCI-MSMS for direct injection of 50 ml of isoamyl acetate into APCI source (Quantification peak) and into 200ml of headspace above a water interface (experimental peak). A_e is the area under the curve of experimental peaks, A_q is the area under the curve for quantification peaks. Rate constant, k_d describes the rate of aroma lost from headspace post aroma injection. Rate constant K_a describes the rate of increase in aroma detection.

Amounts of aroma absorbed during the injection period only is calculated in a similar manner but only considers the aroma detected during the injection period, the experimental area under the curve is expressed relative to the area under the curve of the quantification peak (equation 44):

$$\mathrm{ABS\%_s} = \frac{\mathrm{A_q} - \mathrm{A_s}}{\mathrm{A_q}} * 100 \qquad (44)$$

Where $ABS\%_s$ is the percentage of aroma absorbed during the period t = 0 to t = t_{max} where t_{max} is time taken to reach I_{max}.

7.2.3 Rate of aroma saturation

The rate of aroma level increase during the injection period, k_s is taken to be time taken for aroma levels to reach I_{max} (or injection termination) (equation 45).

$$k_s = \frac{ABS\%_s}{t_{max}} \qquad (45)$$

7.2.4 Statistics

Calculated parameters k_a and ABS% underwent two-way analysis of variance (ANOVA) performed in XLStat with 2-level interactions and multiple comparison by Tukey honest significant difference testing to identify statistically significant differences. Model terms consisted of the explanatory variables Mucin, Salt and an interaction term, Mucin*Salt. A fixed significance level of P <0.05 was implemented throughout the study.

7.3.1 Results

7.3.2 Interface aroma absorption percentage – Two-way ANOVA with interactions and PCA

ANOVA results incorporating Tukey pairwise comparisons are shown in (figure 45). ABS% ANOVA models were significant with P values of <0.0001 for all aroma, interaction terms (Mucin*Salt) were significant model contributors at P <0.0001. Inter-aroma significant differences are represented by different letters, where if X = X then P is >0.05, if X ≠ X then P is <0.05. Global two-way ANOVA with Tukey multiple comparisons assessed the data set for significant differences in aroma absorbance between interface types. Single

component interfaces (i.e. water + mucin or water + salt) differences in ABS% were non-significant regardless of concentration or whether the solute was mucin or salt. Significant modification of aroma ABS% is achievable by altering the concentration of mucin and/or salt when both constituents are present.

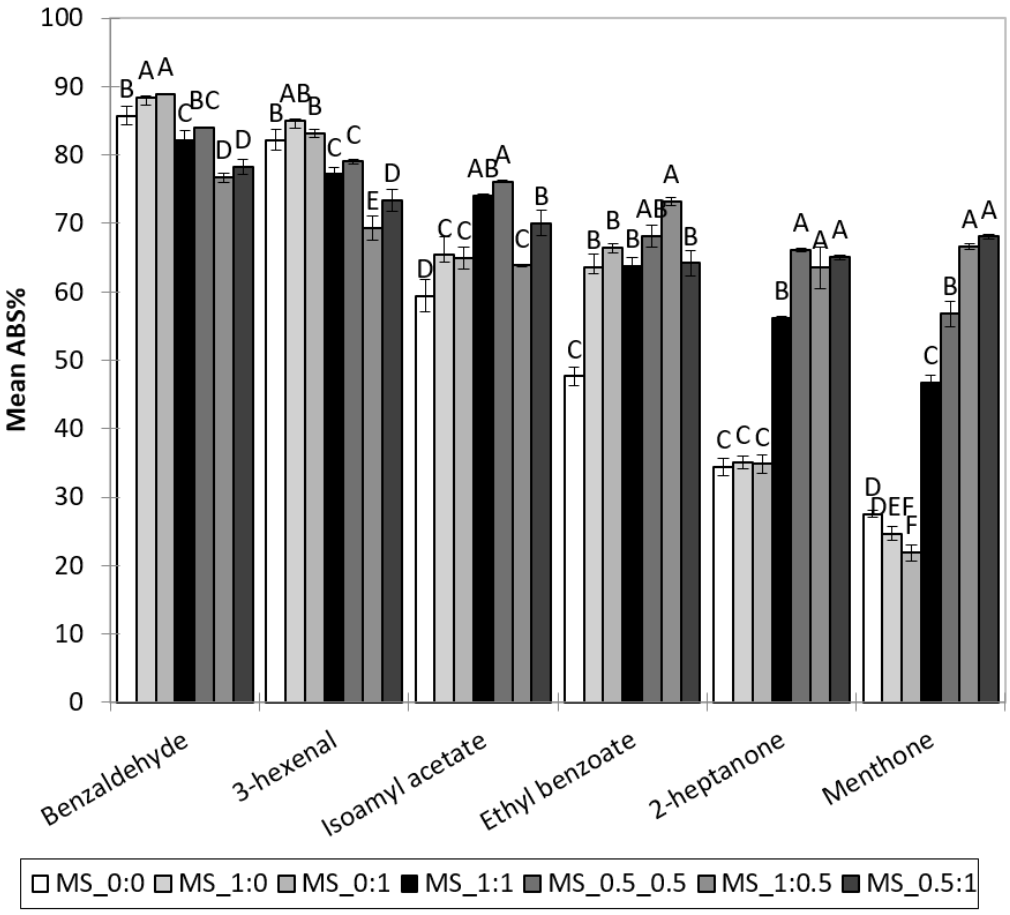

Figure 46 Aroma absorption during infusion and post headspace dilution at interface of varying mucin-salt ratios. Error bars account for variability between three independent repeats.

Total aldehyde absorbance by mucin-salt mixture interfaces was significantly different to water and interfaces of water + mucin and

water + salt. A distinction in the formulation of the mucin-salt mixtures; 'balanced' ratio mixtures (in relation to the original formulation) and 'unbalanced' ratio mixtures. Balanced mucin-salt interfaces, MS_1:1, absorbance of aldehydes were statistically identical to the diluted MS_0.5:0.5 interfaces. Reducing salt concentration (MS_1:0.5) or mucin concentration (MS_0.5:1) of MS_1:1 interface significantly reduced aldehyde ABS%. Reducing mucin concentration in a mucin-salt mixture negatively impacts 3-hexenal ABS% to a greater extent than reducing salt content of mucin-salt mixtures, an observation not mirrored by benzaldehyde.

Mean absorbance to water interfaces was lowest for compounds containing ketone functional groups. Absorbance of the ketone 2-heptanone was not significantly different for interfaces composed of salivary salts + water or for interfaces composed of mucin + water to control water interfaces. Menthone experienced significant albeit, small, increases in aroma absorbance when comparing absorbance to salt + water or mucin + water containing interfaces to the control interface, water. Changes in mucin or salt concentration resulted in no significant difference in menthone absorption relative to water control where mucin or salt where the only solute present.

Mucin-salt mixture interfaces resulted in statistically significant increases in aroma absorbance, a reversal in ABS% behaviour experienced by aldehydes to the same interfaces. A significant distinction between balanced and unbalanced mucin-salt ratios exists for ketones. Altering salt or mucin concentration relative to MS_1:1 interface resulted in a significant increase of ~9% for 2-heptanone and ~22% for menthone. Dilution of both salt and mucin concentrations present in MS_1:1 by half (MS_0.5:0.5) yielded interesting results. ABS% significantly increased so that 2-heptanone ABS% was similar to that of unbalanced interfaces

(MS_1:0.5 and MS_0.5:1), whilst menthone increased significantly to a level midway between MS_1:1 and unbalanced mucin-salt interfaces. Non-significant difference in observed ABS% at MS_1:1 and MS_0.5:0.5 for tested ethyl esters and aldehydes suggest that ABS% modifications are independent of mucin-salt concentration. If MS_1:1 and MS_0.5:0.5 represent identical mucin-salt morphology, then reducing concertation of mucin-salt reduces aggregation of mucin-salt units increasing surface area and potential binding sites for ketones.

Salt-induced mucin morphology changes significantly impacted interfacial aroma absorption. For simple aroma compounds, aroma with one functional group type, absorption behaviour at the presented interfaces were generally, similar. Aldehydes were affected least with inclusion of salivary components; ketones were the most affected suggesting a strong binding affinity of ketones for salt-modified mucin.

Highly absorbed compounds 3-hexenal and benzaldehyde were the most hydrophilic compounds tested as evidenced by log $P_{(ow)}$ and Lop $P_{(aw)}$ values. Aldehydes ABS% was more resistant to change, ABS% was only decreasing by ~10% in the most extreme case and were also the only compound type with an ABS% negatively impacted on by the inclusion of mucin-salt complexes relative to water. In direct opposition to aldehydes, ethyl esters and ketones compounds exist on the lipophilic end of the spectrum and were less well absorbed to water interfaces, mucin-salt complexes increased ABS% of lipophilic compounds to levels similar to that of hydrophilic compounds. Inclusion of mucin-salt complexes appears to decrease surface resistance to hydrophobic compounds, which were in turn, increasingly absorbed. Mucin-salt complexes were able to bind ketones significantly affecting absorptive potential of the interface

and increased lipophilic aroma absorption by lowering surface energy at the air-water interface and creating hydrophobic aggregates attractive to said lyophobic aroma.

7.3.3 Aroma absorption during aroma injection period

All aroma and interface experience high ABS%$_s$ during the aroma injection period, with an ABS%$_s$ range of ~80-97%. As previously noted for (total) ABS% hydrophilic compounds are absorbed to the greatest extent at water interfaces with the aldehydes absorbing the most and the ketones absorbing the least. Increasing interface affinity either through hydrophobic interactions or binding with addition of mucin-salt complexes increased ABS%$_s$ to similar levels. Interfaces with the least variation in aroma ABS%$_s$ contained mucin-salt mixtures with water and mucin + water interfaces featuring the most variation.

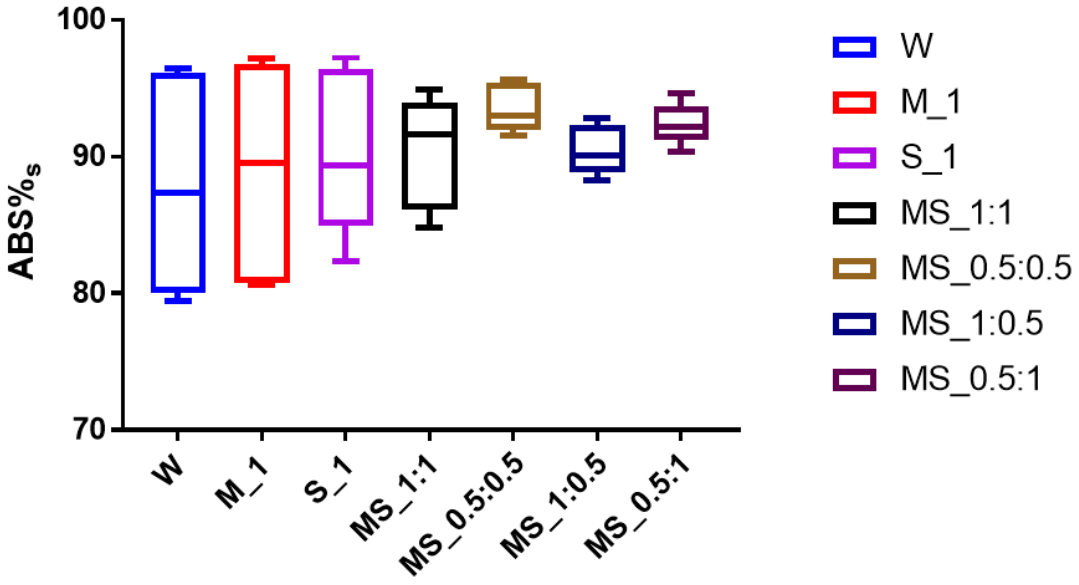

Figure 47 Variation of aroma ABS% for each interface

Two-way ANOVA with Tukey tests identified significant inter-interface variations in aroma ABS%s. Tukey test confidence intervals describes a wider spread of confidence intervals for water, mucin

and salt interface compared to the tighter clustering of mucin-salt interface confidence intervals along with a general decrease in differences between aroma means.

Uniformly high aroma absorbance during injection with little overall variation suggest aroma partitioning during injection is mostly dependent upon the action of the injection syringe constantly supplying aroma to the interface establishing a concentration gradient that favours movement to the interface.

The reduction in variation between different aroma $ABS\%_s$ at mucin-salt interfaces coupled with the increase in $ABS\%_s$ to a spread of 91-94% indicates that there is less resistance to movement across the interface relative to water. Mucin-salt mixtures feature salt-modified mucin, Friel and Taylor (2001) described an increase in mucin-mucin aggregation not normally possible with-out salt due to the net negative charge of mucin. Salt ion induced conformational changes in mucin result in increases in non-polar surface area reducing repulsion between mucin and thus facilitating aggregation, which impacts of the viscosity of mucin-salt bearing solution. Homogenisation of aroma with the inclusion of mucin-salt could potentially be due to an induced Marangoni effect. Aggregation of mucin complexes results in surface tension gradients, disperse non-polar regions disrupt the surface tension of water, as regions of higher surface tension move away from lower regions of surface tension.

Cystic fibrosis, a congenital disease state that results in the accumulation of dried mucus in airways hampering drug delivery. Studies designed to assist in drug delivery development described Marangoni stresses in aqueous solutions of porcine gastric mucin which resulted in an increased spread, post deposition of aerosol delivered droplets. In addition, deposition of aerosol droplets spread

to deeper sub regions of an aqueous layer than thought previously possible (Sharma *et al* 2015). Convective spreading induced by differences in aqueous mucin solutions surface tension with that of a drug carrying aqueous formula were attributed to Marangoni stresses, increasing the uniformity of drug distribution in the investigated medium (Koch *et al* 2011)

7.3.4 Rate of interfaces saturation

The time taken for a peak to reach a plateau is taken to represent aroma interface saturation, or the point where aroma absorption is equal to aroma loss under aroma injection conditions. Aroma levels in the headspace are normalised so that maximum aroma levels equate to 1 and all other values are reported relative to 1. The saturation period is confined to the period 5% of I_{max} to the plateau point. Interface saturation peaks for each aroma are shown in (figure 48), half concentrations of mucin and salt interfaces are not shown.

Initial inspection of increases in levels of aroma detected during the injection period suggested a linear behaviour of aroma at the various interfaces indeed, straight line fits performed in Prism 7 (Graphpad software, California, USA) reported R^2 ranging from 0.97-0.99 for the majority of aroma-interfaces. Ethyl benzoate peaks were an exception, straight line equation fits produced R^2 of ~0.8 in most instances. Exponential growth equations produced better fits with R^2 ranging from 0.95-0.99.

Table 14: Rate of interface saturation, $k_s\ 10^{-2}(s^{-1})$

Aroma	Interface											
	W		M_1		S_1		MS_1:1		MS_1:0.5		MS_0.5:1	
	$k_s\ 10^{-2}$ (s^{-1})	SD	$k_s\ 10^{-2}$ (s^{-1})	SD	$k_s\ 10^{-2}$ (s^{-1})	SD	$k_s\ 10^{-2}$ (s^{-1})	SD	$k_s\ 10^{-2}$ (s^{-1})	SD	$k_s\ 10^{-2}$ (s^{-1})	SD
Benzaldehyde	2.4	0.05	2.3	0.03	2.4	0.06	1.8	0.03	2.4	0.05	2.4	0.02
Isoamyl acetate	2.2	0.04	2.2	0.03	2.3	0.03	1.7	0.05	2.4	0.04	2.3	0.01
3-hexenal	2.2	0.05	2.1	0.04	2.2	0.05	2	0.03	2.5	0.04	2.5	0.02
2-heptanone	2.2	0.05	2.1	0.03	2.2	0.05	1.9	0.04	2	0.05	2.1	0.05
Menthone	2.4	0.04	2.1	0.03	2.2	0.07	1.7	0.03	2	0.05	2	0.05

**Ethyl benzoate results not shown, behaviour conforms to a linear decay.*

Sum of squares tests automated in Prism 7, assessed the statistical likelihood that a single model fit with the same slope and intercept, describes the increase in inter-aroma headspace levels during the injection period for all interfaces. A P value of <0.0001 for the extra sum of squares test was calculated for each aroma indicating a minimum of one curve was significantly different for each aroma. Inter-aroma absolute sum of squares when fitting a singular inter-aroma global model for each interface were generally similar for water, M_1, S_1, MS_1:0.5 and MS_0.5:1. In fact, mean variation of aroma behaviour with changes in interfaces were similar across aroma with the exclusion of MS_1:1 interfaces (and MS_1:0.5 for isoamyl acetate and 3-hexenal), mean sum of squares was ~0.045 across all aroma with the exception of ethyl benzoate. Rate of interface saturation values are shown in (table 14), overall variation during aroma injection was generally only significant for the decrease in saturation experienced at the MS_1:1 interface.

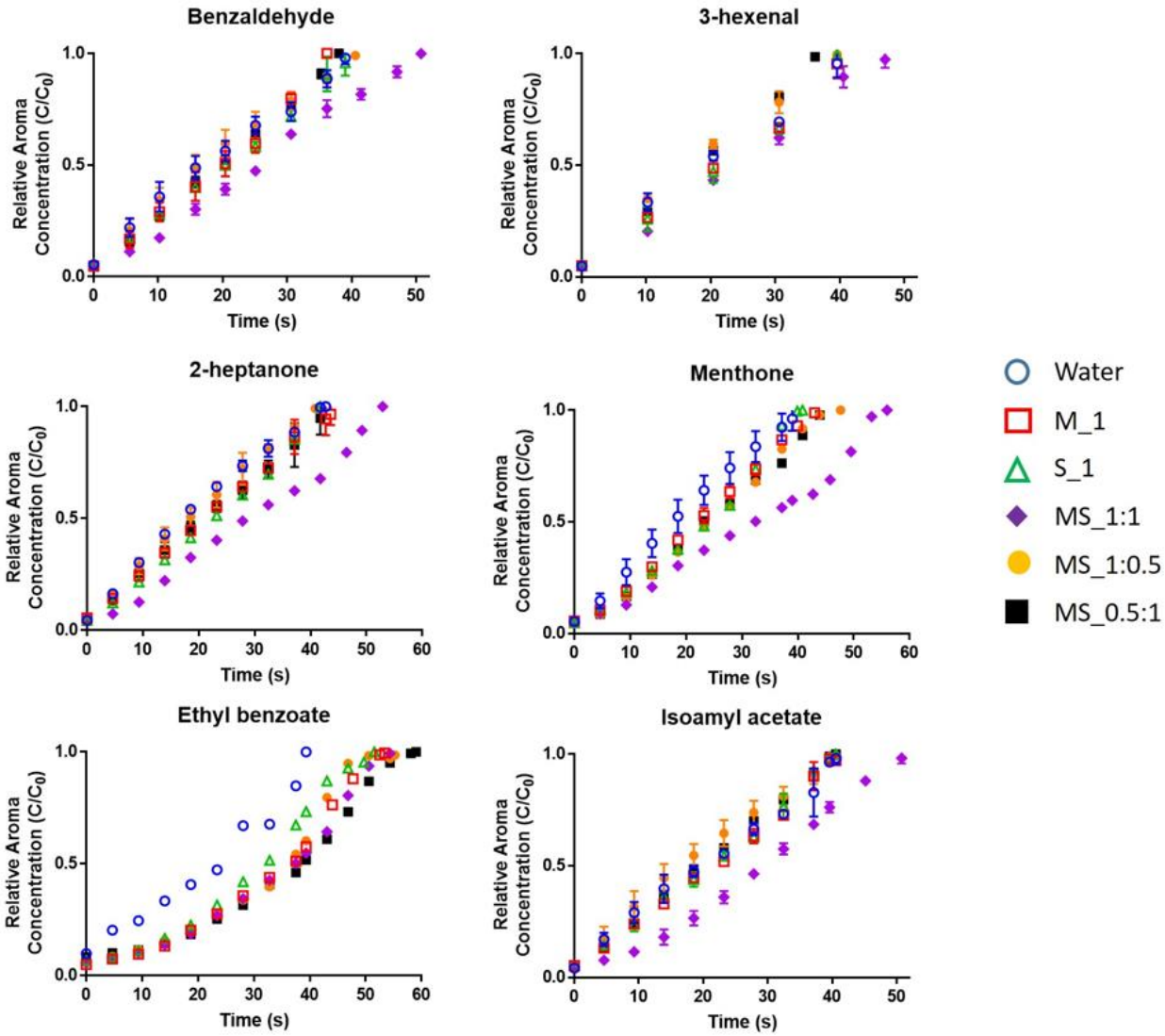

Figure 48 Aroma behaviour of selected aroma compounds during the period of aroma injection

Aroma absorbance during the injection period was uniformly high for all aroma-interfaces ranging from 80-97%. $ABS\%_{tmax}$ at water interfaces was similar to total absorbance, ABS%, at water interfaces. Aldehydes absorbed to a greater extent than ethyl esters which absorbed to a greater extent than ketones.

Correlation analysis performed in Prism 7 correlated several physicochemical parameters with aroma absorption parameters, ABS% and $ABS\%_{tmax}$. Generally, aroma ABS% and $ABS\%_{tmax}$

correlated well with the parameters molar volume and hydrophobicity. Higher values of aroma hydrophobicity or molar volume resulted in decreased absorption at water interfaces. Changing interface composition to include mucin-salt complexes effectively balanced out $ABS\%_{tmax}$ by facilitating increased absorption of the lipophilic compounds which absorbed to a lesser extent at water and binary component interfaces.

Interfaces composed of mucin-salt complexes at ratio of 0.5:1, 1:0.5 and 0.5:0.5, $ABS\%_{tmax}$ values fell within a 5% range of 89 – 94%. The general uniformity of inter-aroma saturation kinetics for all interfaces, excluding MS_1:1 combined with the high levels of aroma absorption suggest that the action of the automated syringe drives the partitioning of aroma to the headspace with more hydrophilic compounds experiencing a greater movement across the interface. Whilst inter-aroma saturation kinetics varied little with the inclusion of solutes (bar MS_1:1 interfaces), quantity of aroma absorbed during the injection period was significantly affected by the inclusion of solutes. A potential explanation for identical kinetics but with changes in quantity absorbed is the changes in colligative properties of a solution. Inclusion of solute, regardless of type results in changes in equilibrium partial pressures of a volatile component in solution. Solute inclusion induces changes in equilibrium volatile headspace concentrations by reducing solution surface area at the solution-air interface.

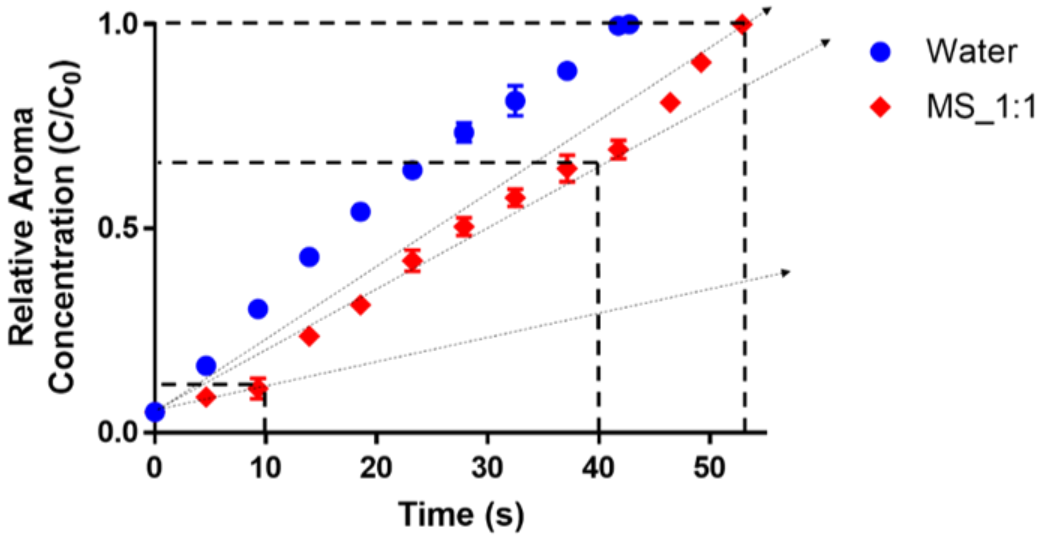

Figure 49 Increase in relative aroma concentration over time for 2-heptanone where water is the control interface and MS_1:1 is water + salt + mucin interface containing maximum concentrations of salivary salts and mucin.

Several special cases identified in the previous text require attention. The ratio of salivary salts and mucin contributing to the artificial saliva of van Ruth (1999) were intended to provide a biological relevant analogue of the components of saliva, those components produced the MS_1:1 interface which is also the interface where the most aroma variation occurs. Ketones experienced the disparity between water and mucin-salt interfaces during the injection period. Inclusion of mucin or salt separately to water interface failed to significantly alter absorption levels $ABS\%_{tmax}$ interfaces were significantly reduced for menthone and 2-heptanone relative to other mucin-salt complexes. As previously stated, the MS_1:1 saturation curve was significantly different to all other interface curves which generally conformed to the same straight-line model, the difference in saturation behaviour potentially explains the significant decrease in $ABS\%_{tmax}$. Saturation curves of 2-heptanone at water and the MS_1:1 interface is shown in (figure 48). 2-heptanone increases in aroma levels with time is

linear with exposure to water interfaces, whereas, increase in aroma levels for the same quantity of 2-heptanone exposed to MS_1:1 interfaces proceed at a reduced rate for the first 10s and at an increased rate for the final 10s. Similar behaviour was also observed for menthone under the same conditions. Post-injection increases in aroma was a common feature for most aroma at MS_1:1.

Explorations of volatile ketone-protein binding interactions exists in the literature. Androit *et al* (2000) described the decrease in the headspace presence of 2-heptanone, 2-octanone and 2-nonanone with the addition and increase in concentration of β-lactoglobulin, attributing the decrease to reversible aroma-protein binding. However, ascribing observed partitioning mechanics for MS_1:1 partitioning of ketones to binding events may not be an accurate assessment of the real situation. Friel and Taylor (2000), Raynal *et al* (2003) reported the changes of mucin morphology by the inclusion of salivary salts and thus, considered mucin and mucin-salt complexes as effectively distinct species with distinct morphology. Furthermore, increased induction of mucin self-aggregation was theorised to occur with the addition of salt. Negatively charged mucin backbones are thought to be shielded by salt-mucin association reducing repulsive forces, promoting the entwining of mucin. Regardless of the changes wrought by salt on mucin Friel and Taylor (2000) reported significant differences between mucin and mucin-salt solutions equilibrium partitioning behaviour of aroma. Combined with increases in solution viscosity, potentially reducing the build-up of aroma at an interface are the potential net effects of mucin-salt self-aggregation. MS_1:1 with the highest mucin-salt concentrations tested, behaves uniquely relative to other mucin-complex interfaces and is thought to experience a greater level of aggregation, affecting the partitioning of aroma to the

interface resulting in decreased saturation rates and aroma absorption. Raynal *et al* (2002), discovered purified mucin (MUC5B) did not feature the gel like properties of saliva, potentially accounting for the general lack in significant differences in $ABS\%_{tmax}$ and k_s for mucin interfaces relative to water interfaces.

7.3.5 Aroma evolution post-injection

Aroma behaviour post-injection is accounted for with partition ratios, (equation 46) values closer to 1 indicate overall aroma ABS% is driven by the initial aroma absorption occurring during the injection event. Values closer to 0 indicate a substantial release of aroma occurs post-injection. As such, k_r provides an indication of an aromas ability to replenish the headspace post infusion.

$$k_r = \frac{ABS\%}{ABS\%_{tmax}} \qquad (46)$$

Initial partition ratio k_r, values for water interfaces can be grouped by type of functional group. Aldehyde partitioning favoured movement to water whilst ketones partitioning favoured movement to the headspace with ethyl esters sitting somewhere between the two carbonyl groups. The addition of single component solutes to water interfaces, i.e. salt or mucin only, have no significant effect on k_r for the aldehydes, isoamyl acetate and the ketones 2-heptanone, carvone and menthone. Relative to water, ethyl benzoate k_r is significantly affected to the same level with inclusion of mucin or salt regardless of concentration. The presence of solute, regardless of type increase the retention of ethyl benzoate, less ethyl benzoate is released post infusion relative to water. Ethyl benzoate is an important distinguisher when describing the absorption potential of

mucin-salt complexes. Ethyl benzoate mean water k_r is approximately 0.5 and is not as readily absorbed as benzaldehyde (~0.89), absorbed ethyl benzoate is not as readily released as menthone (~0.35). With inclusion of salt or mucin regardless of concentration, mean ethyl benzoate k_r increases to 0.72. Importantly, a significant increase in k_r is not observed for other compounds with the change to single component interfaces where partitioning tendency remains similar to water. A slow hydrolysis of ethyl benzoate is known to occur in water to form negatively charged ethyl benzoate ions which when exposed to sodium could form a stabilised salt. Formation of ethyl benzoate+sodium complexes potentially account for the observed increase in absorption of ethyl benzoate by salt interfaces when compared to water interfaces (Cox and Yates 1982).

7.3.6 Exploring aroma persistence kinetics

Factors affecting the kinetics of aroma headspace persistence are the removal of volatilised aroma by the action of the diluting stream and potential reversible and irreversible interactions between aroma and interface constituents. Since the removal of aroma from the headspace is uniform between aroma and interface type, differences in inter-aroma rate change by interface type are based upon aroma-protein interactions and/or changes in interfacial properties. Overall headspace levels under a dilution post-injection is taken to be a measure of aroma persistence. More persistent aroma retains a larger, prolonged presence in the headspace relative to a less persistent aroma.

Normalised concentrations of aroma release with time from I_{max} to 10% of I_{max} or 200s, whichever occurs first, underwent non-linear regression in line estimation software Prism 7 (Graphpad Software, California, USA). A line of best fit based on one-phase and two-

phase exponential decay models were applied to the normalised data producing a rate constant in a similar manner as described in chapter 6.

7.3.7 Kinetics of aroma release post-infusion

Unlike the majority of saturation rates curves, inter-aroma decay rate curves cannot be described by a single straight line fit after transformation. Significant differences in inter-aroma k_d with changes in interface composition indicate that, unlike rate of aroma saturation, headspace persistence was a function of absorbed aroma released, current levels of aroma in the headspace and the action of the headspace dilution stream.

The behaviour of aroma post exposure to interfaces composed of water, low mucin concentration and salt interfaces were best described by one-phase decay kinetics, whilst high mucin concertation and mucin-salt mixture interfaces were best described by two-phase decay kinetics.

Rate decay constants assessed by two-way ANOVA to describe the impact of salt and mucin and interaction between mucin and salt on the post interface exposure release kinetics of aroma. A statistically significant interaction between mucin and salt was identified as evidenced by the significant P values of the model term, mucin*salt for all tested aroma. This indicated that the ratios of mucin to salt is an important factor affecting aroma release.

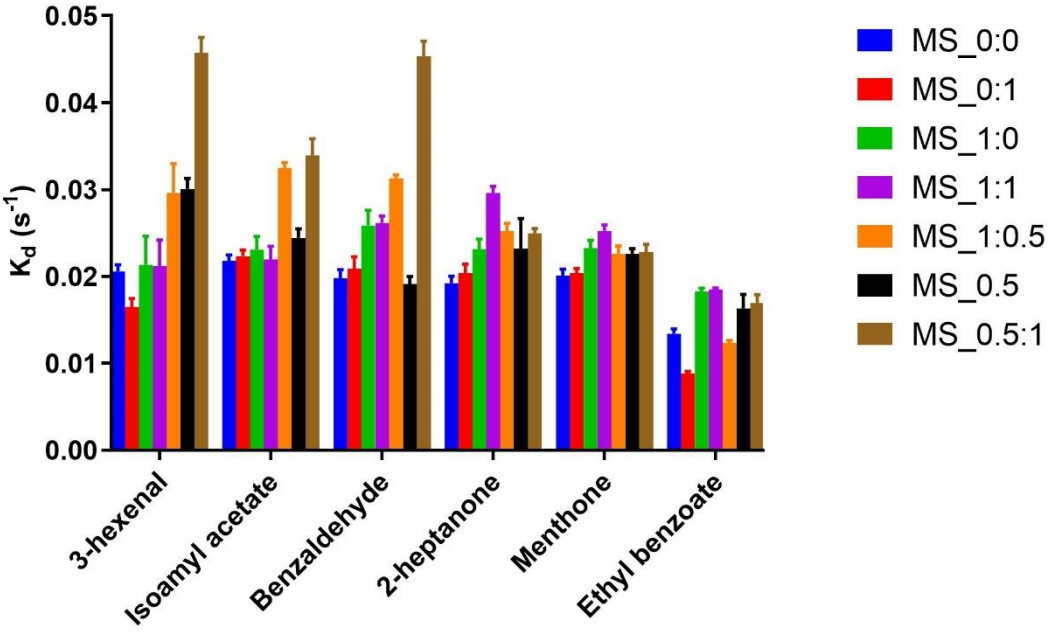

Figure 50 Rate of aroma loss from the headspace of various mucin/salt/water interfaces. Data presented is the mean of 3 independent repeats

Initial Pearson r, correlation analysis indicated significant correlation ($P < 0.0001$) between water, salt low concentration mucin interfaces (table 14). Additionally, Tukey multiple comparisons conducted during ANOVA (XLStat and R) procedures confirmed that the inter-aroma differences in the rate of release post infusion from water, salt and low mucin concentrations were non-significant ($P > 0.005$). Ethyl benzoate proved to be the only exception being the only compound experiencing significant differences ($P < 0.001$) in the rate of release between water, salt and low concentrations of mucin. Potential interactions between hydrolysed ethyl benzoate and sodium ions potentially account for the significant difference in ethyl benzoate k_d with exposure to salt surfaces relative to water surfaces.

No significant correlation of general rates of release was observed between MS_1:1 and any other interfaces indicating a behaviour

unique to MS_1:1 interface. A similar situation was observed in the unique interface saturation kinetics of MS_1:1 interface.

Table 15: Pearson correlation analysis P values

	MS_0:0	MS_1:1	MS_0:1	MS_1:0	MS_0.5:0	MS_0:0.5	MS_0.5:0.5	MS_1:0.5	MS_0.5:1
MS_0:0		0.401	0.099	**0.014**	**0.017**	**0.010**	0.114	**0.010**	0.187
MS_1:1	0.401		0.095	0.132	0.407	0.257	0.912	0.485	0.889
MS_0:1	0.099	0.095		**0.018**	0.147	**0.028**	0.809	0.079	0.270
MS_1:0	**0.014**	0.132	0.018		**0.012**	**0.002**	0.447	**0.045**	0.410
MS_0.5:0	**0.017**	0.407	0.147	0.012		**0.004**	0.330	**0.037**	0.442
MS_0:0.5	**0.010**	0.257	**0.028**	**0.002**	**0.004**		0.407	**0.009**	0.241
MS_0.5:0.5	0.114	0.912	0.809	0.447	0.330	0.407		0.209	0.282
MS_1:0.5	**0.010**	0.485	0.079	**0.045**	**0.037**	**0.009**	0.209		**0.042**
MS_0.5:1	0.187	0.889	0.270	0.410	0.442	0.241	0.282	**0.042**	

**Bold values indicate statistically significant correlations. Italicized columns heads represent interfaces with unique release kinetics.*

Presumably, the character of MS_0.5:0.5 interfaces, where mucin and salt concentrations are present in the same ratio but reduced by half, is similar to that of MS_1:1, however no significant correlations in aroma release ($P = 0.97$) could be achieved between the two interfaces. Altering the mucin-salt ratio from MS_0.5:0.5 to MS_1:0.5 also results in a non-significant correlation with MS_1:1 of aroma release ($P = 0.152$). Correlation of MS_1:1 and MS_0.5:1 aroma release also produces non-significant ($P = 0.27$) results.

Correlation analysis describes mucin+salt solutions, MS_1:1 and MS_0.5:0.5, as statistically distinct entities. Adjusting this core ratio to MS_1:0.5 and MS_0.5:1, reduces only mucin or salt concentrations to half the original level stipulated in the artificial saliva formulation. When reducing the salt concentration to produce the MS_1:0.5 interface, release behaviour correlates significantly with the release behaviour of water ($P < 0.010$). When reducing mucin concentration levels to form the MS_0.5:1 interface, release

behaviour correlates with low significance to that of the MS_1:0.5 interface ($P > 0.42$) only. The results suggest that different mucin salt ratios produce differing aroma release behaviour. Reducing the amount of salt relative to mucin resulted in similar release behaviour to water (MS_0:0), low salt (MS_0.5:0) and mucin only interfaces (MS_1:0 and MS_0.5:0). This suggest that a certain level of salt is required to induce changes in mucin to affect the release behaviour of the aroma tested.

The statistically indistinct differences in global k_d after exposure to water and salt interfaces. Salt is only suspected of modifying ethyl benzoate through an association of water hydrolysed ethyl benzoate and sodium ions, salivary salt have only a limited ability to affect most aroma compounds k_d (assuming no direct aroma-salt association), for salt to exert any effects on aroma k_d then salt must be modifying mucins ability to modulate aroma release. The previously mentioned study by van Ruth and colleagues (2001) when studying equilibrium partitioning of artificial saliva, observed no significant difference in air-water partition coefficients when compared to air-salivary salts partition coefficients.

From a biological point of view, increased availability of salt ions through consumption alter mucin morphological profiles and may have an impact on the aroma released for retro nasal perception.

7.4.1 Conclusion

Headspace exposure to a mucin containing interfaces results in significantly different absorption and release of aroma, the effect is aroma dependant. The inclusion of salt with mucin to an interface modifies the behaviour further. Salt-mucin ratios are important, significant modifiers of aroma absorption and release behaviour. Unique release behaviour as assessed through release kinetics was observed for the maximum amount of

interactions between mucin and aroma is alterable by salt, differing mucin salt ratios result in different mucin conformations that have a direct effect on the absorbance and release of aroma.

Chapter 8 – Conclusions and future work

Increasing the limits of detection of an analytical instrument will always be desirable enabling one to investigate systems normally out of the instruments typical detection range. Enhancing APCI-MSMS limits of detection is achievable by adopting a dual mass filtering step. Monitoring for specific precursor-product ion transitions reduces background noise and increases confidence of aroma detected by monitoring aroma specific molecular transitions. MRM operating modes produced signals with less point-to-point fluctuation, which is the appearance of the signal was 'neater'. Investigations into saturation and release kinetic in particular, benefited from traces with reduced noise. Furthermore, increased sensitivity increases the operating potential of the apparatus, allowing for the detection of molecules at lower ppm.

The increase in operating potential allowed for the use of lower concentrations of aroma compounds, allowing for the assessment of compounds that could potentially saturate surface of interest, lower concentrations of flavour solutions for *in vivo* trials and the ability to develop gas phase infusion methodologies discussed in chapters 5, 6 and 7.

Sensitivity gains through adopting MRM procedures for monitoring breath-by-breath persistence of aroma enabled an exploration of persistence kinetics at lower aroma concentrations along with reduced sampling rates and volumetric flow rates. Furthermore, MRM procedures sensitivity gains enabled the trailing of gas-phase introduction routes for breath-by-breath persistence, a novel technique for APCI-MSMS.

Deposition of aroma to model emulsion systems showed some success in describing the persistence of flavoured water solutions and dilute emulsion systems. Strong correlation was observed for *in vitro* data with *in vivo* data.

Novel automated syringe dispenser-based aroma delivery systems developed allowed for the controlled delivery of volatilised aroma sample to the air-interfaces of interest to observe aroma release in real time and also to indirectly observe aroma absorption by a surface. The repeatability of the gas-phase delivery method allowed for the development of a novel gas phase quantification system, which allowed for the calculation of aroma absorbed and released by a surface of interest. A strength of the novel aroma delivery system is the relative ease in which the data can be described in terms of mass transport, classically, a difficult concept to observe in real time.

Mucin investigations were able to identify several interesting consequences of mucin on aroma absorption and persistence. Aggregation of mucin salt complexes through charge shielding were the identified cause for the homogeneity of aroma absorbance at mucin-salt solutions. Surface tension gradients and Marangoni stresses were thought to be the cause of enhanced aroma absorption of hydrophobic compounds relative to water. Further work would include the use of appropriate dyes or other markers to visualise the effects of convective spread of particulate through an aqueous mucin media. The effects of mucin on VOC are potentially important to industries other than food science, identifying deposition mechanics of aroma compounds to biologically relevant surfaces may help in the development of drugs able to penetrate the dehydrated mucus matter in cystic fibrosis sufferer’s airways.

Chapter 9 - References

Alqahtani, Norah, Suheel K. Porwal, Elle D. James, Dana M. Bis, Jonathan A. Karty, Amy L. Lane, and Rajesh Viswanathan. 2015. "Synergism between genome sequencing, tandem mass spectrometry and bio-inspired synthesis reveals insights into nocardioazine B biogenesis." *Organic and Biomolecular Chemistry* (Royal Society of Chemistry) 13 (26): 7177-7192.

Alqahtani, P., James, E., Bis, D., Karty, A. J., Lane, A. L., Viswanathan, R. 2015. "Synergism between genome sequencing, tandem mass spectrometry and bio-inspired synthesis reveals insights into nocardioazine B biogenesis." *Organic and Biomolecular Chemistry* 13 (26): 7177-7192.

Ambatipudi, Kiran S., Bingwen Lu, Fred K. Hagen, James E. Melvin, and John R. Yates. 2009. "Quantitative analysis of age specific variation in the abundance of human female parotid salivary proteins." *Journal of Proteome Research* 8 (11): 5093-5102.

Anderson, R. E., Benolken, R. M., Dudley, P. A., Landis, D. J. , T. G. Wheeler, T. G. 1974. "Polyunsaturated fatty acids of photoreceptor membranes." *Exp. Eye Res* (18): 205-213.

Andriot, Isabelle, Marcus Harrison, Nicole Fournier, and Elisabeth Guichard. 2000. "Interactions between methyl ketones and β-lactoglobulin: Sensory analysis, headspace analysis, and mathematical modeling." *Journal of Agricultural and Food Chemistry.*

Atkins, P., de Paula, P. 2010. *Physical Chemistry.* 5th edition. OUP Press.

Avison, Shane J. 2013. "Real-time flavor analysis: Optimization of a proton-transfer-mass spectrometer and comparison with an atmospheric pressure chemical ionization mass spectrometer with an MS-nose interface." *Journal of Agricultural and Food Chemistry.*

Badjagbo, Koffi, Martin Ḧeroux, Mehran Alaee, Serge Moore, and Sébastien Sauvé. 2010. "Quantitative analysis of volatile methylsiloxanes in waste-to-energy landfill biogases using direct APCI-MS/MS." *Environmental Science and Technology.*

Bansil, Rama, and Bradley S. Turner. 2006. "Mucin structure, aggregation, physiological functions and biomedical applications." *Current Opinion in Colloid and Interface Science.* Vol. 11. no. 2-3. 6. 164-170.

Berg, J. M., Tymoczko, J. L., Stryer, L. 2002. *Biochemistry.* 5th. New York: W H Freeman.

Bhandawat, Vikas, Johannes Reisert, and King-Wai Yau. 2005. "Elementary Response of Olfactory Receptor Neurons to Odorants." *Science* 308 (5730): 1931.

Biddlecombe, James G., Alan V. Craig, Hu Zhang, Shahid Uddin, Sandrine Mulot, Brendan C. Fish, and Daniel G. Bracewell. 2007. "Determining antibody stability: Creation of solid - Liquid interfacial effects within a high shear environment." *Biotechnology Progress* 23 (5): 1218-1222.

Bignetti, E., Damiani, G., Denegri, P., Ramoni, R., Avanzini, F., Ferrari, G., Rossi, G. L. 1987. "Specificity of an immunoaffinity column for odorant-binding protein from bovine nasal-mucosa." *Chem Senses* (12): 601-608.

Binks, Bernard P., John H. Clint, and Catherine P. Whitby. 2005. "Rheological behavior of water-in-oil emulsions stabilized by hydrophobic bentonite particles." *Langmuir* 21 (12): 5307-5316.

Brandão, Elsa, Susana Soares, Nuno Mateus, and Victor de Freitas. 2014. "Human saliva protein profile: Influence of food ingestion." *Food Research International* (Elsevier Ltd) 64: 508-513.

Britta Brügger. 2014. "Lipidomics: Analysis of the Lipid Composition of Cells and Subcellular Organelles by Electrospray Ionization Mass Spectrometry." *Annual Review of Biochemistry* 83 (1): 79-98.

Bruneel, Joren, Christophe Walgraeve, Stefanie Dumortier, Jonas Stockman, Peter Demeyer, and Herman Van Langenhove. 2018. "Increasing mass transfer of volatile organic compounds in air scrubbers: a fundamental study for different gas–liquid systems." *Journal of Chemical Technology and Biotechnology* (John Wiley and Sons Ltd) 93 (5): 1468-1476.

Buffo, R. A., Rapp, J. A., Krick, T., Reineccius, G. A. 2005. "Persistence of aroma compounds in human breath after consuming an aqueous model aroma mixture." *Food Chem* (89): 103-108.

Burke, William. 2014. "The Ionic Composition of Nasal Fluid and Its Function." *Health* (Scientific Research Publishing, Inc,) 06 (08): 720-728.

Buttery, R. G., Guadagni, D. G., Ling, L. C. 1973. "Flavour Compounds: Volatiles in Vegetable oil and Oil Water Mixtures.

Estimation of Odour Thresholds.” *. Agric. Food Chem* (21): 198-201.

Buttery, R., Guadagni, D., Ling, L. 1973. “Flavor Compounds: Volatilities in Vegetable Oil and Oil-Water Mixtures. Estimation of Odor Thresholds.” *Journal of Agricultre and Food Chemistry* 21 (2): 198 - 201.

Bylaite, Egle, Jens Adler-Nissen, and Anne S. Meyer. 2005. “Effect of xanthan on flavor release from thickened viscous food model systems.” *Journal of Agricultural and Food Chemistry* 53 (9): 3577-3583.

Carey, M. E., Asquith, T., Linforth,R. S. T., Taylor, A. J. 2002. “Modeling the Partition of Volatile Aroma Compounds from a Cloud Emulsion.” *J. Agric. Food Chem* 50: 1985-1990.

Carey, Michelle E., Tom Asquith, Robert S.T. Linforth, and Andrew J. Taylor. 2002. “Modeling the partition of volatile aroma compounds from a cloud emulsion.” *Journal of Agricultural and Food Chemistry* 50 (7): 1985-1990.

Carmen Llena-Puy. 2006. “The role of saliva in maintaining oral health as an aid to diagnosis." Clinical dentistry.” *Clinical dentistry* 11: 449-455.

Casado, Begoña, Lewis K. Pannell, Paolo Iadarola, and James N. Baraniuk. 2005. “Identification of human nasal mucous proteins using proteomics.” *Proteomics* 5 (11): 2949-2959.

Challis, R. C., Tian, H., Wang, J., He, J., Jiang, J., Chen. X., Yin, W., Connelly, T., Ma, L., Yu, C. R., Pluznick, J. L., Storm, D. R., Huang, L., Zhao, K., Ma, M. 2015. “An Olfactory Cilia Pattern

in the Mammalian Nose Ensures High Sensitivity to Odors." *Curr. Biol.* 25 (19): 2503-2512.

Charles S. Sell, C. S., Perring, K. P., Keith. 2006. *Volatility and substantivity. In chemistry of fragrances.* 2nd. Royal Society of Chemistry.

Chong, Yeow Kuan, Chi Chun Ho, Shui Yee Leung, Susanna K.P. Lau, and Patrick C.Y. Woo. 2018. "Clinical Mass Spectrometry in the Bioinformatics Era: A Hitchhiker's Guide." *Computational and Structural Biotechnology Journal.* Vol. 16. Elsevier B.V., 1 1. 316-334.

Cobelli, and Joseph J Claudio. 2019. "Downloaded from www.physiology.org/journal/ajpregu at Univ of Nottingham."

Cooper, G. M. 2000. *The Cell: A Molecular Approach.* 2nd. Goodreads 4.1/5 Amazon 4.4/5 (ASM Press) Boston Univ., MA. Textbook.

Craven, B. A. 2008. "A fundamental study of the anatomy, aerodynamics, and transport phenomena of canine olfaction." The Pennsylvania State University, 42.

Craven, B. A., Patterson, E. G., Settles, G. S. 7. "The Fluid Dynamics of Canine Olfaction: Unique Nasal Airflow Patterns as an Explanation Macrosmia." *J R Soc Interface* 47: 933-943.

Davies, Scott M., Rob S. Linforth, Stuart J. Wilkinson, Katherine A. Smart, and David J. Cook. 2011. "Rapid analysis of formic acid, acetic acid, and furfural in pretreated wheat straw hydrolysates and ethanol in a bioethanol fermentation using atmospheric pressure chemical ionisation mass spectrometry." *Biotechnology for Biofuels.*

de Roos, K. B., Sarlese, J. A. 1996. *In Flavour Science: Recent Developments, Royal Society of Chemistry.* Royal Society of Chemistry.

Demarque, Daniel P., Antonio E.M. Crotti, Ricardo Vessecchi, João L.C. Lopes, and Norberto P. Lopes. 2016. "Fragmentation reactions using electrospray ionization mass spectrometry: An important tool for the structural elucidation and characterization of synthetic and natural products." *Natural Product Reports.* Vol. 33. no. 3. Royal Society of Chemistry, 1 3. 432-455.

Dimitrova, Tatiana D., and Fernando Leal-Calderon. 1999. "Forces between emulsion droplets stabilized with Tween 20 and proteins." *Langmuir* (ACS) 15 (26): 8813-8821.

Dong, Ying, Kuan Yan, Yanhua Ma, Shan Wang, Genye He, Jing Deng, and Zhiyong Yang. 2015. "A sensitive dilute-and-shoot approach for the simultaneous screening of 71 stimulants and 7 metabolites in human urine by LC-MS-MS with dynamic MRM." *Journal of Chromatographic Science* (Oxford University Press) 53 (9): 1528-1535.

Doyen, K., M. Carey, R. S.T. Linforth, M. Marin, and A. J. Taylor. 2001. "Volatile release from an emulsion: Headspace and in-mouth studies." *Journal of Agricultural and Food Chemistry* 49 (2): 804-810.

Doyennette, M., C. De Loubens, I. Déléris, I. Souchon, and I. C. Trelea. 2011. "Mechanisms explaining the role of viscosity and post-deglutitive pharyngeal residue on *in vivo* aroma release: A combined experimental and modeling study." *Food Chemistry* 128 (2): 380-390.

Eccles, R., Mygind, N. 1985. "Physiology of the upper airways in allergic disease." *Clin. Rev. Allergy* 3: 501-551.

Elad, D., Michael Wolf, M., Keck. 2008. "Air-conditioning in the human nasal cavity." *Respiratory Physiology & Neurobiology* 163 (1-3): 121-127.

Elisia, Ingrid, and David D. Kitts. 2011. "Quantification of hexanal as an index of lipid oxidation in human milk and association with antioxidant components." *Journal of Clinical Biochemistry and Nutrition* (The Society for Free Radical Research Japan) 49 (3): 147-152.

Emirzeoglo, M., Sahin, B., Celebi, M., Uzun, A., Bilgic, S., Tontus, H. Q. 2012. "Estimation of nasal cavity and conchae volumes by stereological methods." *Folio. Morphol* 71 (2): 105-108.

Fabre, M., V. Aubry, and E. Guichard. 2002. "Comparison of different methods: Static and dynamic headspace and solid-phase microextraction for the measurement of interactions between milk proteins and flavor compounds with an application to emulsions." *Journal of Agricultural and Food Chemistry* 50 (6): 1497-1501.

Fahy, John V., and Burton F. Dickey. 2010. "Airway Mucus Function and Dysfunction." *New England Journal of Medicine* 363 (23): 2233-2247.

Ferreira, V., Pet'ka, A., Cacho, J. 2006. "Intensity and Persistence Profiles of Flavor Compounds in Synthetic Solutions. Simple Model for Explaining the Intensity and Persistence of Their Aftersmell." *J. Agric. Food Chem* 54 (2): 489-496.

Fisk, I.D. 2014. "Aroma release." In *Flavour Development, Analysis and Perception in Food and Beverages*, by I.D. Fisk, 105-123. Elsevier.

Flower, D. 2000. "Beyond the super family of the lipocalins receptors." *Biochim Biophys Acta* 1482: 327-336.

Frank, D., Appelqvist, I., Piyaasiri, U., Wooster, T. J., Delahunty, C. 2011. "Proton Transfer Reaction Mass Spectrometry and Time Intensity Perceptual Measurement of Flavor Release from Lipid Emulsions Using Trained Human Subjects." *J. Agric. Food Chem* 59: 4891-4903.

Frank, Damian, Udayasika Piyasiri, Nicholas Archer, Jenifer Jenifer, and Ingrid Appelqvist. 2018. "Influence of saliva on individual in-mouth aroma release from raw cabbage (Brassica oleracea var. capitata f. rubra L.) and links to perception." *Heliyon* 5: 1045.

Friel, E. N., and A. J. Taylor. 2001. "Effect of salivary components on volatile partitioning from solutions." *Journal of Agricultural and Food Chemistry.*

Friel, E. N., Taylor, A.J. 2001. "Effect of salivary components on volatile partitioning from solutions." *J. Agric. Food Chem* 49: 3898-3905.

Friel, Ellen N., Rob S.T. Linforth, and Andrew J. Taylor. 2000. "An empirical model to predict the headspace concentration of volatile compounds above solutions containing sucrose." *Food Chemistry* 71 (3): 309-317.

Frings, S. 2001. "Chemoelectrical signal transduction in olfactorysensory neurons of air-breathing vertebrate." *Cell Mol. Life Sci.* 58: 510-519.

Fung, C. J. 2002. "The effect of headspace pressure on the performance of a fluidised-bed bioreactor." *Journal of Chemical Technology and Biotechnology* 77 (10): 1186-1190.

Gan, Heng Hui, Bingnan Yan, Robert S.T. Linforth, and Ian D. Fisk. 2016. "Development and validation of an APCI-MS/GC-MS approach for the classification and prediction of Cheddar cheese maturity." *Food Chemistry.*

Ghosh, Supratim, Devin G. Peterson, and John N. Coupland. 2008. "Temporal aroma release profile of solid and liquid droplet emulsions." *Food Biophysics* 3 (4): 335-343.

Graphics Inc, Photonics. 2008. "Saliva Composition and Functions: A Comprehensive Review."

Guichard, E. 2002. "Interactions between flavour compounds and food ingredients and their influence on flavour perception." *Food Rev Int* 18 (1): 49-70.

Haahr, A. M., W. L.P. Bredie, L. H. Stahnke, B. Jensen, and H. H.F. Refsgaard. 2000. "Flavour release of aldehydes and diacetyl in oil/water systems." *Food Chemistry.* 355-362.

Hahn, I., Scherer, P. W., Mozell, M. M. 1993. "Velocity Profiles Measured for Airfloe Through a Large-Scale Model of the Human Nasal Cavity." *J. Appl. Physiol* 75 (5): 2273-2287.

Harrison, M., Hills, B. P. 1997. "Effects of Air Flow on Flavour Release from Liquid emulsions in the Mouth." *International journal of food science and technology* 32: 1-9.

Harrison, M., Hills, B. P. 1997. "Mathematical Model of Flavor Release from Liquids Containing Aroma-Binding Macromolecules." *J. Agric. Food Chem* 45: 1883-1890.

Harrison, M., Hills, B. P., Bakker, J., Clothier, T. 1997. "Mathematical release of flavours from liquid emulsions." *Journal of Food Science* 62 (4): 653-659.

Hodgson, M. D., Langridge, J. P., Linforth, R. S. T., Taylor, A. J. 2005. "Aroma Release and Delivery Following the Consumption of Beverages." *J. Agric. Food Chem* 53 (5): 1700-1706.

Hodgson, M., Parker, A., Linforth, R. S. T. and Taylor, A. J. 2004. "*In vivo* studies on the long-term persistence of volatiles in the breath." *Flavour Fragr. J.* 19: 470-475.

Hornung, D. E., Mozell, M. M. 1977. "Factors Influencing the Differential Sorption of Odorant Molecules across the Olfactory Mucosa." *J. of Gen. Physiology 69* 69: 346-361.

Hornung, D. E., Youngentob., S. L., Mozell, M. M. 1987. "Olfactory Mucosa/Air Partitioning of Odorants." *Brain Res.* 413: 147-154.

Humphery, S. P., Williamson, R. T. 2001. "A Review of Saliva: Normal Composition, Flow and Function." *J Prosthet Dent.* 85 (2): 162-169.

Hu-Sheng, H. 2010. "Determination of vapour–liquid and vapour–liquid–liquid equilibrium of the chloroform–water and trichloroethylene–water binary mixtures." *Fluid Phase Equilibria* 289: 80-89.

Inoue, Hiroko, Kentaro Ono, Wataru Masuda, Tomohiro Inagaki, Makoto Yokota, and Kiyotoshi Inenaga. 2008. "Rheological Properties of Human Saliva and Salivary Mucins." *Journal of Oral Biosciences* (Japanese Association for Oral Biology) 50 (2): 134-141.

Ivanov, Ivan B., Krassimir D. Danov, and Peter A. Kralchevsky. 1999. "Flocculation and coalescence of micron-size emulsion droplets." *Colloids and Surfaces A: Physicochemical and Engineering Aspects.* Elsevier Science Publishers B.V. 161-182.

Jackson, S., J. Mestecky, Z. Moldoveanu, and P. Spearman, C. 1999. "Collection and processing of human mucosal secretions." *Mucosal immunology Academic Press* 19: 1567-1575.

Karaiskou, Stefania, Georgios Blekas, and Adamantini Paraskevopoulou. 2008. "Aroma release from gum arabic or egg yolk/xanthan-stabilized oil-in-water emulsions." *Food Research International* 41 (6): 637-645.

Katritzky, A. R., Wang, Y., Sild, S., Tamm, T. 1998. "QSPR Studies on Vapor Pressure, Aqueous Solubility, and the Prediction of Water−Air Partition Coefficients." *J. Chem. Inf. Comput. Sci* 38 (4): 720-725.

Kelly, J. T., Prasad, A. K., Wexler, S. 2000. "Detailed flow Patterns in the Nasal Cavity."." *J. Appl. Physiol* 89: 323-337.

Keyhani, K., Scherer, P., Mozell, M. 1997. "A Numerical Model of Nasal Odorant Transport for the Analysis of Human Olfaction." *J. theor. Biol* 186: 279-301.

Koffi, B, Ḧeroux, M., Alaee, M., Moore, S., Sauvé, S. 2010. "Quantitative analysis of volatile methylsiloxanes in waste-to-energy landfill biogases using direct APCI-MS/MS." *Environmental Science and Technology* 44 (2): 600-606.

Kora, Enkelejda Paçi, Isabelle Souchon, Eric Latrille, Nathalie Martin, and Michele Marin. 2004. "Composition Rather than Viscosity Modifies the Aroma Compound Retention of Flavored Stirred Yogurt." *Journal of Agricultural and Food Chemistry* 52 (10): 3048-3056.

Kua, C., Ho, C., Leung, S., Lau S. K. P., Woo, P.C.Y. 2018. "Clinical Mass Spectrometry in the Bioinformatics Era: A Hitchhiker's Guide." *Computational and Structural Biotechnology Journal* 16: 316-334.

Kurtz, D. B., Zhao, K., Hornung, D. E., Scherer, P. 2004. "Experimental and numerical determination of odorant solubility in nasal and olfactory mucosa." *Chem Senses* 29: 763-773.

Lai, S. K., Wang, Y., Wirtz, D., Hanes J. 2009. "Micro- and macrorheology of mucus." *Adv Drug Deliv Rev* 61 (2): 86-100.

Lai, Samuel K, Ying-Ying Wang, Denis Wirtz, and Justin Hanes. 2009. "Micro- and macrorheology of mucus." *Advanced drug delivery reviews* 61 (2): 86-100.

Laing, D. G., Jinks, A. L. 2001. "Psychophysical analysis of complex odor mixtures." *Chimia 55* 55: 413-420.

Lang, J. 1989. *Clinical Anatomy of the Nose, Nasal Cavity and Paranasal Sinuses.".* Thiem Medica New York .

Leopold, D. A., Hummel, T., Schwob, J. E. 2000. "Anterior Distribution of Human Olfactory Epithelium."." *Laryngoscope* 110: 417-421.

Linforth, R. S. T. 2010. *Food flavour technology.* Wiley-Blackwell.

Linforth, R. S. T., Martin, F., Carey, M., Davidson, J., Taylor, A. J. 2002. "Retronasal Transport of Aroma Compounds." *J. Agric. Food Chem* 50 (5): 1111-1117.

Linforth, R., Taylor, A. J. 2000. "Persistence of Volatile Compounds in the Breath after Their Consumption in Aqueous Solutions." *J. Agric. Food Chem* 48: 5419-5423.

Linforth, Rob, and Andy J. Taylor. 2000. "Persistence of volatile compounds in the breath after their consumption in aqueous solutions." *Journal of Agricultural and Food Chemistry.*

Lobel, D., Jacob, M., Volkner, M., Breer, H. 2002. "Odorants of different chemical classes interact with distinct odorant binding protein subtypes." *Chem Senses* 27: 39-44.

Lubbers, Samuel, and Emma Butler. 2010. "Effects of texture and temperature on the kinetic of aroma release from model dairy custards." *Food Chemistry* 123 (2): 345-350.

Ly, M. H., M. Covarrubias-Cervantes, C. Dury-Brun, S. Bordet, A. Voilley, T. M. Le, J. M. Belin, and Y. Waché. 2008. "Retention of aroma compounds by lactic acid bacteria in model food media." *Food Hydrocolloids* 22 (2): 211-217.

M. J. Lawson, M. J., Craven, B. A, Paterson, . E. G.,Settles, G. S. 2012. "A Computational Study of Odorant Transport and Deposition in the Canine Nasal Cavity: Implications for Olfaction." *Chem. Senses* 37 (6): 553-586.

Mackay-Slim, A., Royet, J. 2006. *Structure and Function of the Olfactory System from Olfaction and the Brain.* 1st. Cambridge University Press.

Marin, M., Baek, I., Taylor, A. J. 1999. "Volatile Release from Aqueous Solutions under Dynamic Headspace Dilution Conditions." *J. Agric. Food Chem* 47: 4750-4755.

Marin, Michèle, Inger Baek, and Andrew J. Taylor. 1999. "Volatile release from aqueous solutions under dynamic headspace dilution conditions." *Journal of Agricultural and Food Chemistry* 47 (11): 4750-4755.

Martonen, T. B., Quan, L., Zhang, Z., Musante, C. 2002. "Flow Simulation in the Human Upper Respiratory Tract." *Cell Biochemistry and Biophysics* 37: 27-36.

Mayer, M., Kuller, A., Daiber, P., Neudorf, I., Warnken, U., Schnolzer, M., Frings, S., Mohrlen, F. 2009. "The proteome of the rat olfactory sensory cilia." *Proteomics* 9: 322-334.

McClements, D. J. 2002. "Modulation of globular proteins functionality by weakly interacting cosolvents." *Crit rev food sci nutri* 42: 417-471.

Menco, B. P. 1980. "Qualitative and quantitative freeze-fracture studies on olfactory and nasal respiratory structures of frog, ox, rat, and dog. I. A general survey." *Cell tissue res* 207: 183-209.

Miettinen, Sanna Maija, Hely Tuorila, Vieno Piironen, Kimmo Vehkalahti, and Lea Hyvönen. 2002. "Effect of emulsion characteristics on the release of aroma as detected by sensory evaluation, static headspace gas chromatography, and electronic nose." *Journal of Agricultural and Food Chemistry* 50 (15): 4232-4239.

Mishellany-Dutour, Anne, Alain Woda, Hélène Labouré, Pierre Bourdiol, Pauline Lachaze, Elisabeth Guichard, and Gilles Feron. 2012. "Retro-Nasal Aroma release is correlated with variations in the in-mouth air cavity volume after empty deglutition." *PLoS ONE* 7 (7).

Monaco H. L., Z. G., Spandon P., Bolognesi M., Sawyer L., Eliopoulos E. E. 1987. "Crystal structure of the trigonal form of bovine β-lactoglobulin and of its complex with retinol at 2.5 Å resolution." *J. Mol. Biol.* 197: 695-706.

Moran, D. T., Rowley, JC 3rd, Jafek, B. W., Lovell, M. A. 1982. "The Fine Structure of the Olfactory Mucosa in Man." *J. Neurocytol.* 11 (5): 721-746.

Mosca, Ana Carolina, and Jianshe Chen. 2017. "Food-saliva interactions: Mechanisms and implications." *Trends in Food Science and Technology.* Vol. 66. Elsevier Ltd, 1 8. 125-134.

Mozell, M. M., Jagodowicz, M. 1973. "Chromotographic Seperation of Odorants by the Nose: Retention Times Measured Across *In vivo* Olfactory Mucosa." *Science* 181: 1247-1249.

Nagashima, A., Touhara, K. 2010. "Enzymatic Conversion of Odorants in Nasal Mucus Affects Olfactory Glomerular

Activation Patterns and Odor Perception." *J. Neurosci.* 30 (48): 16391-16398.

Narayan M., B. L. J. 1997. "Fatty acids and retinoids bind independently and simultaneously to β-lactoglobulin." *Biochemistry* 36: 1906-1911.

Nesvizhskii, Alexey I, Andrew Keller, Eugene Kolker, and Ruedi Aebersold. 2003. "A statistical model for identifying proteins by tandem mass spectrometry." *Analytical chemistry* 75 (17): 4646-58.

Nesvizhskii, Alexey I., Andrew Keller, Eugene Kolker, and Ruedi Aebersold. 2003. "A statistical model for identifying proteins by tandem mass spectrometry." *Analytical Chemistry* 75 (17): 4646-4658.

Niessen, W. 2006. *Liquid Chromatography-Mass Spectrometry.* 3rd. CRC Press.

Nomura, T., Takahashi, S., Ushiki, T. 2004. "Cytoarchitecture of the Normal Rat Olfactory Epithelium: Light and Scanning Electron Microscopic Studies." *rchives of Histology and Cytology* 67 (2): 159-170.

Normand, V., Avison, S., Parker, A. 2004. "Modelling the kinetics of flavour release during drinking, Chem senses." *Chem Senses* 29: 235-245.

Normand, Valéry, Shane Avison, and Alan Parker. 2004. "Modeling the kinetics of flavour release during drinking." *Chemical Senses* 29 (3): 235-245.

Oliver, Laura, Lieke Berndsen, George A. van Aken, and Elke Scholten. 2015. "Influence of droplet clustering on the rheological properties ofemulsion-filled gels." *Food Hydrocolloids* (Elsevier) 50: 74-83.

Pagès-Hélary, Sandy, Isabelle Andriot, Elisabeth Guichard, and Francis Canon. 2014. "Retention effect of human saliva on aroma release and respective contribution of salivary mucin and α-amylase." *Food Research International* (Elsevier Ltd) 64: 424-431.

Paravisini, Laurianne, and Elisabeth Guichard. 2016. "Interactions between aroma compounds and food matrix." In *Flavour: From Food to Perception*, by Laurianne Paravisini and Elisabeth Guichard, 208-234. Wiley Blackwell.

Patel, Minesh M., John D. Smart, Thomas G. Nevell, Richard J. Ewen, P. J. Eaton, and John Tsibouklis. 2003. "Mucin/poly(acrylic acid) interactions: A spectroscopic investigation of mucoadhesion." *Biomacromolecules* 4 (5): 1184-1190.

Pelosi, P. 1996. "Perireceptor events in olfaction." *J. Neurobiol* 30: 3-19.

Perez-Vilar, Juan, and Robert L Hill. 1999. "The Structure and Assembly of Secreted Mucins* □ S."

Pevsner, J., Hou, V., Snowman, A. M., Snyder, S. H., (. 1990. "Odorant-binding protein—characterization of ligand-binding." *J Biol Chem* 265: 6118-6125.

Pevsner, J., Sklar, P. B., Snyder, S. H. 1986. "Odorant-binding protein—localization to nasal glands and secretions." *Proc Nat Acad Sci* 15: 4942-4946.

Pevsner, J., Snyder, S. H. 1990. "Odorant-binding protein: odorant transport function in the vertebrate nasal epithelium." *Chemical Senses* 15 (2): 217-22.

Plana-Fattori, Artemio, Ioan C. Trelea, Jean François Le Page, Isabelle Souchon, Philippe Pollien, Santo Ali, Marco Ramaioli, Estelle Pionnier-Pineau, Christoph Hartmann, and Denis Flick. 2014. "A novel approach for studying the indoor dispersion of aroma through computational fluid dynamics." *Flavour and Fragrance Journal* (John Wiley and Sons Ltd) 29 (3): 143-156.

Proctor, D. F. 1977. "The upper airways: nasal physiology , and defense of the lungs." *Am. Rev. Respir. Dis* 115: 97-129.

Proctor, D. F., Andersen, I. 1982. *The Nose, Upper Airway Physiology and the Atmospheric Environment.* Proctor, D. F., Andersen, I., (1982). "The Nose, Upper Airway Physiology and the Atmospheric Environment." .

Purves, D., Augutine, G. J., Fitzpatrick, D. 2001. *Neuroscience. 2nd edition.* Sinauer Associates.

Rabe, S., Banavara, D. S., Krings, U., Berger, R.G. 2002. "Computerized apparatus for measuring dynamic flavour release from liquid food matrices." *J. Agric. Food Chem* 50: 6440-6447.

Rabe, S., Krings, U., Berger, R. G. 2004. "*In vitro* Study of the Influence of Physiological Parameters on Dynamic In mouth Flavour Release from Liquids." *Chem. Senses* 29 (2): 153-162.

Rabe, Swen, Ulrich Krings, and Ralf G. Berger. 2003. "Influence of oil-in-water emulsion characteristics on initial dynamic flavour

release." *Journal of the Science of Food and Agriculture* 83 (11): 1124-1133.

Rabinowitz, J. L., Brand, J. G., Baker, D., Huque, T., Bayley, D. L. 1986. "Comparison of fatty acid patterns of polar and neutral lipid classes and cyclo-oxygenase activity in taste and non-taste epithelium of steer tongues." *Int. JBiochem.* 18 (6): 543-548.

Raynal, Bertrand D E, Timothy E Hardingham, David J Thornton, and John K Sheehan. 2002. "Concentrated solutions of salivary MUC5B mucin do not replicate the gel-forming properties of saliva." *The Biochemical journal.*

Raynal, Bertrand D.E., Timothy E. Hardingham, John K. Sheehan, and David J. Thornton. 2003. "Calcium-dependent protein interactions in MUC5B provide reversible cross-links in salivary mucus." *Journal of Biological Chemistry.*

Reiners, J., Nicklaus, S., Guichard, E. 2000. "Interactions between β-lactoglobulin and flavour compounds of different chemical classes. Impact of the protein on the odour perception of vanillin and eugenol." *Lait* 80 (3): 347-336.

Relkin, Perla, Marjorie Fabre, and Elisabeth Guichard. 2004. "Effect of fat nature and aroma compound hydrophobicity on flavor release from complex food emulsions." *Journal of Agricultural and Food Chemistry* 52 (20): 6257-6263.

Riera, C., Gouezec, E., Matthey-Doret,W., Blank R. I. 2006. "The role of lipids in aroma/food matrix interactions in complex liquid model systems." *Flavour Science: Recent advances and trends* 43: 409-412.

Rozin, P. 1982. "Taste-smell confusions" and the duality of the olfactory sense." Percept. Psychophys." *Perception & Psychophysics* 31: 397-401.

Russell, Y., Evans, P., Dodd, G. H. 1993. "Characterization of the total lipid and fatty acid composition of rat olfactory mucosa." *Experimental and Toxicologic Pathology* 30: 183-188.

Samavati, Vahid, Zahra Emam-Djomeh, Ali Mehdinia, Mohammad Amin Mohammadifar, and Omid Mahmoud. 2012. "Effect of composition on release of aroma compounds." *Iranian Journal of Chemistry and Chemical Engineering* 31 (3): 85-96.

Sánchez-López, José Antonio, Aldo Ziere, Sara I.F.S. Martins, Ralf Zimmermann, and Chahan Yeretzian. 2016. "Persistence of aroma volatiles in the oral and nasal cavities: Real-time monitoring of decay rate in air exhaled through the nose and mouth." *Journal of Breath Research* (Institute of Physics Publishing) 10 (3).

Sangster, J. 1997. *Octanol and water partition coefficients: Fundamentals and physical chemistry.* Cambridge John Wiley and sons.

Sarkar, Anwesha, Kelvin K.T. Goh, and Harjinder Singh. 2009. "Colloidal stability and interactions of milk-protein-stabilized emulsions in an artificial saliva." *Food Hydrocolloids* 23 (5): 1270-1278.

Schenkels, L. C. P. M., Veerman, E. C. I., Nieuw Amerongen, A. V. 1995. "Biochemical composition of human saliva in relation to other mucosal fluids." *Critical reviews in oral biology and medicine* 6 (2): 161-179.

Schömig, Veronika J., Benjamin T. Käsdorf, Christoph Scholz, Konstantinia Bidmon, Oliver Lieleg, and Sonja Berensmeier. 2016. "An optimized purification process for porcine gastric mucin with preservation of its native functional properties." *RSC Advances* (Royal Society of Chemistry) 6 (50): 44932-44943.

Schropp, Bernhard, and Paul Tavan. 2008. "The polarizability of point-polarizable water models: Density functional theory/ molecular mechanics results." *Journal of Physical Chemistry B* (American Chemical Society) 112 (19): 6233-6240.

Sherwood, Carly A., Ashley Eastham, Lik Wee Lee, Jenni Risler, Hamid Mirzaei, Jayson A. Falkner, and Daniel B. Martin. 2009. "Rapid optimization of MRM-MS instrument parameters by subtle alteration of precursor and product m/z targets." *Journal of Proteome Research* 8 (7): 3746-3751.

Sobel, N., Khan, R.M., Hartley, C.A., Sullivan, E.V. and Gabrieli, J.D. 2000. "Sniffing Longer Rather Than Stronger to Maintain Olfactory Detection Threshold." *Chem. Senses* 25 (1): 1-8.

Soldin, Steven J., and Offie P. Soldin. 2009. "Steroid hormone analysis by tandem mass spectrometry." *Clinical Chemistry.* Vol. 55. no. 6. 1 6. 1061-1066.

Steinbrecht, R. A. (. 1998. "Odorant-binding proteins: expression and function." *Annals of the New York Academy of Sciences* (866): 323-332.

Taylor, A J. 2002. "Release and Transport of Flavors *In vivo* : Physicochemical, Physiological, and Perceptual Considerations."

Taylor, A J, R S T Linforth, B A Harvey, and A Blake. n.d. "Atmospheric pressure chemical ionisation mass spectrometry for *in vivo* analysis of volatile ¯avour release."

Taylor, A. J. 1998. "Physical Chemistry of Flavour." *international journal of food science and technology* 33: 53-62.

Taylor, A. J. 2002. "Release and transport of flavours *In vivo* : Physiochemical, physiological and perceptual considerations." *Comprehensive reviews in food science and food safety* 1: 80-89.

Taylor, A. J., Cook, D. J., Scott, D. J. 2008. "Role of odor binding protein: comparing hypothetical mechanisms with experimental data."." *Chemosens Percept* 1: 153-162.

Tegoni, M., Pelosi, P., Vincent, F., Spinelli, S., rie Campanacci V., Grolli, S., Ramoni, R., Cambilla, C. 2000. "Mammalian odorant binding proteins." *Biochimica et Biophysica Acta* 1482: 229-240.

Tomer, K. B., and M. L. Gross. 1988. "Fast atom bombardment and tandem mass spectrometry for structure determination: Remote site fragmentation of steroid conjugates and bile salts." *Biomedical & Environmental Mass Spectrometry* 15 (2): 89-98.

Torner, K B, and M L Grosst. 1988. "Fast Atom Bombardment and Tandem Mass Spectrometry for Structure Determination: Remote Site Fragmentation of Steroid Conjugates and Bile Salts." 89-98.

Tsachaki, Maroussa, Robert S.T. Linforth, and Andrew J. Taylor. 2009. "Aroma release from wines under dynamic conditions."

Journal of Agricultural and Food Chemistry 57 (15): 6976-6981.

Turner, L. H., Chiew, Y. C., Ahlert, R. C., Kosson, D. S. 1996. "Measuring vapor-liquid equilibrium for aqueous-organic systems: Review and a new technique." *American insitute of chemical engineering* 42 (6): 1772-1778.

Van Cauwenberge, P., Sys, L., De Belder, T. D., Watelet, J. B. 2004. "Anatomy and physiology of the nose and the paranasal sinuses." *Immunol. Allergy Clin. N. Am* 24: 1-17.

van Ruth, S. M., Grossmann, I., Geary, M., Delahunty, C.M. 2001. "Interactions between artificial saliva and 20 aroma compounds in water and oil model systems." *J. Agric. Food Chem* 49: 2409-2413.

Van Ruth, Saskia M., Carmel King, and Persephoni Giannouli. 2002. "Influence of lipid fraction, emulsifier fraction, and mean particle diameter of oil-in-water emulsions on the release of 20 aroma compounds." *Journal of Agricultural and Food Chemistry* 50 (8): 2365-2371.

Van Ruth, Saskia M., Catherine H. O'Connor, and Conor M. Delahunty. 2000. "Relationships between temporal release of aroma compounds in a model mouth system and their physico-chemical characteristics." *Food Chemistry.* 393-399.

Van Ruth, Saskia M., Isabelle Grossmann, Mike Geary, and Conor M. Delahunty. 2001. "Interactions between artificial saliva and 20 aroma compounds in water and oil model systems." *Journal of Agricultural and Food Chemistry.*

Vingerhoeds, Monique H., Erika Silletti, Jolan de Groot, Raymond G. Schipper, and George A. van Aken. 2009. "Relating the effect of saliva-induced emulsion flocculation on rheological properties and retention on the tongue surface with sensory perception." *Food Hydrocolloids* 23 (3): 773-785.

Vingerhoeds, Monique H., Theo B.J. Blijdenstein, Franklin D. Zoet, and George A. Van Aken. 2005. "Emulsion flocculation induced by saliva and mucin." *Food Hydrocolloids* (Elsevier) 19 (5): 915-922.

Vogalis, F., Hegg, C. C., Lucero, M. T. 2005. "Ionic Conductance in Sustentacular Cells of the Mouse olfactory Epithelium." *J. Physiology* 562 (3): 785-799.

Voiley, A. 2006. *Flavour retention and release from the food matrix: an overview in Flavour in Food.* Woodhead publishing limited.

Voilley, A., Beghin, V., Charpentier, C., Peyron, D. 1990. "Interactions between aroma substances and macromolecules in model wine." *Food science and Technology* 24: 469-472.

Wang, Xin, Quanquan Lin, Aiqian Ye, Jianzhong Han, and Harjinder Singh. 2019. "Flocculation of oil-in-water emulsions stabilised by milk protein ingredients under gastric conditions: Impact on *in vitro* intestinal lipid digestion." *Food Hydrocolloids* (Elsevier B.V.) 88: 272-282.

Wang, Xinmiao, and Jianshe Chen. 2017. "Food oral processing: Recent developments and challenges." *Current Opinion in Colloid and Interface Science.* Vol. 28. Elsevier Ltd, 1 3. 22-30.

Weiss, Jochen, and D. Julian McClements. 2002. "Mass Transport Phenomena in Oil-in-Water Emulsions Containing Surfactant Micelles: Solubilization." *Langmuir* (American Chemical Society (ACS)) 16 (14): 5879-5883.

Wely, James,. Rorrer, Gregory,.Foster, David. n.d. *Fundamentals of Momentum, Heat and Mass Transfer.* Sixth. Wiley.

Weterings, Martijn, Igor Bodnár, Remko M. Boom, and Michael Beyrer. 2019. "A classification scheme for interfacial mass transfer and the kinetics of aroma release." *Trends in Food Science and Technology.* Elsevier Ltd.

Wright, K. M., Hills, B. P. 2003. "Modelling of flavour release from a chewed bolus in the mouth, Part II the release kinetics, International journal of science and technology." *International journal of food science and technology* 38 (3): 361-368.

Wright, K. M., Hills, B. P., Hollowood, T.A., Linforth, R. S. T., Talyor, A. J. 2004. "Persistence effects in flavour release from liquids in the mouth." *International journal of food science and technology* 38: 343-350.

Wu, S. Y., Perez, M. D., Puyols, P., Sawyer, L. 1997. "β-Lactoglobulin binds palmitate within its central cavity." *J. Biol. Chem* 36: 170-174.

Yang, G. C., Scherer, P. W., Zhao, K., Mozell, M. M. 2007. "Numerical modelling of odorant uptake in the rat nasal cavity." *Chem. Senses* 32: 273-84.

Zalewska, Anna, Krzysztof Zwierz, Krzysztof Zółkowski, and Andrzej Gindzieński. 2000. "Structure and biosynthesis of human salivary mucins." *Acta Biochimica Polonica* 47 (4): 1067-1079.

Zhao, K., Dalton, P., Geoffery, Y. C., Scherer, P. W. 2006. "Numerical Modeling of Turbulent and Laminar Airflow and Odorant Transport during Sniffing in the Human and Rat Nose." *Chem. Senses* 31: 107-118.

Zhao, K., Scherer, P. W., Hajiloo, P. A., Dalton, P. n.d. "Effect of Anatomy on Human Nasal Air Flow and Odorant Transport Patterns: Implications for Olfaction." *Chem. Senses* 29: 365-379.